

AUTOMATED METHODS ON MAGNETIC RESONANCE BRAIN IMAGING IN MULTIPLE SCLEROSIS

Eloy Roura Pérez

Per citar o enllaçar aquest document:
Para citar o enlazar este documento:
Use this url to cite or link to this publication:

<http://hdl.handle.net/10803/394030>



<http://creativecommons.org/licenses/by-nc-sa/4.0/deed.ca>

Aquesta obra està subjecta a una llicència Creative Commons Reconeixement-
NoComercial-CompartirIgual

Esta obra está bajo una licencia Creative Commons Reconocimiento-NoComercial-
CompartirIgual

This work is licensed under a Creative Commons Attribution-NonCommercial-
ShareAlike licence



DOCTORAL THESIS

Automated methods on magnetic
resonance brain imaging in multiple
sclerosis

Eloy Roura Pérez

2016

UNIVERSITAT DE GIRONA
ESCOLA POLITÈCNICA SUPERIOR
Departament d'Arquitectura i Tecnologia de Computadors (ATC)



DOCTORAL THESIS

**Automated methods on magnetic
resonance brain imaging in multiple
sclerosis**

Eloy Roura Pérez

2016

DOCTORAL PROGRAM in TECHNOLOGY

Supervised by:

Dr. Xavier Lladó

Dr. Arnau Oliver

Work submitted to the University of Girona in partial fulfillment of the
requirements for the degree of Doctor of Philosophy

To all who walked along this journey.



Acknowledgements

Today, at the very end of the PhD thesis, I can tell you how satisfied I feel having made this choice four years ago. Venturing in this journey, infinitely long and fuzzy at the beginning, has given me not only the scientific expertise I have gathered but also the opportunity to meet extraordinary people all around the world, who have put their bit and whom I am really grateful for. All what I have learned from them, all the experiences and lovely time spent together and obviously all the outcomes achieved pleasantly reward the efforts made during this thesis, it was definitely worth it.

I would like to show my deepest gratitude to my advisors Dr. Xavier Lladó and Dr. Arnau Oliver for promoting me relying on my work and my commitment with this amazing research group. Working at VICOROB within the NeuroImage Computing group has allowed me to maintain inspiring scientific discussions with my closest team-workers Sergi and Mariano. Besides, coffee breaks, lunchtime, dinners, running, paddle, philosophical discussions and other social activities in and out of the PIV building with the rest of colleagues Marc, Pepe, Ricard C., Gerard P., Albert G., Ferran R., Sandra, Cristian, Josep, Habbib, Konstantin, Mojdeh, Guillaume, Sik, Aina, Robert, Joan M., Jordi, Xevi, Yago, Oliver, Ricard P., Eloy G., Albert P., Pablo, Ferran T., and Xesca have been also helpful during tough times. I would like to mention the great job of the administrative staff Joseta, Mireia and Anna.

This work would neither be possible without the collaboration of Dr. Lluís Ramió-Torrentà from the Hospital Dr. Josep Trueta of Girona, Dr. Joan Carles Vilanova from the Clínica Girona, Dr. Deborah Pareto and Àlex Rovira from the Hospital Vall d'Hebron of Barcelona and Dr. Nùria Bargallò, Dr Ricard Cervera and Nicolae Sarbu from Hospital Clinic of Barcelona. They have provided most of the images used in this PhD thesis while the rest have been obtained in the different research stays. This leads me to thank the

International Federation of MS for awarding me with the Du Pré Grant 2012 and the University of Girona for funding my research during the last three years with the grant BR-GR13 and the corresponding travel grants the two last years. Thanks to this funding, I have visited the Institute of Neurology of London under the supervision of Dr. Claudia Wheeler-Kingshott with the great support of Dr. Torben Schneider and the rest of the fellows room Moreno, Nils, Hug, Frank, David, Varun and Uran. I have also visited the Brain Imaging Center at McGill University in Montreal collaborating in a project with Dr. Arnold Douglas, Dr. Sridar Narayanan, Dr. Louis Collins and Dr. Parya Mommavez having a great encouragement of Dave, Rob, Kunio, Dumitru and Haz-Edine. Finally, I also had the opportunity to visit the Department of Pediatrics at the Medical Centre of the University of Washington in Seattle, under the supervision of Dr. Colin Studholme and the collaboration of Mengyuan. I also would like to thank the rest of co-authors of my publications for sharing their knowledge.

After having mentioned all who walked along in the professional field, I would like to thank those who have suffered in the other side, those who have perfectly bear my unreasonable bad attitude at stressed days helping me to fight these adversities, I would like to deeply thank my parents, family and friends for all this support received.

Publications

This thesis is a compendium of the following research articles, which meet the requirements in the PhD technology program:

- **Eloy Roura**, Nicolae Sarbu, Arnau Oliver, Sergi Valverde, Sandra González, Ricard Cervera, Nuria Bargalló and Xavier Lladó. Automated detection of Lupus white matter lesions in MRI images. *Submitted to Frontiers in Neuroinformatics*. 2016. Frontiers. Quality index: [JCR MCB IF 3.261, Q1(8/57)].
- **Eloy Roura**, Arnau Oliver, Mariano Cabezas, Sergi Valverde, Deborah Pareto, Joan Carles Vilanova, Lluís Ramió-Torrentà, Àlex Rovira and Xavier Lladó. A toolbox for multiple sclerosis lesion segmentation. *Neuroradiology*. Vol. 57, Issue 10, pp. 1031-1043. 2015. DOI: 10.1007/s00234-015-1552-2. Springer. Quality index: [JCR RNMMI IF 2.485, Q2(41/125)].
- **Eloy Roura**, Torben Schneider, Marc Modat, Panaj Daga, Nils Mulhert, Declan Chard, Sebastien Ourselin, Xavier Lladó and Claudia AM Wheeler-Kingshott. Exhaustive multi-channel registration evaluation of conventional and diffusion MRI on MS patients. *Functional Neurology*. Vol. 30, Issue 4, pp. 645-656. 2015. DOI: 10.11138/FNeur/2015.30.4.245 Quality index: [JCR N IF 1.855, Q3(187/252)].
- **Eloy Roura**, Arnau Oliver, Mariano Cabezas, Joan Carles Vilanova, Àlex Rovira, Lluís Ramió-Torrentà and Xavier Lladó. MARGA: Multispectral Adaptive Region Growing Algorithm for brain extraction on axial MRI. *Computer Methods and Programs in Biomedicine*. Vol. 113, Issue 2, pp. 655-653. 2014. DOI: 10.1016/j.cmpb.2013.11.015. Elsevier. Quality index: [JCR CSTM IF 1.897, Q1(15/102)].

The rest of publications derived from this PhD thesis are the following:

Journals

- Sergi Valverde, Arnau Oliver, **Eloy Roura**, Deborah Pareto, Joan Carles Vilanova, Lluís Ramió-Torrentà, Jaume Sastre-Garriga, Xavier Montalban, Àlex Rovira and Xavier Lladó. Quantifying brain tissue volume in multiple sclerosis with automated lesion segmentation and filling SPM8 toolboxes. *NeuroImage Clinical*. 2016. DOI: 10.1016/j.nicl.2015.10.012. Elsevier. Quality index: [JCR N IF 2.526, Q2(6/14)].
- Sergi Valverde, Arnau Oliver, Mariano Cabezas, **Eloy Roura** and Xavier Lladó. Comparison of ten brain tissue segmentation methods using revisited IBSR annotations. *Journal of Magnetic Resonance Imaging*. Vol. 41, Issue 1, pp. 93-101. January 2015. DOI: 10.1002/jmri.24517. Wiley. Quality index: [JCR RNMMI IF: 3.210 Q1(23/125)].
- Mariano Cabezas, Arnau Oliver, **Eloy Roura**, Jordi Freixenet, Joan Carles Vilanova, Lluís Ramió-Torrentà, Àlex Rovira, and Xavier Lladó. Automatic multiple sclerosis lesion detection in brain MRI by FLAIR thresholding. *Computer Methods and Programs in Biomedicine*. Vol. 115, Issue 3, pp. 147-161. July 2014. DOI: 10.1016/j.cmpb.2014.04.006. Elsevier. Quality index: [JCR CSTM IF 1.897, Q1(15/102)].

Conferences

- **Eloy Roura**, Arnau Oliver, Mariano Cabezas, Sergi Valverde, Deborah Pareto, Joan Carles Vilanova, Lluís Ramió-Torrentà, Àlex Rovira and Xavier Lladó. An SPM12 extension for multiple sclerosis lesion segmentation. *SPIE Medical Imaging 2016*. February 2016, San Diego, USA.
- **Eloy Roura**, Arnau Oliver, Mariano Cabezas, Sergi Valverde, Deborah Pareto, Joan Carles Vilanova, Lluís Ramió-Torrentà, Àlex Rovira and Xavier Lladó. A toolbox for segmenting multiple sclerosis lesions using T1w and FLAIR images. *ECTRIMS 2015. Multiple Sclerosis*. October 2015, Barcelona, Spain. [JCR CN IF:4.472 Q1(25/191)].

- Sergi Valverde, Arnau Oliver, **Eloy Roura**, Deborah Pareto, Joan Carles Vilanova, Lluís Ramió-Torrentà, Jaume Sastre-Garriga, Xavier Montalban, Àlex Rovira and Xavier Lladó. Evaluation of two automated lesion segmentation and filling pipelines for brain tissue segmentation of multiple sclerosis patients. *ECTRIMS 2015. Multiple Sclerosis*. October 2015, Barcelona, Spain. [JCR CN IF:4.472 Q1(25/191)].
- **Eloy Roura**, Arnau Oliver, Mariano Cabezas, Jordi Freixenet, Xavier Lladó, Joan Carles Vilanova, Àlex Rovira and Lluís Ramió-Torrentà. Extracting the brain in axial MR images with an adaptive segmentation technique. *ECTRIMS 2013. Multiple Sclerosis*. October 2013, Copenhagen, Denmark. [JCR CN IF:4.472 Q1(25/191)].
- **Eloy Roura**, Torben Schneider, Marc Modat, Panaj Daga, Nils Mulhert, Declan Chard, Sebastien Ourselin, Xavier Lladó and Claudia AM Wheeler-Kingshott. Multi-channel registration of conventional and diffusion MRI on MS patients. *The International Society for Magnetic Resonance in Medicine (ISMRM)*. April 2013, Salt Lake city, Utah.
- Yago Díez, Xavier Lladó, Arnau Oliver, Robert Martí, **Eloy Roura**, Mariano Cabezas, Onur Ganiler, Jordi Freixenet, Joan Carles Vilanova, Lluís Valls, Lluís Ramió-Torrentà, Deborah Pareto and Àlex Rovira. Registration of serial brain MRI scans from multiple sclerosis patients. Analysis of 3D intensity-based methods. *ECTRIMS 2012. Multiple Sclerosis*. October 2012, Lyon, France. [JCR: CN, IF:4.255 Q1(27/191)].
- **Eloy Roura**, Torben Schneider, Panaj Daga, Marc Modat, Nils Mulhert, Jordi Freixenet, Declan Chard, Sebastien Ourselin, Xavier Lladó and Claudia AM Wheeler-Kingshott. Multi-channel registration of FA and T1-weighted images to standard space: patients with Multiple Sclerosis. *The International Society for Magnetic Resonance in Medicine (ISMRM)*. May 2012, Melbourne, Australia.

Acronyms

ADC	Apparent Diffusion Coefficient
BET	Brain Extraction Tool
BSE	Brain Surface Extractor
CAD	Computer-Aided Diagnosis
CHB	Childrens Hospital Boston
CNS	Central Nervous System
CSF	Cerebrospinal Fluid
DIS	Dissemination in Space
DIT	Dissemination in Time
DOF	degree-of-freedom
DSC	Dice Similarity Coefficient
DTI	Diffusion Tensor Image
DWI	Diffusion Weighted Image
FA	Fractional Anisotropy
FLAIR	Fluid Attenuated Inversion Recovery
FP	False Positive
GE	Gradient Echo
GM	Gray Matter
MARGA	Multispectral Adaptive Region Growing Algorithm
MI	Mutual Information
MICCAI	Medical Image Computing and Computer Assisted Interventions
MR	Magnetic Resonance
MRI	Magnetic Resonance Imaging
MS	Multiple Sclerosis
NAMIC	National Alliance for Medical Image Computing
NMI	Normalised Mutual Information

N3 Non-parametric, Non-uniform intensity Normalisation
PDw Proton Density Weighted
PPV Positive Predictive Value
PPMS Primary-Progressive Multiple Sclerosis
PRMS Primary-Relapsing Multiple Sclerosis
RF Radio frequency
RG Region Growing
ROI Region of Interest
RRMS Relapsing-Remitting Multiple Sclerosis
SE Spin Echo
SPM Statistical Parametric Mapping
SPMS secondary-progressive Multiple Sclerosis **SSD** Sum of Squares Distances
TE Echo Time
TP True Positive
TP Repetition Time
TPR True Positive Rate
T1w T1 weighted
T2w T2 weighted
UNC University of North Carolina
WM White Matter
WML White Matter Lesions

List of Figures

1.1	MS prevalence around the world.	3
1.2	Main symptoms of MS.	5
1.3	Brain MRI representation.	7
1.4	Different MR images of the brain.	8
1.5	VICOROB Projects.	11
2.1	Different diffusion MR images of the brain.	19
2.2	Head MRI representation.	20
2.3	MRI intensity corrections.	21
2.4	Global scheme of the registration process.	24
2.5	Brain tissue segmentations.	26
2.6	3T MRI of an MS patient.	27

List of Tables

1.1 Tissue intensity distributions by image contrast.	9
---	---

Contents

Abstract	xiii
Resum	xv
Resumen	xvii
1 Introduction	1
1.1 Motivation	1
1.2 Thesis context	2
1.2.1 Multiple Sclerosis	2
1.2.2 Lupus Erithematosus	4
1.2.3 Magnetic resonance imaging	5
1.2.4 Image processing	6
1.3 Research background	9
1.4 Objectives	10
1.5 Document structure	12
2 Thesis background	15
2.1 MRI details	15
2.1.1 Conventional MRI	17
2.1.2 Diffusion MRI	17

2.2	Pre-processing	19
2.2.1	Brain extraction	19
2.2.2	Intensity corrections	20
2.2.3	Registration	22
2.3	Processing	25
2.3.1	Brain tissue segmentation	25
2.3.2	WML segmentation	25
3	MARGA: Multispectral Adaptive Region Growing Algorithm for brain extraction on axial MRI	29
4	Multi-channel registration of FA and T1w images in the presence of atrophy: application to Multiple Sclerosis	49
5	A toolbox for multiple sclerosis lesion segmentation	63
6	Automated detection of Lupus white matter lesions in MRI images	77
7	Main results and discussion	87
8	Conclusions	91
8.1	Research stays	91
8.2	Contributions	92
8.3	Future work	93

Abstract

Nowadays, medical imaging is one of the most important tools for doctors when studying the human body. Given the wide variety of images, the information provided, and the huge amount of research and clinical practice performed around the world, we could say that medical imaging has become a new science. The imaging techniques used depend mainly on the part of the body and the disease studied, in order to better appreciate the characteristics of the tissue. In the case of the brain, one of the techniques most widely used is the conventional and diffusion magnetic resonance imaging (MRI), although Computed Tomography (CT) is also used. The focus of this thesis, is to study these MRI by means of computer vision, analysing and developing automated methods to assist doctors in the detection and monitoring of neurological diseases affecting the central nervous system, of which the brain is the main part. Multiple Sclerosis (MS) is a clear example of these diseases, characterised by the presence of white matter lesions (WML), which can be detected in this image modality. Lupus is also an example, in which the white matter is affected by these plaques, but usually presenting a smaller lesion burden.

Currently, doctors perform manual analyses of MRI scans, which are volumes in 3D implying a great deal of computation time. By manual analysis we mean carrying out the detection and segmentation of WML. The quantification of these WML is crucial for the diagnosis of MS and is also an important predictor in Lupus. This task is performed repeatedly by different radiologists who provide a subjective description, always within some limits and following specific criteria. This fact introduces a high variability that negatively affects the results, especially in longitudinal studies, where even a single radiologist can have different opinions in different time points. This subjectivity difficulties to develop automatic algorithms as the definition of what is correct is inherently unclear.

First of all, in this thesis, we have focused on the image pre-processing in order to

enhance the image information. The main aspects of this enhancement rely on removing any image noise and correcting any intensity bias induced by the scanner. Also, as isolating the brain region from the whole image is a key step in the pre-processing, this technique is known as "skull-stripping". On this last point, we have contributed a new technique based on a multispectral, adaptive, region growing algorithm, which enhances the current state-of-the-art on the brain segmentation process.

We include, as a pre-processing step, the image registration process, which is a key step in order to using complementary information from different modalities as well as comparing different subjects. In this thesis we also propose a novel pipeline to carry out the registration process by using information from multiple modalities to improve the results of this registration process.

Furthermore, we have also studied the current techniques for the detection and segmentation of WML, proposing a new method based on a previous proposal. This approach uses two image modalities, one to obtain tissue information that will be used to detect the lesions in the other. Finally, we have achieved an automated and user-friendly tool with comparable, or even better, results in some cases than the state-of-the-art.

As a result of this thesis, we present on the one hand a new approach for brain segmentation from an MRI and another approach for registering various MRI modalities in the same space. On the other hand, we present a tool able to automatically detect and segment WML. This tool is publicly available and designed to operate under the SPM platform commonly used in hospitals due to its easy user interaction. This tool has been developed on the basis of a thorough analysis of the state-of-the-art of the different techniques involved.

Resum

La imatge mèdica és avui dia una de les eines principals dels metges per estudiar el cos humà. Donada la gran diversitat d'imatges, la informació que ens proporcionen, i la quantitat d'estudis i pràctiques clíniques que es duen a terme arreu del món, podríem dir que la imatge mèdica s'ha convertit en una nova ciència. Les tècniques d'imatge utilitzades depenen majoritàriament de l'òrgan i la malaltia estudiada, per tal que les característiques del teixit s'apreciïn millor. En el cas del cervell, la imatge per excel·lència és la imatge de ressonància magnètica (MRI) convencional i de difusió, tot i que la Tomografia Axial Computeritzada (TAC) és extensament utilitzada. En aquesta tesi ens centrem en estudiar MRI mitjançant la visió per computador, analitzant i desenvolupant mètodes automàtics per tal d'ajudar als metges en la detecció i el seguiment de malalties neurològiques que afecten al sistema central nerviós, on el cervell n'és la part principal. Un exemple clar d'aquest tipus de malaltia és l'Esclerosi Múltiple (EM), caracteritzada per la presència de lesions a la matèria blanca, les quals poden ser detectades en aquesta modalitat d'imatge. Lupus és també un exemple on la matèria blanca es veu afectada per aquest tipus de lesions, tot i que solen tenir una mida més reduïda.

Actualment els metges analitzen manualment les ressonàncies magnètiques, que són volums en 3D, i per tant analitzar totes les imatges d'un pacient comporta un temps de valoració radiològica molt elevat. Quan parlem d'anàlisi manual, ens referim sobretot a la detecció i segmentació de les lesions de matèria blanca esmentades. La seva quantificació és un fet crucial en el diagnosi de l'EM i un factor de predicció important en el Lupus. Aquesta tasca l'efectuen diferents radiòlegs una i altra vegada, i el resultat de cadascú acaba sent una descripció subjectiva del pacient, sempre dins uns límits i seguint uns criteris establerts. Aquest fet implica una variabilitat, a vegades bastant elevada, que afecta negativament als resultats, sobretot en estudis longitudinals, on fins i tot un mateix

radiòleg pot tenir diferents opinions en diferents espais de temps.

En aquesta tesi ens centrem, per una part, en el pre-processat de la imatge per tal d'eliminar el soroll i corregir les inhomogeneïtats en les intensitats, ambdòs errors introduïts per l'escàner. A més, l'obtenció de la regió del cervell de dins de tota la imatge, és una etapa important en el pre-procés, i aquesta tècnica és coneguda com a “skull-stripping”. En aquest punt hi hem contribuït amb una nova tècnica basada en un algorisme de “region growing” adaptatiu i de multiespectre, el qual millora la segmentació del cervell dels treballs actuals de l'estat de l'art.

Incloem com a pre-processat el registre d'imatges, fet primordial per tal de poder utilitzar la informació complementària en les diferents modalitats així com comparar diferents casos. En aquesta tesi proposem una “pipeline” per tal de dur a terme el registre mitjançant la informació de múltiples modalitats per tal de millorar els resultats d'aquest procés.

Per altra banda, hem estudiat també les tècniques actuals de detecció i segmentació de lesions en la matèria blanca, proposant un mètode nou basat en anteriors propostes. Aquest mètode utilitza dues modalitats d'imatge, una de les quals s'utilitza per obtenir informació dels teixits la qual serà utilitzada per detectar les lesions en l'altre. Finalment, hem aconseguit una eina amb uns resultats comparables, o fins i tot millor en alguns casos, que l'estat de l'art, i que és totalment automàtica i fàcilment utilitzable.

Com a resultat d'aquesta tesi, presentem una nova proposta per tal de segmentar el cervell a partir una MRI i una altra per tal de registrar diferents modalitats de MRI en un mateix espai. Per altra banda, presentem una eina automàtica capaç de detectar i segmentar lesions en la matèria blanca de pacients d'EM i Lupus. Aquesta eina és pública i dissenyada per tal de funcionar sota la plataforma SPM, la qual utilitzen habitualment en els hospitals gràcies a la seva fàcil interacció amb l'usuari. Aquesta eina s'ha dut a terme a partir d'un anàlisi exhaustiu de l'estat de l'art de les diferents tècniques involucrades.

Resumen

La imagen médica es hoy en día una de las herramientas principales de los médicos para estudiar el cuerpo humano. Dada la gran diversidad de imágenes, la información que nos proporcionan, y la cantidad de estudios y prácticas clínicas que se llevan a cabo en todo el mundo, podríamos decir que la imagen médica se ha convertido en una nueva ciencia. Las técnicas de imagen utilizadas dependen mayoritariamente del órgano y de la enfermedad estudiada, para que las características del tejido se aprecien mejor. En el caso del cerebro, la imagen por excelencia es la imagen de resonancia magnética (RM) convencional y de difusión, aunque la Tomografía Axial Computarizada (TAC) es también un recurso extensamente utilizado. En esta tesis nos centramos en estudiar imágenes de RM mediante la visión por computador, analizando y desarrollando métodos automáticos para ayudar a los médicos en la detección y el seguimiento de enfermedades neurológicas que afectan al sistema central nervioso, donde el cerebro es la parte principal. Un ejemplo claro de este tipo de enfermedad es la Esclerosis Múltiple (EM), caracterizada por la presencia de lesiones en la materia blanca, las cuales pueden ser detectadas en esta modalidad de imagen. El Lupus es también un ejemplo donde la materia blanca se ve afectada por este tipo de lesiones, aunque suelen tener un tamaño más reducido.

Actualmente los médicos analizan manualmente las resonancias magnéticas, que son volúmenes en 3D, y por tanto analizar todas las imágenes de un paciente conlleva un tiempo de valoración radiológica muy elevado. Cuando hablamos de análisis manual, nos referimos sobre todo a la detección y segmentación de las lesiones de materia blanca mencionadas. Su cuantificación es un hecho crucial en el diagnóstico de la EM y un factor de predicción importante en Lupus. Esta tarea la efectúan diferentes radiólogos una y otra vez, y el resultado de cada uno termina siendo una descripción subjetiva, siempre dentro de unos límites y siguiendo unos criterios establecidos. Este hecho implica una

variabilidad, a veces bastante elevada, que afecta negativamente a los resultados, sobre todo en estudios longitudinales, donde incluso un mismo radiólogo puede tener diferentes opiniones en diferentes espacios de tiempo.

En esta tesis nos hemos centrado, por una parte, en el pre-proceso de la imagen para eliminar el ruido y corregir las inhomogeneidades en las intensidades, ambos introducidos por el escáner. Además, obtener la región del cerebro de entre toda la imagen, es una etapa importante en el pre-proceso, técnica conocida como “skull-stripping”. En este punto hemos contribuido con una nueva técnica basada en un algoritmo de “region growing” adaptativo y de multiespectro, el cual mejora la segmentación del cerebro de los trabajos actuales del estado del arte.

Incluimos como pre-proceso el registro de imágenes, hecho primordial para poder utilizar la información complementaria en las diferentes modalidades así como comparar diferentes casos. Por lo tanto, en esta tesis proponemos una “pipeline” para llevar a cabo el registro mediante la información de múltiples modalidades para mejorar los resultados de este proceso.

Por otra parte hemos estudiado también las técnicas actuales de detección y segmentación de lesiones en la materia blanca, proponiendo un método nuevo basado en anteriores propuestas. Este método incorpora dos modalidades de imagen, una de las cuales se utiliza para obtener información de los tejidos la cual es utilizada, a su vez, para la detección de las lesiones en la otra. Hemos conseguido una herramienta con unos resultados comparables, o incluso mejores en algunos casos, que el estado del arte, y que es totalmente automática y fácilmente utilizable.

Como resultado de esta tesis, presentamos por una parte una nueva propuesta para segmentar el cerebro a partir de una MRI y una para registrar diferentes modalidades de MRI en un mismo espacio. Por otra parte presentamos una herramienta automática capaz de detectar y segmentar lesiones en la materia blanca de pacientes de EM y Lupus. Esta herramienta es pública y diseñada para funcionar bajo la plataforma SPM, la cual se utiliza habitualmente en los hospitales gracias a su fácil interacción con el usuario. Esta herramienta se ha realizado a partir de un análisis exhaustivo del estado del arte de las diferentes técnicas involucradas.

Introduction

This chapter outlines the motivation for the work developed in this thesis. It also presents an overview of the covered topics on which this thesis is based. Afterwards, it describes our team's previous work within this scope and the proposed objectives. After this chapter, the reader will have general overview of the thesis content, while in the next Chapter 2 a more detailed description of the techniques is given covering the contents of the four papers presented in the thesis. The first two contributions (see Chapter 3 and 4) are related with the pre-processing section 2.2 and the two last papers (see Chapter 5 and 6) belong to the processing section 2.3.

1.1 Motivation

Technology is evolving in such a way that humans are not able to exploit its entire potential, not even to the point of using these innovations in daily practice. This is unstoppable nowadays in all fields of science, such as the environment, biology, services, medicine, etc. The key question is how to exploit all these resources, how to combine all those technological innovations in order to obtain as many benefits as possible. This is why research is a key step in squeezing out everything that this technological evolution has to offer human beings, so there is still a lot of work to do.

Several factors have contributed to the development of medicine, from mere drugs to complex surgical equipment and medical imaging. Unfortunately, diseases have been always a part of being a human being, a fact that renders us vulnerable and dependent on this science. The more advances made in medicine the better quality of life and longer life expectancy we humans can enjoy, even though a myriad of factors influence this issue. Given this situation, the research in this field affects the entire globe, and, thanks to the

investment of private companies (mostly pharmaceuticals) as well as governments, we can carry out projects focused on medicine improvements.

Regarding medical research, medical imaging has become a crucial tool used to study the interior of the body for a variety purposes, such as medical intervention, disease diagnosis, disease evolution control, etc. The most common imaging technologies are the following: radiography, magnetic resonance imaging (MRI), ultrasound, endoscopy, elastography, tactile imaging, thermography, medical photography and nuclear medicine functional imaging techniques like positron emission tomography.

In this thesis, we will focus on MRI of the brain, since several diseases like Multiple Sclerosis (MS), Alzheimer, Lupus, Dementia, and Strokes affect the brain in different ways, presenting white matter lesions (WML), atrophy, and matter loss. Brain MRI scans consist of a 3D volume of the patients which doctors and radiologists have to process slice by slice in order to detect abnormalities in the brain. This becomes a tedious and very time consuming task that may lead to inaccuracies due to human error. On the other hand, from the computer science point of view, one can see those tasks as a set of sequential processes that produce different outputs, making decisions based on the application of certain rules over certain inputs. Therefore, by means of computer vision, the image processing can be performed automatically sometimes achieving better accuracy and reproducibility.

Considering different diseases and their abnormalities affecting the brain, in this thesis we will focus on MS, which affects the central nervous system (CNS) presenting damage to the white matter of the brain, sometimes related to physical, mental and psychiatric problems.

1.2 Thesis context

1.2.1 Multiple Sclerosis

Multiple Sclerosis is an unpredictable chronic neurological condition affecting the CNS and causing the most disability in young adults. Most people are diagnosed between the ages of 20-40, but it can affect younger and older people. Recent epidemiological studies show that 2.3 million people have been diagnosed with MS worldwide, of which almost three times more women than men are affected. The causes are still unknown, but interaction with multiple genetic and as-yet-unidentified environmental factor(s) are potential candidates [1]. Moreover, geographic studies show the prevalence of MS around

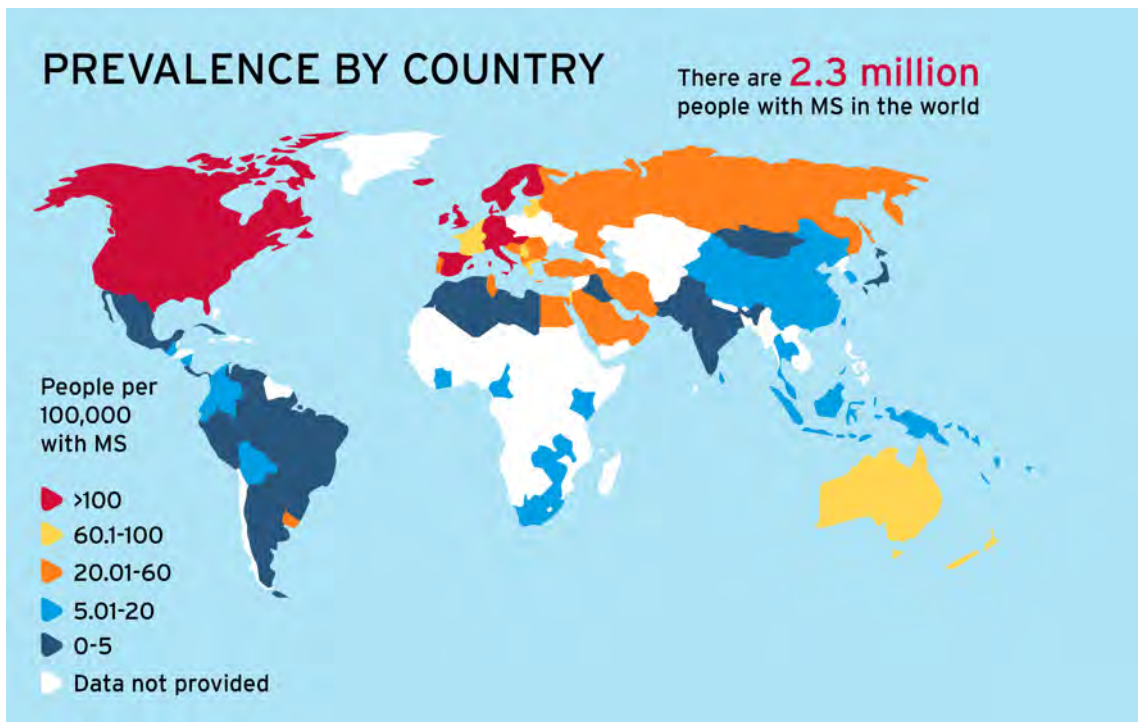


Figure 1.1: MS prevalence around the world <http://www.oysterhc.co.uk/uncategorised/ms-horrible/> accessed 13.05.2016.

the world (see Figure 1.1), affirming that migration from high to lower-prevalence in areas before the age of 15, reduces the likelihood of developing MS. Looking at the map in Figure 1.1, we can see that Europe, the United States, Canada, New Zealand, and sections of Australia have more MS sufferers than Asia and the tropics.

MS is characterised by demyelination, i.e. damage of the myelin, a fatty protein that insulates the axons of nerve cells (that part of the cell that transmits messages to other nerves cells). Therefore, demyelination in the brain and spinal cord leads to a disruption of the communication within the brain and between the brain and the body. When this interruption appears in the early stages of the disease, the CNS can repair some areas by demyelination, resolution of inflammation, and compensatory mechanisms, but that ability decreases as the disease progresses and recurrent attacks appear. As the disease prompts the immune system to attack the myelin, lesions develop on the brain and can only be seen in MRI scans.

Typically, the progression of MS consists of a relapsing and remitting course. This type of condition is known as relapsing-remitting MS (RRMS). Sufferers are relatively symptom-free for periods of time that are interrupted by attacks that can put them in hospital for

weeks, or even months, at a time. These attacks worsen the symptoms (see Figure 1.2) and are followed by full, partial, or no recovery of some function or another. The interval between relapses varies, there can be many years between the first manifestation and the first relapse. On average, 65% of people with RRMS develop secondary-progressive MS (SPMS), this progressive part may begin shortly after the onset or may occur even decades later. The last two types of this condition are less common and usually affect people who develop MS after age 40. Primary-progressive MS (PPMS) affects just 10% of all people with MS, and is characterised by a gradual progression of disability without any recovery periods. Finally, the least common form (5%) is the progressive-relapsing MS (PRMS) where the disability progression is steady, but punctual attacks may appear.

1.2.2 Lupus Erihematosus

Lupus Erihematosus is a chronic disease affecting the human immune system by attacking normal healthy tissues of different parts of the body such as joints, skin, kidneys, heart, lungs, and brain [2, 3]. Lupus erithomatosus affects around 5 million people around the world, while the most common and severe form of this condition (70%) is the Systemic Lupus Erihematosus (SLE), also known as Disseminated Lupus Erihematosus [2–4]. Other types of Lupus, not treated in this thesis, are discoid, drug-induced, and neonatal. As in MS, the underlying causes are still unknown but genes and certain drugs might be the main factors. Gender and age, are also similar attributes with MS since women are more likely to develop Lupus than men, and it also appears early in age, between 15 and 45 years, although it can occur at any time. Geographic and racial distribution of MS may differ from MS, since it is 2 to 4 times more frequent in non-white populations around the world, where Asians and African Americans are the most affected in the world [2–4].

Independently of the type of lupus, joint pain and swelling is present in almost every patient, among other common symptoms such as fatigue, fever, chest pain, hair loss, skin rash, etc. Besides, depending on the parts of the body (organs) affected, the symptoms may vary causing breathing problems, abnormal heart rhythms, nauseas, etc. When the brain is affected, headaches, numbness, tingling, seizures, vision problems, and personality changes can be present. Patients with problems on the nervous system can develop neuropsychiatric SLE, which is the main cause of morbidity and mortality [5–8].

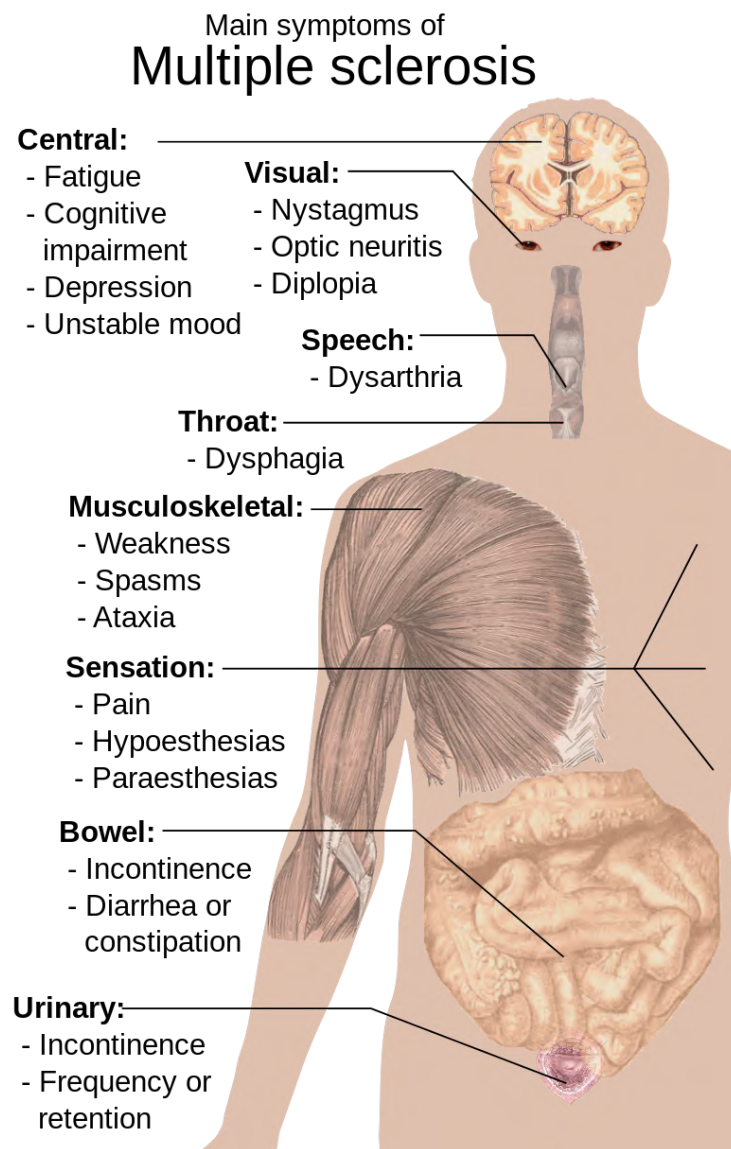


Figure 1.2: Main symptoms of MS <http://neurosciencenews.com/neurology-ms-gray-matter-393/> accessed 11.10.2015.

1.2.3 Magnetic resonance imaging

MRI is a technique that produces high quality images of organs and structures inside the body. It is based on the principles of nuclear magnetic resonance imaging, although the name was changed in the late 1970's due to the negative connotations associated with the word nuclear. This technique has undergone many technological advances since its beginning [9, 10] acquiring a wide range of modalities with high resolution. Nowadays, this is one of the best imaging techniques available to clinicians in order to understand

the brain.

Brain MRI consists of a 3D model of the brain, which can be acquired in three different orientations: axial, coronal, and sagittal (see Figure 1.3). The resolution is given by a 3×3 matrix, each axis being one of its orientation. Axis z denotes the number of slices, which are 2D images of $x \times y$. Even though the final image resolution is given in voxels, this is only how we represent the volume of the real world first described in mm in the acquisition from the scanner and finally in the reconstruction for the users. For example, an image obtained at $0.5 \times 0.5 \times 0.5$ mm, can be then reconstructed to $1 \times 1 \times 1$ mm meaning that each voxel in the image represents 1mm^3 of the real brain and there is 1mm between each slice. Instead, the image can be acquired at $1 \times 1 \times 3$ mm without applying any interpolation at reconstruction time, thus the gap between slices will be 3mm, so the resolution would be lower, 3mm^3 per voxel. Another fact that plays an important role in image acquisition is the magnitude of the magnetic field used by the scanner, which is measured in Tesla at a common values of 1.5T or 3T (see Section 2.1 for more details). A whole brain is illustrated in Figure 1.3, which has been acquired at 1.5T magnitude scanner in the axial orientation with a resolution of $1 \times 1 \times 3$ mm, i.e. 256×256 by 44 slices.

1.2.4 Image processing

MRI is a highly sensitive technique for the analysis of the human body. In this thesis we focused on the brain, specifically on brains damaged by MS. MRI is nowadays the only, and essential, tool for detecting MS plaques in the CNS, but it can also provide other biomarkers able to detect abnormalities inside the brain in the early stages as well as future impairments. This imaging technique helps to build a better control of the disease's evolution and in the effectiveness of the treatments. It also allows a better comprehension of the disease's natural history [11–14].

Following the new revisions of the McDonald's criteria [15–17], diagnostics for MS include the dissemination of CNS lesions in space (DIS) and time (DIT), which can be established with a single scan. The European MAGNIMS (Magnetic Resonance Imaging in MS) multicentre collaborative research network has demonstrated that a clinical isolated syndrome (CIS) can be diagnosed as MS if it presents at least one T2 lesion in at least 2 of 4 locations considered characteristic for MS (juxtacortical, periventricular, infratentorial, and spinal cord). These criteria have been exhaustively analysed in [18], where the same members of MAGNIMS have provided extensive recommendations for the use of MRI in the diagnosis of suspected MS patients. Performing this task manually is tedious

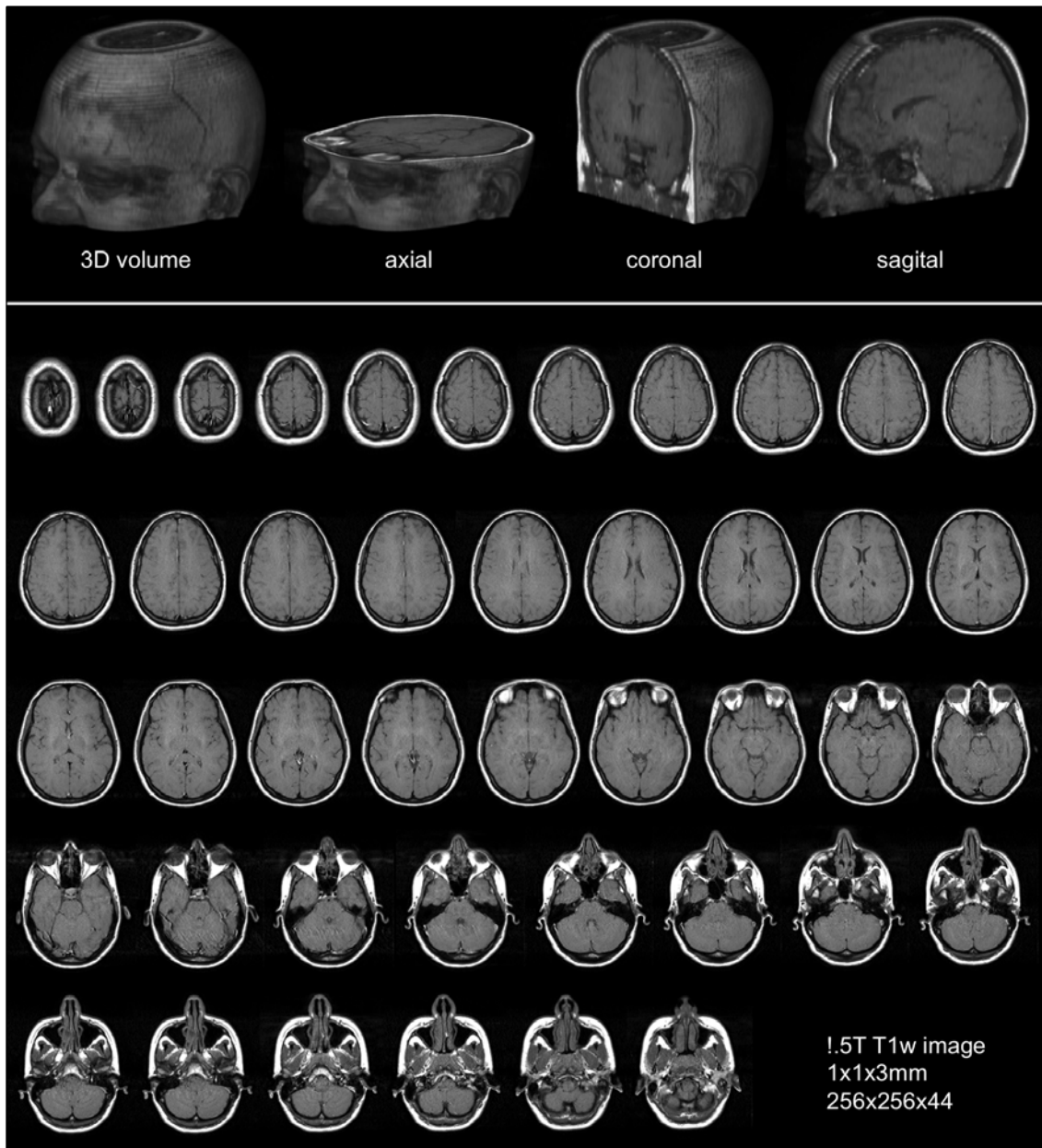


Figure 1.3: Brain MRI representation. The first row illustrates the 3D volume and its 3 different orientations (axial, coronal, and sagittal respectively from left to right). Since this volume has been acquired with a scanner of 1.5T in the axial orientation, this figure illustrates the 44 slices in its primary orientation.

and prone to inaccuracies due to possible inter- and intra-observer variability, therefore, computer-aided diagnosis (CAD) tools play an important role in assisting doctors in the interpretation of MRI.

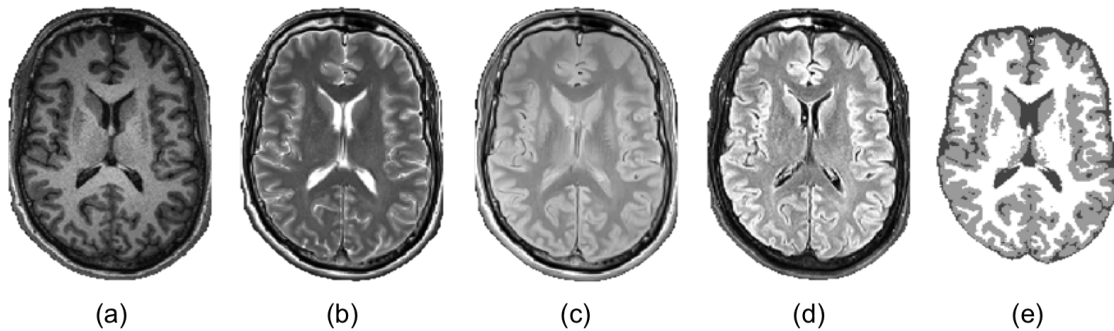


Figure 1.4: Different MR images of the brain: a) T1w image, b) T2w image, c) PDw image, d) FLAIR image, and e) Tissue mask image (white = white matter, light gray = gray matter, and dark gray = cerebrospinal fluid).

Building a CAD tool involves several processes in order to prepare the images for a specific purpose, in our case brain WML segmentation. First of all, one has to deal with the noise and undesired artefacts in the raw images [19]. Some of them (motion artefacts due to inadvertent head movement, peak artefacts due to a high signal value, blood and cerebrospinal fluid flow artefacts, etc.) may be recovered during the scanning procedure, but others, such as inhomogeneities in the magnetic field as well as patient properties, lead to inhomogeneities across the image, known as bias field error, and must be corrected by post-scanning processes.

Depending on the final application, other issues may affect the image processing. For example, non-brain tissues (skull, fat, eyes, etc.) affect image intensity distributions. Brain extraction tools are developed to obtain an image of the brain from the whole MRI. Other common processes are the comparison of different time-points to control the disease's evolution, or even between different subjects. In order to perform these comparisons of specific regions automatically, images have to be aligned in the same space, thus registration processes for both intra- and inter- subjects are needed. When an intra-subject registration of the same time-point is performed, the process is known as co-registration.

Given that we are looking for WML, the segmentation of the three main brain tissues (white matter (WM), gray matter (GM), and cerebrospinal fluid (CSF)), is also a common process (see Figure 1.4e), as well as lesion segmentation. The tissues present different contrasts depending on the scanner's parameters as shown in Figure 1.4 and described in Table 1.1.

High signal intensities detected in T2 weighted (T2w), Proton Density weighted (PD)

Table 1.1: Tissue intensity distributions by image contrast.

	T1weighted	T2 weighted	PD weighted	FLAIR
WM	bright	dark	dark	intermediate
GM	intermediate	intermediate	intermediate	bright
CSF	dark	bright	intermediate	dark

and Fluid Attenuated Inversion Recovery (FLAIR) images indicates edema, inflammation, demyelination, reactive gliosis and/or axonal loss, reflecting their increased tissue water content. They can be either acute or chronic MS lesions known as hyperintense lesions. Approximately 10% to 20% of these lesions present a low signal intensity (compared to WM) in T1w image, and they differ from the well-known black holes. Enhancing lesions can be detected in gadolinium-enhanced T1w images by applying a contrasting agent (gadolinium) before the image acquisition.

1.3 Research background

The Computer Vision and Robotics group (VICOROB) of the University of Girona has been working on medical image analysis since 1996, mainly in segmentation and registration of mammography images. Thanks to their prior knowledge acquired through several medical projects, the group started to focus their research on brain MRI analysis six years ago. This new line of research started with the segmentation of MS lesions and has expanded to other fields such as temporal analysis, registration (temporal and inter-subject) and atrophy analysis.

All these studies have been carried out through several research projects:

1. [2009 – 2012] PI09/91918 “SALEM: Segmentación Automática de Lesiones de Esclerosis Múltiple en imágenes de resonancia magnética” awarded by the Instituto Carlos III.
2. [2010 – 2012] VALTEC09-1-0025 “Salem: toolkit para la segmentación automática de lesiones de Esclerosis Múltiple en resonancia magnética” awarded in 2009 by the Generalitat de Catalunya within the ”Projectes de valorització VALTEC”.
3. [2015 – 2017] TIN2014-55710-R: “Herramientas de neuroimagen para mejorar el diagnóstico y el seguimiento clínico de los pacientes con Esclerosis Múltiple” awarded in 2014 by the Spanish call Retos de investigación 2014.

4. [2015 – 2019] BiomarkEM.cat: To develop, validate and transfer to clinical practice robust and totally automated tools for measuring new lesions and changes in the brain’s volume in MS patients. Awarded in 2015 by the Fundació Marató de TV3.

The goal of all these projects is either to create or to use novel datasets with imaging data from three different hospitals using three different scanning machines from different manufacturers and to study and develop techniques to segment MS lesions as well as to perform atrophy measurements that can be transferred to experts for clinical use. Within these projects, in which this PhD was the continuation of two previous PhD theses in the group, there has been a strong relationship with medical expert teams in the field of multiple sclerosis. Specifically:

- From the Hospital Vall d’Hebron: Dr. Rovira, who is the director of the “Unitat de Ressonància Magnètica-Centre Vall d’Hebron” (URMVH) and has participated in several research projects funded by public and private institutions in the last few years, as well as Dr. Pareto and technicians Huerga and Corral. This group is part of the MAGNIMS network, a European network of centres that share an interest in the MS study through MRI.
- From the Clínica Girona / Hospital Santa Caterina: Dr. Vilanova and Dr. Barceló are the codirectors of the “Unitat de Ressonància Magnètica” at the Clínica Girona and are members of several national and international radiology societies.
- From the Hospital Josep Trueta: Dr. Ramió-Torrentà, who is the current coordinator of the “Unitat de Neuroimmunologia i Esclerosi Múltiple”, as well as Drs. Robles and Beltrán, who work for the radiology unit.

Since the beginning of the brain research activity in our team, several outputs have been obtained (see the graphic of Figure 1.5). We started in 2009 with a master thesis and bachelor projects, and so far two PhD theses have been produced, and, a part from this one, two more are currently running.

1.4 Objectives

This PhD thesis has been developed as a part of the projects mentioned above, and the main goal is

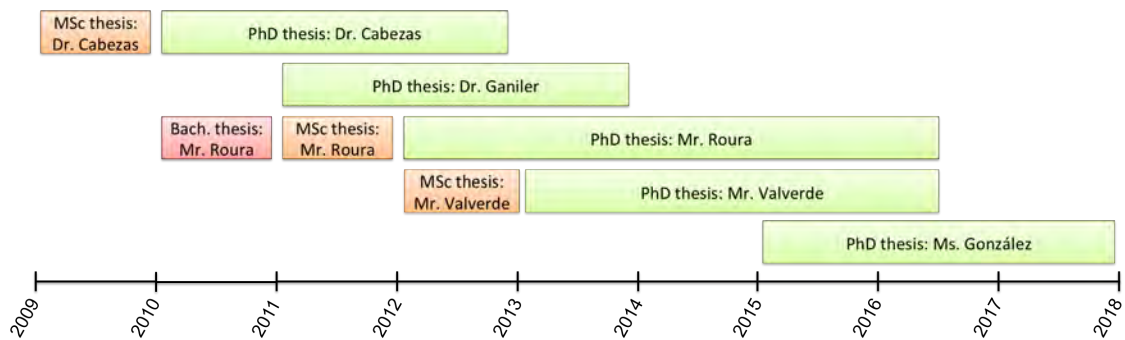


Figure 1.5: Projects on brain image analysis produced since 2009 by the VICOROB group.

to develop automated image processing tools to help in the image analysis of brain MRI and in particular to detect and segment WML.

This objective refers to the segmentation process of images of patients at a specific stage but we do not consider follow-up scans. With the segmentation of those transversal studies we aim to quantify the number of lesions as well as the lesion's volume.

As mentioned in the image processing section, to segment WML of MS patients, several pre-processes are required beforehand, which we have dealt with through several stages of this thesis. We therefore started tackling the weaknesses found in the pre-processing steps, defining our goal as being **to compare and improve the brain extraction tools in the literature**. This aim involved an exhaustive analysis of the current state of the art to better understand their advantages and drawbacks.

Secondly, we have analysed the effect of the pre-processing steps. The objective of this second sub-goal was to set up a pre-processing pipeline, i.e. considering different tools for brain extraction, image denoising, and intensity correction, for datasets of 1.5T and 3T. All these steps play an important role in all the image processing approaches focused on quantifying the lesion load, the atrophy measurements and monitoring the disease's evolution, among others. Therefore, having such a study in order to fix a standard pipeline that produces reproducible good results has been a big contribution to this community.

The combination of different image modalities allows us to gather complementary information from a single voxel, a fact that can help to set a probability as belonging to a certain tissue or structure of the brain, and also to observe different behaviours depending on the image contrast. However, in order to benefit from this extra information, all the image acquisitions from the same subject must be aligned first. This process is known as the image registration process [20,21]. The question that arises when combining different

image modalities is whether, when comparing different subjects, the fact of having several images with different information on the same subject helps to drive the registration process. Therefore, another goal of this thesis is **to set up a multi-channel registration pipeline**.

The sub-goals mentioned above are part of the main contribution of **developing a new, automated WML segmentation tool**. This tool will be tested on more than 100 patients from different sources. We will run all the experiments with a multi-centre database comprising 1.5T and 3T images of MS patients, but we will also use public databases to test our tool in order to compare it with the state of the art. Eventually, this tool will be adapted to segment WML of other diseases as well as MS.

Finally, once we have developed all our methods and configured all the pipelines needed for WML segmentation, we will integrate this tool into the well known SPM¹ platform. Since WML quantification (either by number or, maybe better, by volumetric measurements) is a key step in diagnosing and monitoring this disease's progression as well as its response to therapy, this tool is an interesting contribution for clinicians, and one will be able to incorporate in the hospitals we are collaborating with.

1.5 Document structure

This thesis is structured as follows:

- **Chapter 1. Introduction.** Motivation, topics, objectives and backgrounds have been described in this chapter.
- **Chapter 2. Thesis background.** This chapter presents a detailed analysis of the image processing methods used in this thesis. The chapter is divided in three main sections consisting on the MRI details, the pre-processing techniques and the main processing methods.
- **Chapter 3. MARGA: Multispectral Adaptive Region Growing Algorithm for brain extraction on axial MRI.** We present a new approach for the brain extraction process and its comparison with three of the best tools for this purpose in the literature.
- **Chapter 4. Exhaustive multi-channel registration evaluation of conventional and diffusion MRI on MS patients.** We propose a multi-channel re-

¹<http://www.fil.ion.ucl.ac.uk/spm/software/>

gistration pipeline of diffusion (FA) and conventional (T1w) MRI by using public softwares.

- **Chapter 5. A toolbox for multiple sclerosis lesion segmentation.** We present a new pipeline for WML segmentation in MS patients integrated in a standard platform.
- **Chapter 6. Automated detection of Lupus white matter lesions in MRI images.** We adapt the WML segmentation to the Lupus disease by changing the strategy and integrating all the steps in the same tool. We provide a straightforward toolbox that is easy to use.
- **Chapter 7. Results and Discussion.** We summarise the outcomes in this thesis and discuss all the results obtained.
- **Chapter 8. Conclusions and Future work.** The contributions are outlined in this chapter and we also discuss the future lines.

Thesis background

In this chapter, we first introduce some details on the MRI acquisitions and image modalities generated. Afterwards, we describe all the basic processes involved in the image processing pipeline when detecting and delineating WML. We can divide these processes in pre-processing, i.e. preparing the images to apply the processes of the final application, referred as post-processing methods.

2.1 MRI details

In the first chapter we described the principles of the MRI, we gave to the reader some insights about resolution, acquisition, reconstruction, and visualisation. In what follows, we will go deeper into the acquisition process, the main source of this technique. The acquisition of a single image is performed by the MRI scanner, which consists of the following components:

- **Spins:** Nuclear magnetisation detected by the MR. This is the particle spin movement, e.g. in the case of a spinning charged particle, a magnetic field is created.
- **B_0 :** A strong external magnetic field and static generated by an MRI scanner, which is typically measured in Tesla units, a unit equal to 10000 Gauss. As an example of scale, a 3 Tesla (or 3T) MRI scanner generates a B_0 field 60000 times stronger than the natural magnetic field of roughly 0.5 Gauss on the Earth's surface.
- **Radio frequency (RF) wave:** This is the electromagnetic pulse needed to get the signal. It is also generated by the scanner and is applied for only a brief period (oscillates at radio frequencies).

- **Magnetic field gradients:** To figure out the spatial information of the signal received and place it in the space by means of additional magnetic fields.

Magnetic resonance images primarily reflect water and fat concentration; specifically, they reflect the signal from hydrogen nuclei because of their abundance in the body. The hydrogen nuclei are made up of protons and neutrons, both of which spin around their own axis. When no external magnetic field is applied, their axes are randomly aligned until the B_0 magnetisation acts. At this point, the magnetic axes of the nuclei align with the magnetic axis of B_0 . The cumulative magnetic moments created by this process generate the net magnetisation vector [22]. In order to obtain the MR signal, a radio frequency pulse is applied producing a flip by a certain angle to the net magnetisation vector. From this flip, longitudinal and transverse magnetisation vector components are obtained. When the RF energy is turned off, the net magnetisation vector goes back to its origin realigning the B_0 axis. During this process, the longitudinal magnetisation increases or recovers (T1 recovery) and the transverse magnetisation decreases or decays (T2 and T2* decays). Depending on the tissues, values for T1, T2 and T2* vary, thus, when the receiver coil catches the MR signal and the computer reconstructs the final image, the voxel intensity will be different between tissues.

The pulse sequence parameters are key to the creation of image contrast. Repetition time (TR) and echo time (TE) are the two key parameters that set the timing of the RF and gradient pulses, both measured in milliseconds:

- **TR:** is the time between the application of the RF excitation pulse and the start of the next RF pulse.
- **TE:** is the time between the application of the RF pulse and the peak of the echo detected.

In MRI, two different MR pulse sequences can be found: the spin echo (SE) where two RF pulses are used, and the gradient echo (GE), generated by a single RF pulse in conjunction with a gradient reversal [23]. GE sequences can record the echo much more quickly, a fact that allows us to reduce the TE. Moreover, when using low-flip-angle excitations (less than 90°) the TR can also be shorter. Hence, this kind of sequence is useful when fast scans are needed, although it does not correct for local magnetic field inhomogeneities. The rest of the MR sequences are mere variations of these two obtained by different parametrisation.

2.1.1 Conventional MRI

The most common sequences in regular MRI used in MS diagnosis are:

- **T1 weighted:** related to TR ($TR < 1000\text{ms}$, $TE < 30\text{ms}$). Shorter TRs allow us to distinguish between fat and water.
- **T2 weighted:** related to TE ($TR > 2000\text{ms}$, $TE > 80\text{ms}$). Longer TEs allow us to detect differences between fat and water.
- **PD weighted:** echo time similar to T1w ($TR > 2000\text{ms}$, $TE < 30\text{ms}$). This is the result of a dual echo sequence on the T2w.
- **FLAIR:** stands for fluid attenuated inversion recovery. This is a T2w with the CSF signal suppressed, an inversion recovery pulse is used to null the signal from the CSF.

PDw is the concentration of protons in tissue in the form of water and macromolecules (proteins, fat, etc.). Regarding T1w and T2w differences, they remain in the relaxation time after the protons revert back to aligning the external magnetic field. In Figure 1.4, one can see what the different image contrasts look like.

2.1.2 Diffusion MRI

The brain contains more than 100 billion neurons that communicate with each other via axons for the formation of complex neural networks [24]. Our understanding of the brain's structural connectivity is surprisingly limited, due in part to the lack of non-invasive imaging techniques to study axonal anatomy. Diffusion Tensor Imaging (DTI) is an MRI technique introduced in the mid 1990s [25] that provides information about the connections in the brain's regions. The main clinical domain of application has been neurological disorders, especially WM disorders. DTI can reveal abnormalities in white matter fibre structure and provide models of the brain's connectivity. This imaging technique can delineate the axonal organisation of the brain, which we could not appreciate with conventional MRI.

Basically, diffusion represents the thermal (or Brownian) motion of water molecules, and also their flow according to Fick's first law [26]. We can better understand diffusion with a simple analogy, i.e. the shape of ink dropped on a piece of paper. When the shape stays circular, diffusion is isotropic, when this shape is elongated along one of the axis, the

diffusion is anisotropic, suggesting a higher density of fibres oriented in this direction [24]. Similar to conventional MRI, the information obtained by this technique is based on signal intensity, S , following Equation 2.1:

$$S = PD(1 - e^{-TR/T1})e^{-TE/T2}e^{-bD} \quad (2.1)$$

where S is based on the PD, T1 and T2 relaxation times and the timing of excitation TR and TE. Respectively, b and D are the diffusion-weighting factor and the diffusion term. To obtain the diffusion coefficient, one needs to obtain two images changing the b value while the other parameters remain the same. From this equation, we can see how we can expect more signal loss when D is higher. The amount of signal loss also depends on the gradient application, the b values. Computing D at each pixel, we can build a map of the diffusion coefficient, commonly known as an apparent diffusion coefficient (ADC). Since the diffusion can be measured only along the applied gradient axis, and the orientation fibres in pixels is determined by the largest ADC, to accurately find it, one would need to apply these gradients along thousands of axes, which becomes unfeasible. This issue is simplified in Basser et al. [25], describing the model of diffusion tensor imaging thought as a 3D ellipsoid. The axes of this ellipsoid are called eigenvectors and the measures of their lengths eigenvalues, which define the so-called eigensystem, a 3 by 3 symmetric matrix obtained at each pixel. The three eigenvalues (diagonal of the matrix) represent the diffusivity of the principal axes of the tensor, while their orientation is given by the three eigenvectors. The principal eigenvector is associated with the largest eigenvalue and it turns out to be parallel to the orientation of the diffusion tensor. From the DTI, several indexes can be extracted, among which fractional anisotropy (FA) is the most widely used [27]. This image can be seen in Figure 2.1b, a greyscale image normalised between 0 (isotropic) and 1 (anisotropic). A color-coded orientation map (red, blue and green assigned to X, Y and Z axes respectively) can also be extracted from the DTI (see Figure 2.1c), which indicates local fibre orientation determined by the longest axis (principal eigenvector). Given this information, a 3D streamline can be reconstructed by following this orientation (highest anisotropy). This process is known as tractography [28, 29], and requires a seed or a set of seeds to start the propagation based on the main orientations (see Figure 2.1d).

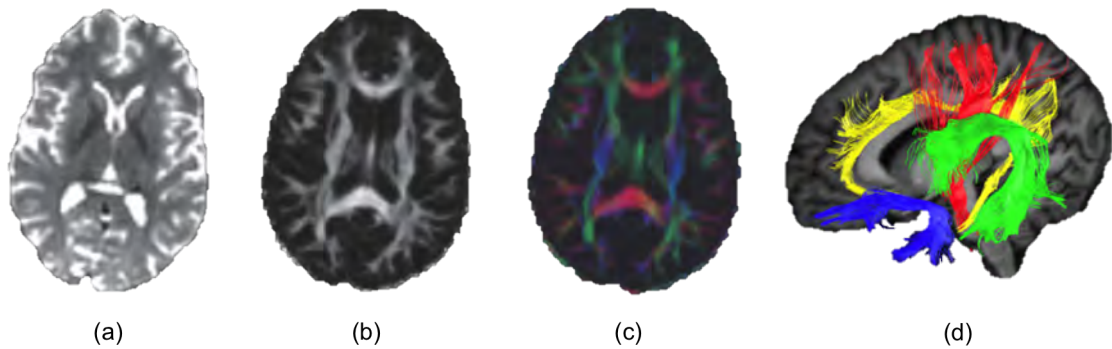


Figure 2.1: Different diffusion MR images of the brain: (a) diffusion weighted, (b) FA, (c) color-coded map, and (d) tractography.

2.2 Pre-processing

2.2.1 Brain extraction

The main purpose of this thesis is to obtain an automatic tool able to segment WML in order to help doctors' diagnosis in their daily clinical practice. We base this task on analyses of brain MRI that we obtained directly from the scanner by automatic procedures. Even though we refer to these images as brain MRI, they actually contain the whole head, and sometimes the neck. When these images are manually processed, falling apart the brain from the rest of the head is not a difficult task, specially when this is performed by an expert (a radiologist or a neurologist). Instead, automatising the image analysis processes requires focusing on the region of interest (ROI), in this case the brain itself, i.e. WM, GM, and CSF tissues, avoiding structures such as the skull, eyes, and dura (see Figure 2.2). The presence of non-brain regions affects the image histogram distribution and alters the segmentation performance of both tissues and lesions.

The process of obtaining the brain mask is known as either brain extraction or skull stripping. Several methods have been published [30–36], of which the most commonly used are the Brain Extraction Tool (BET) [32, 37] and the Brain Surface Extractor (BSE) [38]. Good results from these methods have been published in articles in which they have been compared [39, 40], although, as we will see in the approach presented in the next chapter, the Multispectral Adaptive Region Growing Algorithm for brain extraction in axial MRI (MARGA) [40], some of the limitations of these current techniques can be improved for specific data.

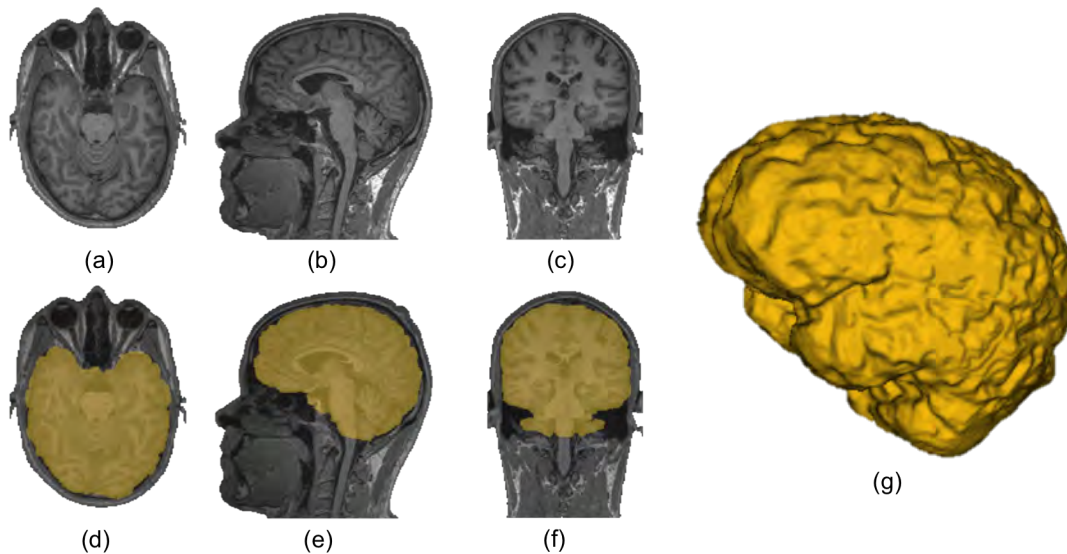


Figure 2.2: Head MRI representation. The three orientations are illustrated: (a) axial, (b) sagittal, and (c) coronal. The brain mask is overlaid in (d)(e)(f) and its 3D representation in (g).

2.2.2 Intensity corrections

Intensity inhomogeneities are inherent to MRI for numerous reasons: variable imaging parameters, overlapping intensities, noise, motion, echoes, blurred edges, normal anatomical variations and susceptibility artifacts [41] (see Figure 2.3). These issues can adversely affect quantitative image analysis when developing CAD tools.

As stated in [42], these problems are modelled as follows:

$$I(x) = \beta(x) + \varepsilon \quad (2.2)$$

where $I(x)$ defines the real intensity measured for each voxel x , β denotes the multiplicative smooth bias field and ε is the additive noise. Therefore, this effect is attenuated by reducing the image noise followed by a bias field correction. Several works have been proposed to deal with these two issues, [43, 44]. Note that image intensity correction processes will be performed over the ROIs we focus on, i.e. over the brain mask obtained in the skull stripping process.

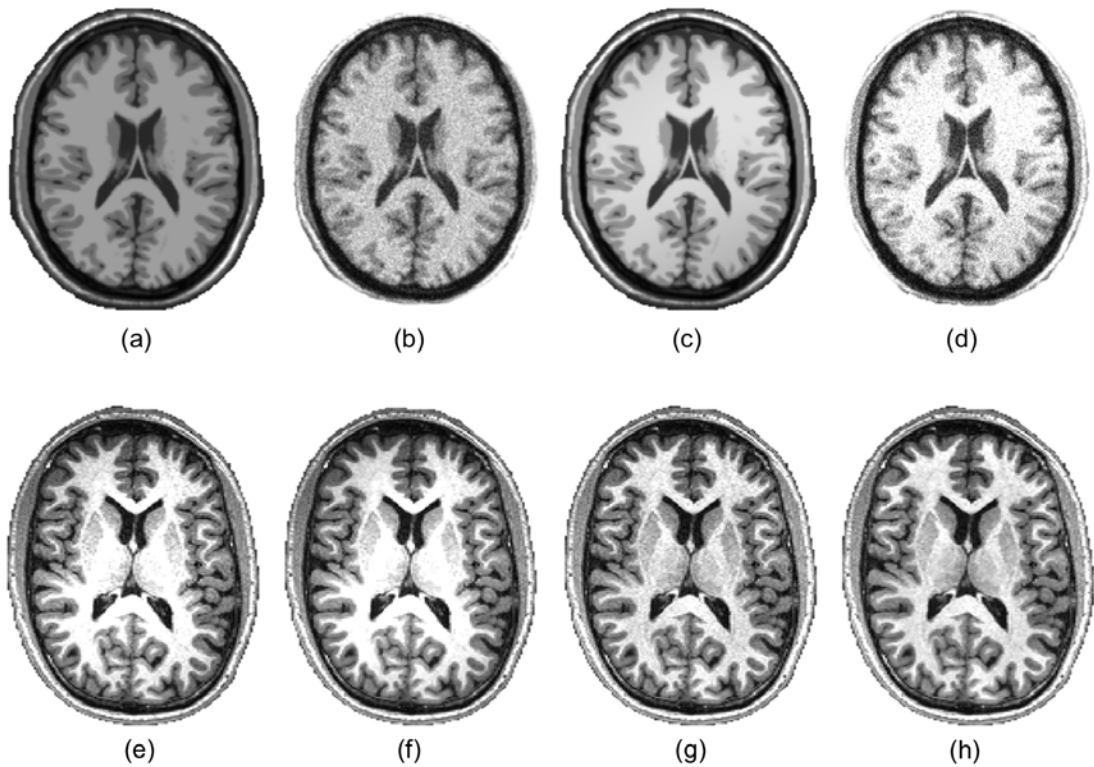


Figure 2.3: MRI intensity corrections. First row represents a BrainWeb T1w simulated image: (a) original image, (b) 9% of noise image, (c) 40% of bias field image, and (d) image with both effects applied. The second row represents the opposite process of a real 3T T1w image: (e) original image, (f) image denoised, (g) image with bias field corrected, (h) image with both effects corrected.

Noise reduction

Noise is a random additive distortion added to any image acquisition system [45], and is not present in the real object or subject but that can be caused by different aspects such as poor illumination, transmission errors or image sensors. These errors can derive from different models. The noise signal introduced into the MRI can be seen in Figure 2.3(b) as a kind of grainy film model with BrainWeb simulated images. This same effect is seen in Figure 2.3(d), although bias and intensity bias have also been applied. We focus firstly on the signal noise, since it is independent of the original intensity. To reduce this noise, or even to eliminate it, we use an anisotropic diffusion filter, which implements an N-dimensional version of the classic Perona and Malik filter [46] (see Figure 2.3(f)).

Bias field correction

This common artefact found in MRI, also known as intensity inhomogeneities or intensity non-uniformity, refers to the intensity variability of the tissue. This effect is shown in Figure 2.3(c)(d) where the bottom part is darker than the top, and the opposite is shown in Figure 2.3(e)(f). The bias can be induced by either the scanner parameters or the patient's movements inside the scanner. Although several methods have been proposed, the most commonly used are those from Statistical Parametric Mapping (SPM) [47], and the well known non-parametric, non-uniform intensity normalisation (N3) method [48], all of which have been optimised for new MRI techniques [49, 50] over the years. The results for these methods can be seen in Figure 2.3(g)(h), where uniform intensities are present throughout the various tissues.

2.2.3 Registration

The registration process consists of aligning two objects that are in different spaces. Regarding automatic medical image analysis, the registration process is a fundamental step for both inter- and intra- subject analysis. On the one hand, in order to quantify the evolution of a disease, the patient must be subject to follow-up scans at regular intervals, and the position of the head inside the scanner can be different every time so the different scans must be aligned in order to be comparable. On the other hand, when the brain of a new patient with some unknown symptoms is compared with a healthy subject, i.e. a healthy brain without anatomical malformations, they also have to be aligned. We understand that two brains are perfectly aligned when the index of a given voxel of two different brains corresponds to the same part of the brain, independently of the possible damage.

Registration applications in medical image analysis are numerous [51–55], and there are also myriad brain studies where registration is a key step (even though this is sometimes transparent to the user), for instance group-wise atlas generation [56], atlas-based segmentation [57–59] and lesion segmentation [42, 60–63], etc. Nevertheless, the final aim of registration deals with different lines [64, 65], this is a key step in many image processing methods. For instance, a basic distinction can be made between inter- and intra- subject registration, where the former is used to align different sequences from the same subject (multi-modal also known as co-registration process) [40, 63, 66, 67] while in the later, both the source and target images usually belong to the same sequence from different subjects (mono-modal). Sometimes prior information from the atlas is used to drive segmentation methods, known as atlas based segmentation approaches [67]. This strategy requires a

previous registration either in the atlas space or the subject space. Another purpose also addressed in this thesis is the brain atrophy simulation when registering healthy subjects to patients with enlarged ventricles for example [63, 68].

Technically, registration methods follow the same strategy, see the typical scheme shown in Figure 2.4. Basically, they aim at deforming a source image to match a target image as much as possible by an optimisation process of some energy function and a transformation model. The registration process consists of the following 4 modules:

1. *Metrics: Similarity measures.* A way to measure the correspondences between the source and the target image. This can be either feature based or intensity based. These similarity measures can also be used for the evaluation of the registration performance. The most commonly used metrics in medical image registration are: sum of squares distances(SSD), mutual information (MI) [69,70], normalised mutual information (NMI) [71], and cross correlation [72].
2. *Transformation models.* There is no single definition of an optimal method, but as many definitions as there are practical applications. Techniques are numerous and inspired by a wide range of theories or strategies: the statistics and information theory, the theory of continuum mechanics or viscoelastic fluids, the theory of thermodynamics, optical flow, splines, wavelets, block matching, etc [64,73–77]. Several surveys and reviews [70, 78–82] have compared the various registration techniques, but they are mainly based on two steps:
 - Rigid and affine registration: the 6 degree-of-freedom (DOF) rigid registration algorithm is focused on position alignment (translations and rotations). Also, a 12 DOF affine registration method includes shape recovering (scaling and shearing). The greatest differences (position, orientation and size) between the target and source are reduced by this process.
 - Non-rigid registration: allows the deformation of each pixel locally depending on their local similarity and position. Sometimes these algorithms need a regularisation term in order to control the deformations since they can adopt undesirable effects. Deformation models differentiate between these methods, elastic or hyperelastic models [83], viscous fluid [84, 85] and Demons (optical flow) [73, 74], more suitable for large deformations, and free form deformation (B-splines) methods [75], a smooth and continuous deformation controlled by a mesh of control points.

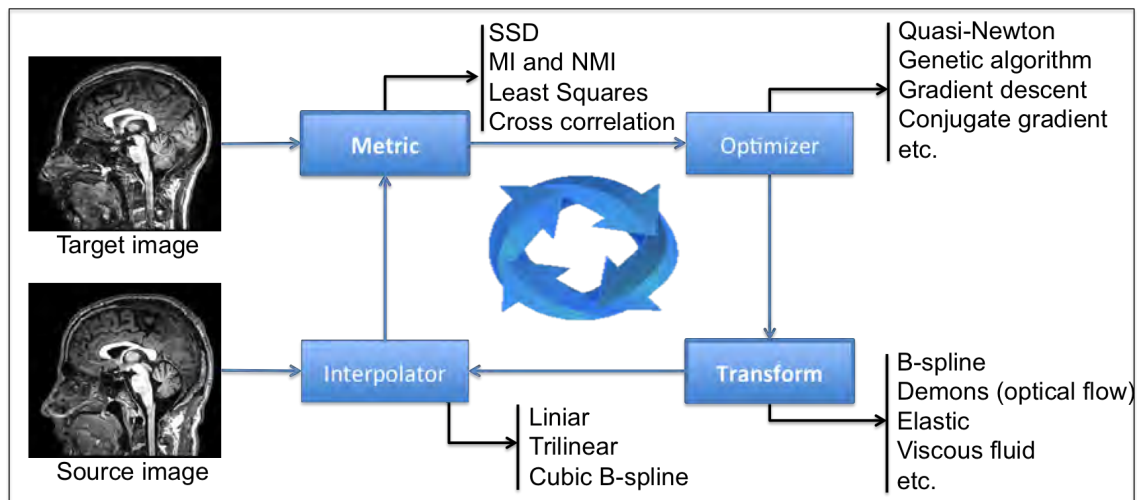


Figure 2.4: Global scheme of the registration process (SSD = Sum of Squares Distances, MI = Mutual Information, NMI = Normalised Mutual Information). This is an iterative process that aims at aligning the two input images by warping the source image step by step until it reaches a desired similarity with to the target image.

3. *Interpolator.* To resample the transformed source image into the physical space of the target image building a continuous image from its discrete samples. While the simplest interpolation technique, nearest-neighbour, has a low computational time, its accuracy, i.e. the precision of the resampling, can be greatly improved by more complex techniques such as the trilinear, quadratic, spline, B-spline or the cubic B-spline.
4. *Optimisation.* Image registration can be seen as an optimisation process of an objective function that tries to minimise a cost function by searching for the appropriate parameters in the transformation model. The cost function is composed of the similarity metric between the transformed source image and the target image and may also contain a regularisation term in order to preserve the topology. The optimisation process can be carried out in a multiresolution or multiscale framework, which have been shown to be robust and fast [86–89]. These techniques are used to speed up the optimisation process, where the original high-resolution images are subsampled into images at lower resolution, which require less computation.

The article presented in Chapter 4 focuses on MRI registration of MS patients. The aim of this work is to provide a pipeline able to register both anatomical and diffusion MRI to a standard space with the presence of MS lesions and atrophy.

2.3 Processing

2.3.1 Brain tissue segmentation

The automatic classification of brain tissues, consisting of the three main tissue types (WM, GM and CSF), is also important for neuroscientific studies, such as cortical surface extraction [90,91], atrophy and volume measurements [92–94], brain extraction [40,95,96], MS lesion segmentation [42,63,97], etc.

As explained in the MRI section, tissues have different contrasts depending on their acquisition, a fact that helps the image segmentation. Due to the significance of this process, a wide range of approaches based on different techniques have been proposed, all of which perform mostly with T1w data. The well-known Markov random field is the basis of the FAST [98], which is part of the FMRI Software Library, and SVPASEG [99]. SPM5/8/12 are three of the available versions of the SPM toolbox. This toolbox includes several image processing methods, one of which is the tissue segmentation based on a Gaussian Mixture Model, atlas registration and a bias field correction performed iteratively [100]. Other are FANTASM [101] based on Fuzzy Clustering techniques, and KNN [102], which implements the common k-Nearest Neighbour. In Figure 2.5, the brain tissue distributions from the atlas used in the SPM12 toolbox, and one example of a T1w 3T subject segmented with SPM12 are shown. The brain tissue segmentation is also an important step when detecting neurological lesions, usually present in WM but also seen in GM. Therefore, the tissue information is commonly used for lesion detection, although, at the same time, the lesions may affect the tissue segmentation accuracy [103,104].

2.3.2 WML segmentation

Nowadays MS diagnosis focus especially on detecting WML [15–17] in the brain tissue. These plaques of demyelination are typically observed in MRI with different contrasts depending on the image sequence. They are commonly seen as hyperintense lesions in T2w, PD and FLAIR and usually appear as dark areas in T1w images (see Figure 2.6).

An MRI is a 3D volume composed of a large number of slices containing information on the whole brain, thus analysing these images manually is a monotonous and burdensome task that may affect the accuracy of the experts and lead to inter- and intra-rater variabilities. However, its fully automated process is challenging [105,106] due to image variabilities caused by factors such as different scanners or protocols. This is a very im-

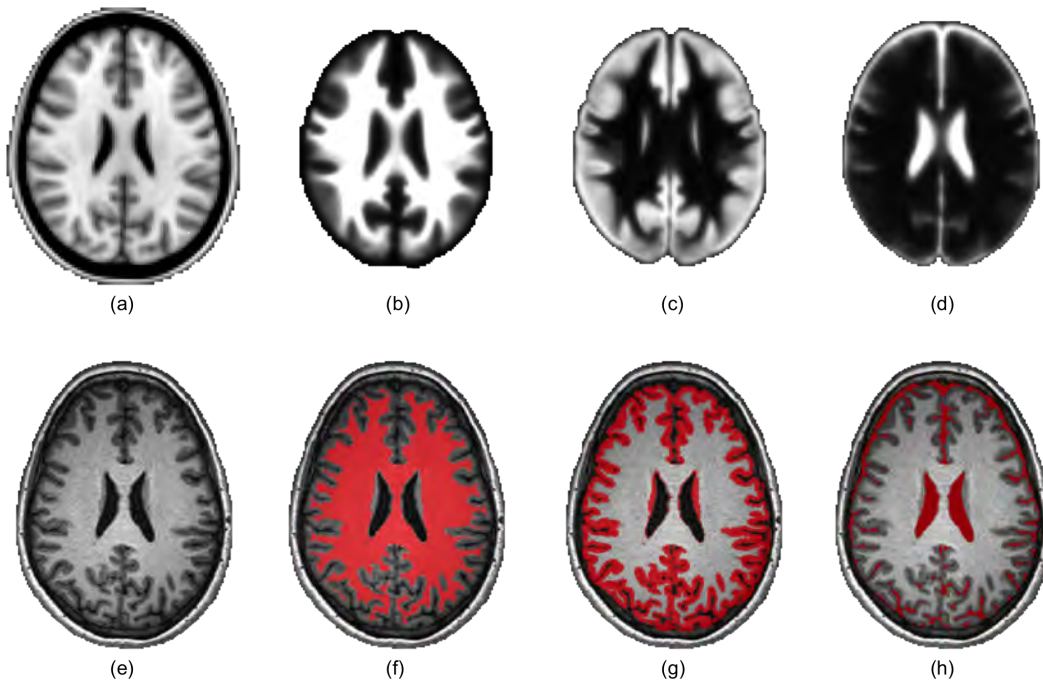


Figure 2.5: Brain tissue segmentations: (a) Average atlas and its prior tissue maps ((b) WM, (c) GM and (d) CSF) used in SPM12 for tissue segmentation. The second row represents (e) the original T1w 3T MRI data and the tissue mask results in red: (f) WM, (g) GM and (h) CSF.

portant problem in the MS community and, therefore, many attempts have been proposed to try to solve it [42,60,61,63,97,107,108]. Although none of these processes have been established as the standard tool, they have provided this community with publicly available software capable of reaching good results with low user interaction.

As this is a wide field of research, one can find numerous projects in the literature, which can be classified by different strategies and techniques [105,106]. In general terms, we can distinguish two main strategies:

1. **Supervised methods.** These approaches base their segmentation on using a priori information usually obtained by manual annotations. They are also known as training-specific approaches, and a prior knowledge is obtained from several features in the input images. Usually, these features are manually extracted in order to construct the classifier [61,108–113], a process that may require an extremely high computational cost depending on the feature space.
2. **Unsupervised methods.** The information needed for these approaches is the input

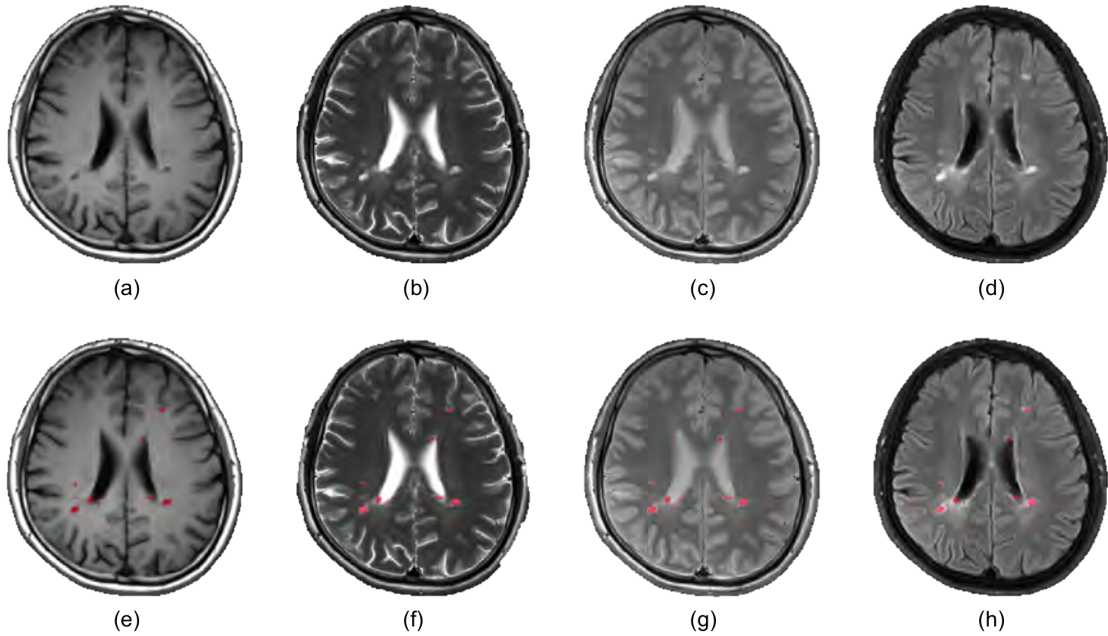


Figure 2.6: 3T MRI of a MS patient: (a) T1w, (b) T2w, (c) PD, and (d) FLAIR. The second row shows the same images as above with the lesion mask overlaid in red.

image itself [114–118], a fact that increases its convenience in applying it in daily clinical practice. There are strategies based on tissue properties where a previous tissue segmentation is used as we show in Chapter 5 and 6, and a very large literature is found using this same strategy [42,63,67,97,107,119–126]. The tissue segmentation step uses a priori built atlas, thus they are considered supervised methods also known as atlas-based tissue segmentation.

MRI is also the gold standard for studying the brain in SLE [127–131], where the most common neuroimage findings are vascular diseases and inflammatory-like lesions. Similar to the MS lesions, these vessel lesions appear hyperintense on FLAIR, T2w and PDw images while on T1w images are hypointense [130]. This fact suggests that similar approaches used on MS lesion segmentation could be used for lupus WML segmentation.

MARGA: Multispectral Adaptive Region Growing Algorithm for brain extraction on axial MRI

In this chapter, we propose a new approach for brain extraction on MRI based on the complementary information of T1w and T2w images. This method has been evaluated in both simulated and real data, and compared with three of the well-known state-of-the-art approaches.

The proposed method has been published in the following paper:

Paper published in Computer Methods and Programs in Biomedicine (CMPB) Volume: 113, Issue: 2, Pages: 655-673, Published: February 2014 DOI: 10.1016/j.cmpb.2013.11.015 JCR CSTM IF 1.897, Q1(15/102)



MARGA: Multispectral Adaptive Region Growing Algorithm for brain extraction on axial MRI

Eloy Roura^{a,*}, Arnau Oliver^a, Mariano Cabezas^a, Joan C. Vilanova^b, Àlex Rovira^c, Lluís Ramió-Torrentà^d, Xavier Lladó^a

^a Department of Computer Architecture and Technology, University of Girona, Girona, Spain

^b Girona Magnetic Resonance Center, Girona, Spain

^c Magnetic Resonance Unit, Department of Radiology, Vall d'Hebron University Hospital, Barcelona, Spain

^d Multiple Sclerosis and Neuroimmunology Unit, Dr. Josep Trueta University Hospital, Institut d'Investigació Biomèdica de Girona, Girona, Spain

ARTICLE INFO

Article history:

Received 29 June 2013

Received in revised form

30 September 2013

Accepted 25 November 2013

Keywords:

Biomedical engineering

Image analysis

Image segmentation

Skull stripping

Magnetic resonance imaging

ABSTRACT

Brain extraction, also known as skull stripping, is one of the most important preprocessing steps for many automatic brain image analysis. In this paper we present a new approach called Multispectral Adaptive Region Growing Algorithm (MARGA) to perform the skull stripping process. MARGA is based on a region growing (RG) algorithm which uses the complementary information provided by conventional magnetic resonance images (MRI) such as T1-weighted and T2-weighted to perform the brain segmentation. MARGA can be seen as an extension of the skull stripping method proposed by Park and Lee (2009) [1], enabling their use in both axial views and low quality images. Following the same idea, we first obtain seed regions that are then spread using a 2D RG algorithm which behaves differently in specific zones of the brain. This adaptation allows to deal with the fact that middle MRI slices have better image contrast between the brain and non-brain regions than superior and inferior brain slices where the contrast is smaller. MARGA is validated using three different databases: 10 simulated brains from the BrainWeb database; 2 data sets from the National Alliance for Medical Image Computing (NAMIC) database, the first one consisting in 10 normal brains and 10 brains of schizophrenic patients acquired with a 3 T GE scanner, and the second one consisting in 5 brains from lupus patients acquired with a 3 T Siemens scanner; and 10 brains of multiple sclerosis patients acquired with a 1.5 T scanner. We have qualitatively and quantitatively compared MARGA with the well-known Brain Extraction Tool (BET), Brain Surface Extractor (BSE) and Statistical Parametric Mapping (SPM) approaches. The obtained results demonstrate the validity of MARGA, outperforming the results of those standard techniques.

© 2013 Elsevier Ireland Ltd. All rights reserved.

1. Introduction

Magnetic resonance image (MRI) analysis is nowadays involved in a wide range of clinical applications in order to

enhance the medical diagnosis in terms of reducing processing time and improving accuracy on the final decision. When brain diseases are studied, the only part the experts are interested in is the brain itself, i.e. white matter (WM), gray matter (GM) and cerebrospinal fluid (CSF) tissues. However, other

* Corresponding author at: P-IV, Campus Montilivi, University of Girona, 17071 Girona, Spain. Tel.: +34 972 419812; fax: +34 972 418259.

E-mail addresses: eloyroura@eia.udg.edu (E. Roura), aoliver@eia.udg.edu (A. Oliver), mcabezas@eia.udg.edu (M. Cabezas), llado@eia.udg.edu (X. Lladó).

0169-2607/\$ – see front matter © 2013 Elsevier Ireland Ltd. All rights reserved.

<http://dx.doi.org/10.1016/j.cmpb.2013.11.015>

tissues and structures of the head (i.e. skull, eyes, and dura) appear also in the MR images. The main goal of the skull stripping process is to separate the brain from those parts that are not brain tissues. This process is a key step in many high level automatic processes such as tissue segmentation and atrophy quantification [2,3], brain registration [4–7], brain analysis for different diseases [8–12] or cognitive aging [13], among others. In general, techniques that compute measurements on brain volume or cortical thickness require a very accurate brain extraction.

Automating the brain segmentation in neuroimaging is a crucial step in many studies and it allows to eliminate human variance corresponding to the doctors subjective criteria and to liberate them of this time-consuming procedure, being this point a key factor to allow the analysis of larger clinical studies. Over the last years, several skull stripping approaches have been presented, reaffirming the crucial importance of this step. The commonest fully automated methods are the Brain Extraction Tool (BET) [14] and the Brain Surface Extractor (BSE) [15], although recently, novel approaches have been proposed [1,16,17]. These approaches can be classified according to their strategy. For example, BSE is a pure edge based approach. Initially, the scans are smoothed by an anisotropic diffusion filter and the edges are identified by using the Marr–Hildreth edge detector [18]. Afterwards, a component is selected as brain based on the size, location and intensity within the frame using a sequence of morphological and connected component operations. Finally, a morphological dilation operation is applied to fill the small holes. Recently, Kale et al. [19] adapted this strategy segmenting human facial tissue. Another well-known strategy consists in initially thresholding the volume using histogram information and subsequently refines this rough segmentation using different techniques. For instance, the recent approaches of Balan et al. [17] and Somasundaram and Kalaiselvi [16] used morphological operations (erosion, largest connected component, dilation, closing and fill in the holes) to that aim. In contrast, the BET algorithm uses the initial segmentation as a starting point of a deformable model that is expanded towards the brain edge. On the other hand, Park and Lee [1] used this initial information to locate two different region seeds (corresponding to brain and non-brain regions) which, afterwards, are expanded by a region growing algorithm based on general brain anatomy information. The region growing method is a well known segmentation algorithm widely used in other applications medical [20,21].

Nevertheless, none of these algorithms has emerged as a perfect tool since all of them present limitations and issues to be solved. For instance, BET tends to oversegment the brain tissues, adding regions outside the brain into the segmentation result. This issue is even bigger in the BSE algorithm [22–25]. Moreover, it is also well-known that BET and BSE presented bad results in data sets with poor spatial resolution and noisy images [22–24]. To improve their performance, both algorithms require a conscious configuration of the parameters according to each database. Besides, as stated by Park and Lee [1], the methods that use mathematical morphology are sometimes sensitive to small data variation and it is difficult to find the optimum morphology size for separating brain tissues from non-brain tissues. On the other hand, approaches

like the one of Park and Lee [1] require the images being captured in coronal view, being this fact a hard constraint in many applications where the clinical routine requires the images to be acquired in axial view.

Skull stripping algorithms are implemented for conventional MRI since anatomical images provide an excellent contrast for the different brain tissues, being the T1-weighted (T1w) image the most used MRI scan. For instance, BET and BSE were originally developed using this scan, although they have also been tested with T2-weighted (T2w) images [22]. Recently, other works have been presented to work over T2w images [16]. However, to our knowledge, none of these algorithms combines different scans. As shown in Fig. 1, T1w and T2w images provide different and complementary information that can help to better extract the brain from the rest of the head.

Given this scenario, in this paper we propose, analyze and discuss, the Multispectral Adaptive Region Growing Algorithm (MARGA¹), an extension of the region growing approach of Park and Lee [1] that enables its use to axial views and provides more reliable results for different patient populations and different MRI scanners (1.5 T and 3 T). The developed method is able to adapt itself to deal with changes of scanner machines, acquisition parameters, etc., with the aim of reducing the expert interactivity. In particular, we divide the MRI scan into three different spatial zones (middle, inferior and superior) where the segmentation strategy is slightly different to better adjust to the tissue intensity distributions. Furthermore, we introduce the use of T1w and T2w images within the segmentation framework with the idea that different intensity contrasts help on enhancing the resulting brain masks.

Besides, we demonstrate the validity of the new approach comparing the obtained results with the ones from the original work of Park and Lee [1] from both coronal and axial oriented scans. Moreover, we also present a qualitative and quantitative evaluation of the MARGA approach with BET [14], BSE [15] and the Statistical Parametric Mapping (SPM) [2], using three different data sets: (1) 10 simulated brains from the BrainWeb database, (2) 25 brains (10 normal brains, 10 brains of schizophrenic patients and 5 brains from lupus patients) acquired with two different 3 T scanners from the National Alliance for Medical Image Computing (NAMIC) public database, and (3) 10 brains of multiple sclerosis patients acquired with a 1.5 T scanner. The use of data sets containing different pathologies allows us to test the algorithm in more challenging conditions. The obtained results show that MARGA outperforms the other analyzed techniques in both 1.5 T and 3 T scanners. The first two rows of Fig. 1 show an example of a brain acquired using the 1.5 T scanner, while the last two show a brain acquired using a 3 T scanner, where the resolution of the images is higher.

2. Methods

The skull stripping proposal presented in this paper is inspired on the recent work of Park and Lee [1] in which satisfactory

¹ Sourcecode available at <http://atc.udg.edu/salem/margaToolbox>.

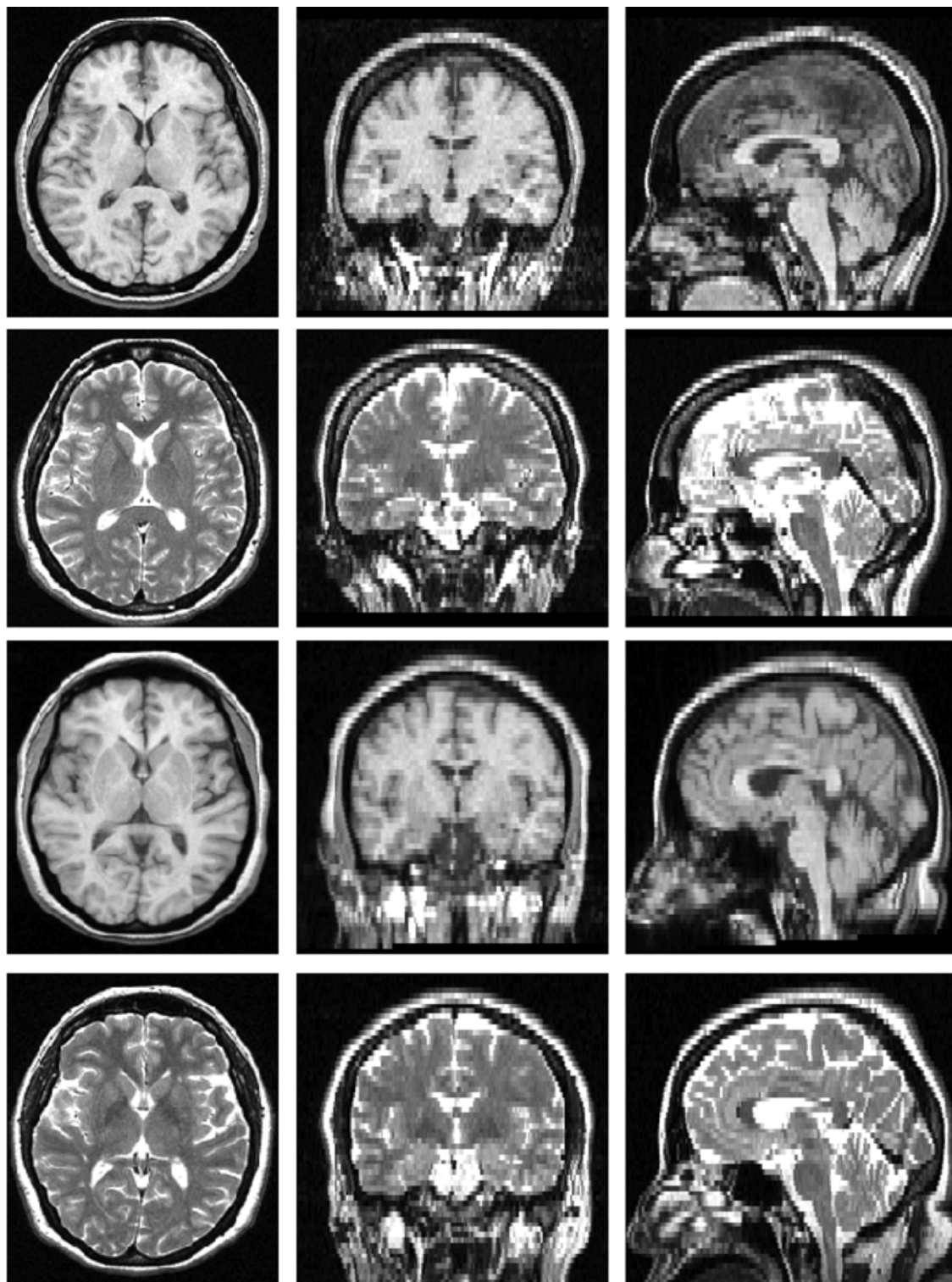


Fig. 1 – Brain MRI examples from a 1.5 T GE scanner (first and second row) and a 3 T scanner (third and fourth row) of T1w images (first and third rows) and T2w images (second and fourth rows). From left to right: axial, coronal and sagittal orientation.

segmentation results were reported when using coronal orientation images from different databases. However, we have noticed that their approach presents some inherent problems when either using brain volumes with lower quality

acquisition (1.5 T scans) or when using axial oriented images. This last issue may be partially solved by reorienting images to coronal view, but this transformation decreases the image resolution in its new orientation (even more in 1.5 T) and

therefore aggravates the first problem, producing results such as the ones illustrated in Fig. 2, where non-brain regions are included in the final mask.

Our contributions in this work allow to overcome these limitations, extending their approach in order to apply it directly to axial images. This new process through the brain slices implies restructuring the original strategy dividing the brain

the 3D volume $S(x, y, z)$, while S^{ij} denotes the (i, j) th voxel of the 2D image $S(x, y)$. Moreover, two other structures are used: a vector of voxels that will be called $nb(x)$ and a vector of regions that will be called $CC(q)$, being CC^q the (q) th region of the vector. Subindexes used in the names are added to clarify the meaning of the variables.

Algorithm 1. Skull stripping procedure.

```

Input:  $img(x, y, z)$ ; Original MRI unaltered.

Output:  $rg(x, y, z)$ ; MRI masked.
*****
 $roiImg(x, y, z) \leftarrow RoiEstimation(img(x, y, z));$ 
 $initialSlice(x, y) \leftarrow img(x, y, K/2);$ 
 $M(x, y) \leftarrow getInitialMask(initialSlice(x, y));$  // Algorithm 2
FOR ( $k = K/2$  to 0) do
   $rg_{seeds}(x, y) \leftarrow SeedRegions(roiImg^k(x, y), M(x, y));$  // Algorithm 3
   $rg^k(x, y) \leftarrow RegionGrowing(roiImg^k(x, y), rg_{seeds}(x, y));$  // Algorithm 4
   $rg^k(x, y) \leftarrow FillHoles(rg^k(x, y));$  // Algorithm 7
   $M(x, y) \leftarrow rg^k(x, y);$ 
END
 $M(x, y) \leftarrow rg^{K/2}(x, y);$ 
FOR ( $k = K/2 + 1$  to  $K$ ) do
   $rg_{seeds}(x, y) \leftarrow SeedRegions(roiImg^k(x, y), M(x, y));$ 
   $rg^k(x, y) \leftarrow RegionGrowing(roiImg^k(x, y), rg_{seeds}(x, y));$ 
   $rg^k(x, y) \leftarrow FillHoles(rg^k(x, y));$ 
   $M(x, y) \leftarrow rg^k(x, y);$ 
END
 $rg(x, y, z) \leftarrow RemoveBrainStem(rg(x, y, z));$  // Algorithm 5
 $rg(x, y, z) \leftarrow FillHoles(rg(x, y, z));$ 

```

into three different zones (superior, inferior, and central zone) to adapt the parameters of the algorithm to changes in intensity distributions. Besides, we combine the use of T1w and T2w images, which contain complementary information, to help providing more accurate boundaries specially in CSF regions. Notice that these regions have low intensity in T1w images while they have a higher intensity in T2w images.

2.1. Implementation of the original approach

The general scheme of the Park and Lee [1] strategy is shown in Fig. 3, where all the white and green boxes are the original steps followed in their approach, although the green ones have been re-implemented here using a slightly different strategy. Roughly, the skull stripping process is divided into three main steps: preprocessing, backward segmentation (2D slice by slice segmentation towards the inferior part of the volume) and forward segmentation (2D slice by slice segmentation towards the superior part of the volume). In the preprocessing step the main goal is to determine a region of interest from which the segmentation will be initialized. From the starting slice (which corresponds to the central slice of the brain), an initial mask is computed and a region growing process is applied towards the first and the final slice of the brain volume. Algorithm 1 presents the main structure of our implementation, which is done using the ITK software library.²

In what follows we describe in more detail each step of the algorithm, showing also the proposed implementation using the ITK library. Within the algorithms of the paper we refer to a 3D volume of an image S as $S(x, y, z)$, while $S(x, y)$ refers to a 2D image. When using $S^k(x, y)$ we refer to the k th slice of

2.1.1. Estimation of the region of interest

The first step is to find the space enclosed by the skull, hence removing the background voxels. This step is based on the analysis of intensity histogram of the full volume, and the aim is to remove the long low tails at each end. Generally, the low values belong to the background and the brighter voxels to the spike due to image reconstruction or to arteries [14].

Park and Lee [1] followed the thresholding strategy proposed by Smith [14] by using the cumulative intensity histogram. The cumulative histogram is obtained by adding to each histogram bin the cumulative number of observations of the previous bins up to the specified bin. Two thresholds were defined for removing the tails, a lower threshold set to 2% ($T_{2\%}$) and an upper one set to 98% ($T_{98\%}$). Therefore, pixels with very low and very high intensities that widely differ from the real image are removed.

A third threshold was defined in order to separate the background from the head itself. According to Smith [14], this threshold is defined at the 10% of the intensity between the previous two. Therefore, the region of interest (ROI) could be defined as the region accomplishing:

$$roiImg(x, y, z) = \begin{cases} 1, & \text{if } img(x, y, z) > 0.1 * (T_{98\%} - T_{2\%}) + T_{2\%} \\ 0, & \text{otherwise} \end{cases} \quad (1)$$

Finally, after removing all the undesirable voxels, some holes may appear inside the $roiImg(x, y, z)$ that have to be filled in, as shown in Fig. 4.

2.1.2. Getting the initial mask for the initial slice

An initial mask ($M(x, y)$) containing only brain tissue is obtained using the central slice, where the process of isolating the brain from the non-brain regions is relatively easy since

² <http://www.itk.org/>.

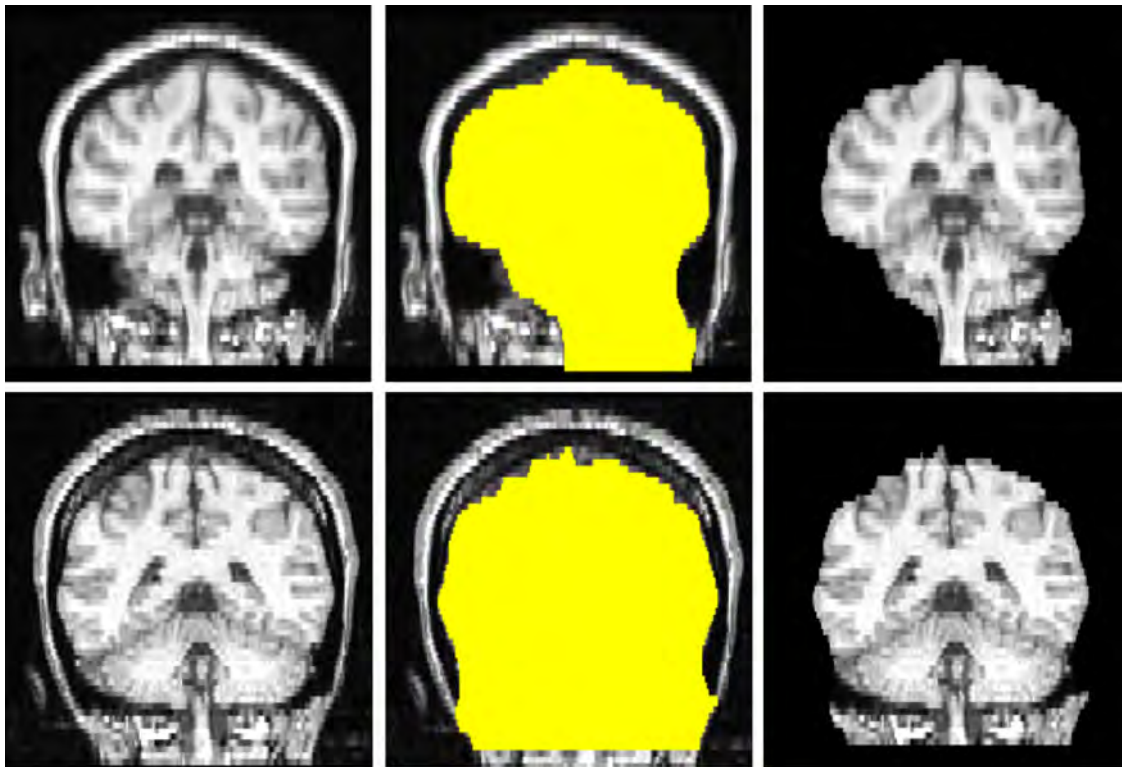


Fig. 2 – Example of bad brain segmentations with the original approach of Park and Lee [1] when using a 1.5 T reoriented coronal scan. From left to right: original image; mask overlapped over the original image; brain extracted result.

most of the brain regions are well separated from non-brain regions by CSF, which has a lower intensity value than the nearby brain regions and other structures.

Therefore, this rough binary mask is obtained from the initial slice by applying thresholding, followed by sequential binary morphological procedures, which included the following steps:

- *Thresholding*. In order to perform the thresholding step, rather than using the range-constrained least valley detection method [26] to remove the CSF we based this step on the Otsu thresholding method [27] already implemented on ITK.³
- *Erosion*. After the thresholding step, the brain and non-brain regions may still be connected due to factors like noise,

cal erosion is performed. We used the ITK implementation⁴ with a spherical kernel of 5 voxels [28,29].

- *Largest connected component*. Since in the middle slices the brain is larger than the non-brain regions, the largest connected component corresponds to the brain tissues. We have also performed this step using an available ITK filter.⁵
- *Dilation*. In order to restore the initial size before the erosion, a dilation operation [28,29] have to be applied with the same structural element used in the erosion step. In our implementation we use the ITK implementation.⁶

In summary, the steps required to obtain the initial mask are shown in Algorithm 2.

Algorithm 2. Getting the initial mask for the initial slice.

```

Input: slice(x,y); Initial slice .
Output: M(x,y); Initial slice masked.
*****
M(x,y) ← OtsuTh(slice(x,y)); //Otsu Thresholding
M(x,y) ← Er(M(x,y)); //Erosion
M(x,y) ← LCC(M(x,y)); //Largest Connected Component
M(x,y) ← Dil(M(x,y)); //Dilation

```

lack of CSF or anatomical continuity between both regions. Aiming to completely separate both regions a morphologi-

³ http://www.itk.org/Doxygen/html/classitk_1_1OtsuThresholdImageFilter.html.

⁴ http://www.itk.org/Doxygen/html/classitk_1_1BinaryErodeImageFilter.html.

⁵ http://www.itk.org/Doxygen/html/classitk_1_1ConnectedComponentImageFilter.html.

⁶ http://www.itk.org/Doxygen/html/classitk_1_1BinaryDilateImageFilter.html.

2.1.3. Lower and upper thresholds

The obtained mask provides a rough segmentation of the brain in the central slice. To obtain a more detailed segmentation Park and Lee proposed the use of a region growing algorithm, which is delimited in each slice (k) by a lower (T_{lower})

(CC) of $rg_{seeds}(x, y)$: (1) brain (R_B), (2) non-brain (R_N) and (3) undetermined (R_U). The components that belong to this last region are determined in subsequent steps. Algorithm 3 describes these rules in more detail.

Algorithm 3. Classifying the seed regions (brain/non-brain/undetermined).

```

Input:  $rg_{seeds}(x, y)$ ; Slice with the seed regions marked but not classified.
           $M(x, y)$ ;
Output:  $rg_{seeds}(x, y)$ ; Slice with its regions classified in  $R_B, R_N$  and  $R_U$ 
          *****
 $CC(q) \leftarrow getCC(rg_{seeds}(x, y))$ ; //To obtain the connected components in a slice
FOR each  $CC^q$  in  $CC(q)$ 
  IF  $(M(x, y) \cap CC^q) \neq \emptyset$  and  $|CC^q| \geq \epsilon$ 
    //The  $CC^q$  is greater than 5 voxels and intersects  $M(x, y)$ 
     $R_B \leftarrow R_B \cup CC^q$ 
  else if  $(M(x, y) \cap CC^q) = \emptyset$  and  $|CC^q| \geq \epsilon$ 
    //The  $CC^q$  is greater than 5 voxels but does not intersect  $M(x, y)$ 
     $R_N \leftarrow R_N \cup CC^q$ 
  else
    //The  $CC^q$  is smaller than 5 voxels
     $R_U \leftarrow R_U \cup CC^q$ 
END

```

and an upper threshold (T_{upper}). These thresholds were empirically fixed to $T_{lower} = 35\%$ and $T_{upper} = 80\%$ of the cumulative histogram for the k th slice. However, T_{lower} is subsequently adjusted computing the difference between the mean intensities of the k th slice and the total volume, allowing to adapt itself to the intensities of the different volume slices. Fig. 5 shows graphically the cumulative histogram and the corresponding thresholds for a typical middle slice.

2.1.4. Determination of seed regions

The region growing starts with two seed regions, corresponding each one to brain and non-brain tissues. Both seed regions ($rg_{seeds}^k(x, y)$) are determined after an initial thresholding by the T_{upper} over the current slice of the ROI ($roiImg^k(x, y)$).

$$rg_{seeds}(x, y) = \begin{cases} 1, & \text{if } T_{upper} \leq roiImg^k(x, y) \\ 0, & \text{otherwise} \end{cases} \quad (2)$$

In these rules, $M(x, y)$ corresponds to the mask obtained at the end of the RG process of the previous slice, except for the initial slice where $M(x, y)$ is computed as explained above. The idea is that brain regions are those which intersect with that mask, while non-brain regions are those which do not intersect. Given that many components could appear with a very few number of voxels, those regions with less than ϵ voxels (fixed to 5 voxels) are assigned as undetermined.

2.1.5. Region growing process

The approach of Park and Lee follows a 2D RG procedure based on a slice by slice analysis. Hence, the RG is an iterative process over each k th slice consisting in the steps shown in Algorithm 4.

Algorithm 4. Region growing procedure.

```

Input:  $slice(x, y)$ ; Region growing temporal mask.
           $rg_{seeds}(x, y)$ ; Slice with seed regions classified in  $R_B, R_N$  and  $R_U$ .
Output:  $rg(x, y)$  slice masked
          *****
 $rg_{tmp}(x, y) \leftarrow rg_{seeds}(x, y)$ 
//% of the cumulative histogram of the current slice
 $T_{upper} \leftarrow getTupper(rg_{tmp}(x, y))$ ;
//% of the cumulative histogram of the current slice adjusted with the mean intensity
//difference between the current slice and the total volume.
 $T_{lower} \leftarrow getTlower(rg_{tmp}(x, y))$ ;
FOR  $thr = T_{upper} - 1$  to  $T_{lower}$ 
   $rg_{tmp}(x, y) \leftarrow voxelAssignment(slice(x, y), rg_{tmp}(x, y), thr)$ ; //Algorithm 5
   $rg_{tmp}(x, y) \leftarrow componentAssignment(rg_{tmp}(x, y))$ ; //Algorithm 6
END
 $rg(x, y) \leftarrow rg_{tmp}(x, y)$ ;

```

Subsequently, a set of rules allows to discriminate among three different regions from all the connected components

In each slice the process starts with the determination of seed regions described above. These seed regions grow up by

decreasing the upper threshold, hence allowing to take more voxels into account. These new voxels are reconsidered and assigned to a region (brain, non-brain, undetermined) by the assignment rules indicated in Algorithm 5.

2.1.6. Fill in the holes

Depending on the images and their intensity distribution, the CSF and also the GM can have low level intensities. Park and Lee found out that due to this fact some holes could appear inside the brain zones. However, they presented these morphological operations as an optional process depending on

Algorithm 5. Voxel assignment rules.

```

Input:  $slice(x,y)$ ; Original slice within the RoI.
          $rgtmp(x,y)$ ; Region growing temporal mask.
          $thr$ ; Upper threshold.

Output:  $rgtmp(x,y)$ ; Region growing temporal mask with voxels  $> thr$  assigned.
*****

 $[R_B, R_N, R_U] \leftarrow getBrainRegions(rgtmp(x,y))$ ;

FOR each  $voxel^{i,j} \in slice(x,y) > thr$  and NOT assigned
     $nb(x) \leftarrow computeNeighbors(voxel^{i,j})$  //Compute a 4 connectivity neighborhood of  $voxel^{i,j}$ 

    //Check the  $nb(x)$  intersection with the previous regions classified
    IF  $(nb(x) \cap R_B) \neq \emptyset$ 
        IF  $(nb(x) \cap R_N) \neq \emptyset$  //Adjacent to both zones
             $R_N \leftarrow R_N \cup voxel^{i,j}$ ;
        else //Adjacent to the brain zone
             $R_B \leftarrow R_B \cup voxel^{i,j}$ ;
    else
        IF  $(nb(x) \cap R_N) \neq \emptyset$  //Adjacent to the non-brain zone
             $R_N \leftarrow R_N \cup voxel^{i,j}$ ;
        else //Isolated
             $R_U \leftarrow R_U \cup voxel^{i,j}$ ;
    END

 $rgtmp(x,y) \leftarrow setBrainRegions([R_B, R_N, R_U], rgtmp(x,y))$ ;

```

With these rules we obtain a classification of the new voxels depending on their neighborhood with connectivity 4 ($\leftarrow \uparrow \rightarrow$). If a particular voxel is in contact only with brain regions then is classified as brain, otherwise if the voxel is in contact with brain and non-brain regions is classified as non-brain.

Afterwards, once the new voxels are assigned, some components might be still unassigned and might also be connected to some of the brain or non-brain zones. Thus, Algorithm 6 contains the new set of component assignment rules defined following the same strategy than before:

the application. In contrast, in our approach, the filling in the holes becomes a mandatory step, mainly due to the change in the slice acquisition. In the axial view, internal CSF structures (the ones responsible of the holes) are larger than the ones obtained when using the coronal view, as can be clearly seen in Fig. 1.

In the original approach, this step was implemented by using morphological operations. A dilation allowed to fill in the holes, while a subsequent erode was necessary to reduce the size increased when applying the dilate operation. However, in axial orientation some holes still remain in the mask. Therefore, to solve this problem we modify this step by

Algorithm 6. Component assignment rules.

```

Input:  $rgtmp(x,y)$ ; Region growing temporal mask with  $q$  connected components undetermined ( $CCU(q)$ )
Output:  $rgtmp(x,y)$ ; Region growing temporal mask with the  $q$  connected components re-assigned.
*****

 $[R_B, R_N, R_U] \leftarrow getBrainRegions(rgtmp(x,y))$ ;
 $CCU(q) \leftarrow getCCUundetermined(rgtmp(x,y))$ ;

FOR each  $CC_U^q$  in  $CCU(q)$ 
     $nb(x) \leftarrow computeRegionNeighbors(CC_U^q)$  //Compute neighborhood of the boundary of the  $CC_U^q$ 

    //Check the  $nb(x)$  intersection with the previous regions classified
    IF  $(nb(x) \cap R_B) \neq \emptyset$ 
        IF  $(nb(x) \cap R_N) \neq \emptyset$  //Adjacent to both regions
             $R_N \leftarrow R_N \cup CC_U^q$ ;
        else //Adjacent to the brain zone
             $R_B \leftarrow R_B \cup CC_U^q$ ;
    else
        IF  $(nb(x) \cap R_N) \neq \emptyset$  //Adjacent to the non-brain region
             $R_N \leftarrow R_N \cup CC_U^q$ ;
    END

 $rgtmp(x,y) \leftarrow setBrainRegions([R_B, R_N, R_U], rgtmp(x,y))$ ;

```

looking for the connected components that were not included in the mask. Formally:

$$rg_{fh}(x, y) = \begin{cases} 1, & \text{if } M(x, y) \notin LCC(!M(x, y)); \\ 0, & \text{otherwise.} \end{cases} \quad (3)$$

In that situation, the largest connected component will correspond to the background, while the remaining ones will be filled in. Fig. 6 illustrates this improvement. Fig. 6(a) shows the mask without dilation neither erosion, Fig. 6(b) shows the mask obtained applying the dilate and erode morphological operations, where there are still some holes inside the mask, and, finally, Fig. 6(c) shows the obtained mask when using the proposed filling holes algorithm. The implementation of this step is shown in Algorithm 7.

Algorithm 7. Hole filling (2D).

```

Input:  $rg(x, y)$ ; Region growing masked slice.
Output:  $rg_{fh}(x, y)$ ; Region growing masked slice with the holes filled.
*****
 $background(x, y) \leftarrow LCC(inverse(rg(x, y)))$ ;
FOR each voxel in  $background(x, y)$ 
  //Set  $rg_{fh}(x, y) = 1$  when  $\notin background$ 
  IF  $background(x, y) = 0$ ;
     $rg_{fh}(x, y) \leftarrow 1$ ;
  else
     $rg_{fh}(x, y) \leftarrow 0$ ;
END

```

2.1.7. Removing the brain stem

To complete the full description of the pipeline proposed by Park and Lee, another optional process has to be introduced to remove the brain stem. This process consists in finding the slice where the brain stem starts, which is found looking for the maximum area differences between slices. Therefore, the masks of current and subsequent slices are removed, as illustrated in Algorithm 8.

Algorithm 8. Removing the brain stem.

```

Input:  $rg(x, y, z)$ ; Masked image.
Output:  $rg(x, y, z)$ ; Masked image without the brain stem.
*****
 $sliceNum \leftarrow SliceWithLargestDiffArea(rg(x, y, z))$ ;
FOR each  $k \in rg^k(x, y) \geq sliceNum$ 
  //Set  $rg^k(x, y)$  to empty
   $rg^k(x, y) \leftarrow \emptyset$ ;
END

```

2.2. MARGA approach

As explained in the introduction, the above implemented method fails in some cases due to the low resolution of images and the different slice orientation acquisition (see Fig. 2). Therefore, we propose to modify the original algorithm introducing some key steps, which are shown in blue in Fig. 3. In general, the segmentation process maintains the same strategy proposed by Park and Lee [1]. However, the inclusion of multispectral information as well as the division of the brain in three different regions allows to overcome those issues.

In what follows we describe in more detail the modifications introduced in order to obtain the full brain volume mask.

2.2.1. Dividing the brain in three parts

The segmentation process starts with the ROI determination and getting the seed regions from the initial slice (middle slice). From that slice, the procedure progresses towards the inferior and superior brain extremes. However, we divided the brain into three different parts, as it is graphically shown in Fig. 7, and a different strategy for segmentation is followed in each zone. In central slices, the different brain structures are well delimited, and therefore, the 2D segmentation algorithm explained in Section 2.1 is directly applied. In contrast, in the superior and inferior parts, the distinction between the different structures is much less evident, and the segmentation becomes increasingly challenging. In those parts, we propose to adaptively decrease the limits of interaction of the RG

in order to prevent that surrounding non-brain regions are added into the brain mask.

Therefore, in the superior (*MaxSliceThr*) and inferior (*MinSliceThr*) parts of the brain, the lower threshold increases gradually when progressing throughout the volume slices, always maintaining the relation $0 \leq T_{lower} \leq T_{upper} \leq 1$. Hence, a lower range of intensities is allowed during segmentation. Besides, we ensure that only one connected component appears in the mask, removing small components that may appear in the slice. In general, the brain tends to be connected

in only one volume, and thus, the obtained mask should be uniform and the largest segmented area. Finally, the segmentation process can be stopped in both superior (*MaxSlice*) and inferior (*MinSlice*) parts where there is no more brain area and it is not necessary to process or because the T_{lower} has reached the T_{upper} .

2.2.2. Use of complementary information (T1w and T2w)

As mentioned before, we also propose the use of multispectral information in order to perform the skull stripping. Specifically, we use both T1w and T2w images to perform the

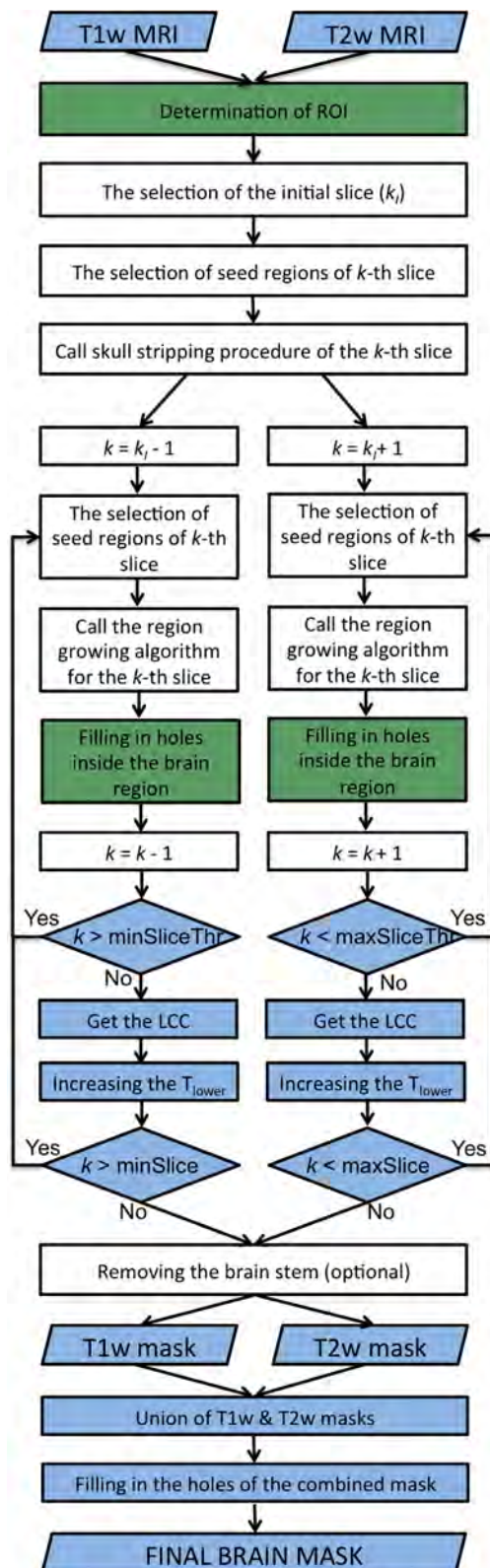


Fig. 3 – Overall scheme of the skull stripping procedure. Boxes in white correspond to the original steps presented in the work of Park and Lee [1]. Colored boxes indicate our adaptations and contributions introduced in the original approach (in green: adaptations; in blue: new steps). (For interpretation of the references to color in this figure legend, the reader is referred to the web version of the article.)

segmentation. As shown in Fig. 1, in T1w images the higher intensities always belong to the WM tissue whereas on T2w they belong to the GM and CSF. Therefore, we propose to use both scans in order to segment the WM, GM and CSF tissues from the rest of the skull.

Specifically, our approach consists in segmenting T1w and T2w images using the presented pipeline and combines the obtained binary masks using the morphological union operation. However, in order to not oversegment the brain, the thresholds applied on the images have to be more restrictive. Due to this fact, the final mask in a single sequence may miss part of the tissues. For instance, on T1w images the cortex (GM) is the most difficult part to segment since its intensity contrast may be similar to parts of the head that do not belong to the brain. Contrary, the segmentation on T2w is focused on the GM which is brighter than the WM. Since both segmentations are focused on different tissues of the brain, the final union allows to obtain a more accurate brain segmentation.

Fig. 8 shows an example of the benefits of using multispectral information. When using each sequence independently the brain is undersegmented. However, the combination of both results, which may be significantly different, allows to correctly segment the brain. Specifically, the algorithm tends to undersegment the T1w images in the frontal part, where the brain tissues have similar intensities than other structures, like the ocular bones. In contrast, in the T2w images, this part is clearly distinguishable. However, in this latter sequence, the white matter appears darker, and due to the thresholding step, in some slices it may be assigned to background, hence producing also an undersegmentation of the mask. Therefore, the combination of both sequences allows to obtain a more accurate segmentation since the physically undersegmentation causes are different and complementary in each sequence. Note that both causes may be associated with both the low quality of 1.5 T scans and its original axial orientation acquisition.

2.2.3. 3D hole filling step

As already mentioned in Section 2.1.6, in the original approach the hole filling step was an optional postprocessing step. However, due to the axial slice orientation acquisition, this step has become now a mandatory step when segmenting both T1w and T2w volumes.

Besides, a similar final step is necessary to avoid holes at the end of the union step. In some cases, small holes may appear in the middle of the mask and also in the boundaries that need to be filled in. We extended Algorithm 7 to perform a 3D volume filling holes.

3. Experimental results

In this section we firstly present the three databases used to obtain the results. Afterwards we quantitatively and qualitatively test the performance of the RG and MARGA approaches. Besides, we compare the results with the most used state-of-the-art skull stripping algorithms (BET, BSE and SPM).

The Dice Similarity Coefficient was used to quantitatively compare the obtained results with ground-truth masks. This measure indicates the amount of area overlap between the



Fig. 4 – Example of ROI estimation. From left to right: original image, threshold mask image, threshold mask image with the holes filled.

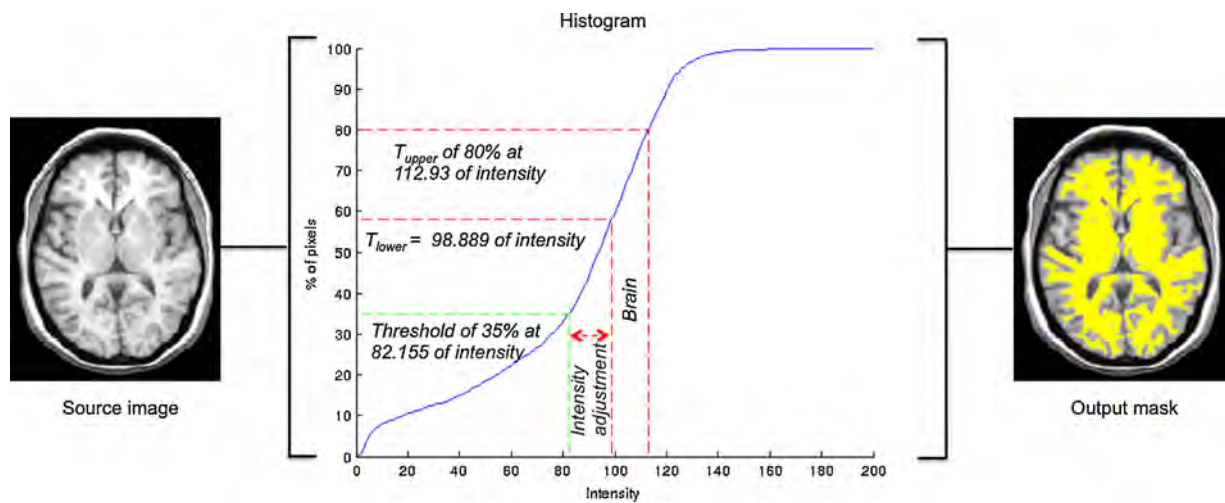


Fig. 5 – Cumulative histogram labeled with the lower intensity threshold at 35% and the upper intensity threshold at 80%.

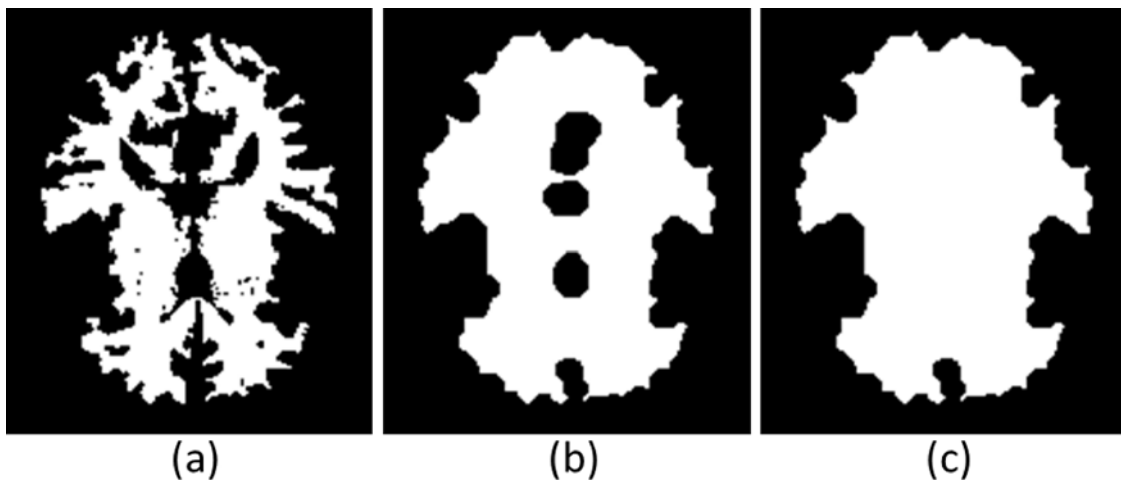


Fig. 6 – The three steps of the mask generation: (a) mask without any morphological operation, (b) mask after dilation and erosion, and (c) mask with all the operations applied.

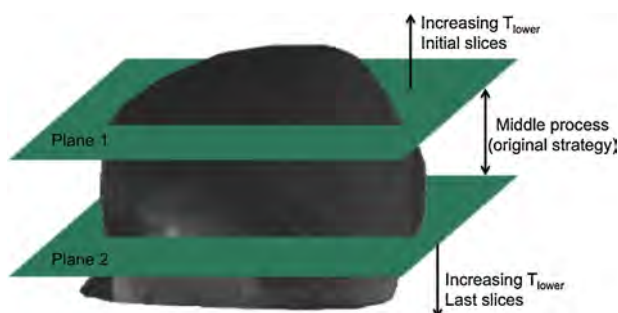


Fig. 7 – Visual example of the volume divisions proposed in our approach.

automatically detected (A) and the manually delineated (B) brain volumes. This measure is computed as:

$$DSC = \frac{2 \cdot |A \cap B|}{|A| + |B|} = \frac{2 \times TP}{2 \times TP + FP + FN} \quad (4)$$

where TP are the correct detections, FP are incorrect detections, and FN are missing detections, all measured in voxel terms.

3.1. Data sets

We test our algorithm using three databases of very different nature: the BrainWeb synthetic data, and two data sets of real cases, the first one being acquired with 3 T MRI scanners, and the second one using a 1.5 T scanner.

1 BrainWeb – simulated MRI volumes for normal brain. 10 simulated brain cases were obtained from this synthetic database with slice thickness fixed to 1 mm for both T1w and T2w images. Five degrees of noise (calculated relative to the brightest tissue) were chosen for 0% and 40% of intensity non-uniformity. The discrete anatomical model applied to generate the simulated brain MRI data was used as ground truth data. Both the discrete model and the 10 simulated brains were transformed to coronal orientation before starting the experiments in order to accomplish the requirements of Park and Lee [1].

2 NAMIC database

- 3 T GE scanner. 20 cases publicly available from the MIDAS/National Alliance for Medical Image Computing (NAMIC).⁷ From this set, 10 were normal controls while the other 10 were schizophrenic patients. The MRI acquisition protocol included two MRI pulse sequences. The first one consisted in contiguous spoiled gradient-recalled acquisition (fastSPGR) with the following parameters; TR 7.4 ms, TE 3 ms, TI 600 ms, 10° flip angle, 25.6 cm² field of view, matrix 256 × 256, voxel dimensions 1 mm × 1 mm × 1 mm. The second acquisition produced a series of contiguous T2w images (TR 2500 ms, TE 80 ms, 25.6 cm² field of view, 1 mm slice thickness), voxel dimensions 1 mm × 1 mm × 1 mm. All the series contains 128 axial slices. Along with the images,

the database provided a brain mask for each scan, which in our experiments are considered as the gold standard.

- 3 T Siemens scanner. 5 patients with lupus WM lesions are also publicly available in NAMIC.⁸ This set also provides a brain mask for each scan (gold standard in our experiments) and T1w and T2w MRI. All the images within each scan are co-registered and its acquisition contains 256 axial slices of 25.6 cm² field of view, matrix 256 × 256, voxel dimensions 1 mm × 1 mm × 1 mm. The differences with the previous NAMIC data set are the number of slices and the intensity rank, which is lower in the second one.
- 3 SALEM database – 1.5 T GE scanner. This (non-public) database comprised data from 10 patients with clinically confirmed multiple sclerosis. Each patient underwent MR imaging by using the same protocol (T1w, T2w, PDw and FLAIR images), although only T1w and T2w were used here. The scanner used was a 1.5 T GE Signa HDxt with 3D fast spoiled gradient T1w (TR 30 ms, TE 9 ms), fast spin echo T2w (TR 5000–5600 ms, TE 74–77 ms). All images were acquired in axial-view with slice thickness of 3 mm. No ground truth was available for this database.

3.2. Testing the RG approach

In order to validate our implementation of the original approach of Park and Lee [1], we tested it with both the synthetic MRI volumes from the BrainWeb repository in coronal orientation and the SALEM database with both axial and coronal orientations. The use of the BrainWeb database allows us to check our implementation of RG, since in the original work the authors used this database to analyze the performance of the approach. The use of the SALEM database allows to show the limitations of the approach in a real scenario.

RG was tested using the BrainWeb (with the same parameters), and compared with the BET [14] algorithm. According to Park and Lee [1], the best parameters configuration for this database was $T_{lower} = 0.35$ and $T_{upper} = 0.80$, and thus, these were the values used in this test. The obtained results illustrate similar outputs to the ones reported in the original method. This was numerically confirmed obtaining similar DSC results to the ones reported in Park and Lee [1]. The performance of our implementation is qualitatively shown in Fig. 9. Some misalignments with the ground truth can be seen in particular zones, where the standard techniques tend to enlarge the mask specially on the neck and spinal cord.

On the other hand, the SALEM data set contained MRI of lower resolution and with axial orientation. The obtained results presented many misclassifications, as is graphically shown in second row of Fig. 10. The results on the axial slices mainly miss cortex tissue, while the sagittal and coronal orientation, in addition to these parts, also present oversegmentation on the top and the bottom of the slices. Moreover, when reorienting this database to coronal view, we obtained the results shown in Fig. 2, where many misclassified tissues appeared. These poor results motivated the proposal of MARGA, obtaining the results shown in the last row of Fig. 10.

⁷ <http://insight-journal.org/midas/collection/view/190>.

⁸ <http://insight-journal.org/midas/collection/view/191>.

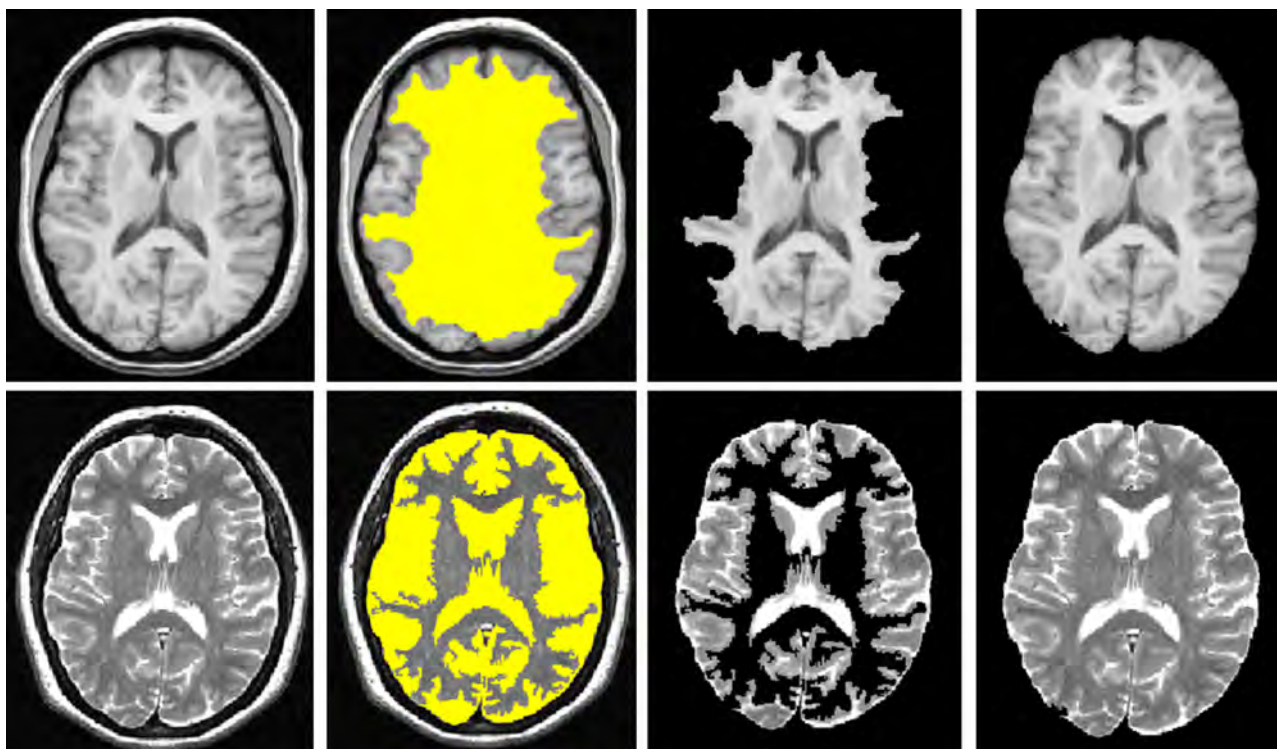


Fig. 8 – First row and second row correspond to T1w and T2w images, respectively. Form left to right: original image, obtained mask, region of the mask, and the final mask obtained by the union of T1w and T2w masks when applied onto the original image.

3.3. Testing MARGA with real data

We tested the performance of our modified approach with the two databases of real data, where the original RG approach failed in most of the cases. In order to quantitatively test the results of our approach with state-of-the-art algorithms, we compared MARGA with the well-known BET [14], BSE [15] and SPM [2] tools. Although the latter does not provide a direct brain mask but a tissue segmentation, following the work of Boesen et al. [30] one can generate the brain mask by thresholding the sum of GM, WM and CSF probability masks.

3.3.1. NAMIC database

The first NAMIC data set is composed by 20 scans of 3T with the corresponding ground truth (brain mask) for each case. Table 1 summarizes the obtained results along with the ones provided by BET, BSE and SPM. The mean DSC for each algorithm was 0.965 ± 0.012 for MARGA, 0.936 ± 0.015 for BET, 0.907 ± 0.021 for BSE, and 0.922 ± 0.021 for the SPM. Our algorithm provided the best DSC average, while BET provided 3.5%, SPM 5.6%, and BSE 6.4% less of accuracy. To analyze the statistical significance of these comparisons we carried out a one-way ANOVA analysis for comparing the performance of the different methods. Since the p_{value} was near zero, the performance of at least one method was significantly different from the other ones. Bonferroni correction method was then used to counteract multiple comparisons [31–34]. Fig. 11 confirms the statistical significant difference between MARGA and the rest of methods.

Qualitative results for the four algorithms are shown in Fig. 12, comparing their result with the provided ground-truth. The two upper rows correspond to the subject 01020, where notable differences appear between our approach and the rest of techniques. For the MARGA approach the two masks (green and red) are almost equal to their intersection, while standard tools differ specially on the cortex. For the BET and BSE techniques the intersection is always smaller than the ground truth, while for the SPM the intersection is the ground truth mask itself since the SPM segmentation is larger than the ground truth. On the other hand, the two last rows correspond to subject 01042, where MARGA, BSE and SPM techniques depict a similar performance, being the automatically obtained masks bigger than the ground truth, while the BSE provides again a smaller mask. In both cases this qualitative analysis is quantitatively confirmed by the DSC shown in Table 1.

Moreover, we have also tested the performance of MARGA when using just a single modality (T1w or T2w) during the segmentation process. Analyzing the results, we observed that better DSC percentage was obtained when using T2w (0.948 ± 0.031) than when using T1w (0.855 ± 0.034). Notice that both values are lower than those obtained with the combined used of T1w and T2w images (0.965 ± 0.012). Fig. 8 shows a qualitative example of the segmentation results obtained (T1w, T2w and the combination of T1w and T2w masks, respectively). The same parameter configuration was used for the three tests. It is important to remark that we adopted a conservative behavior on the segmentation growing process,

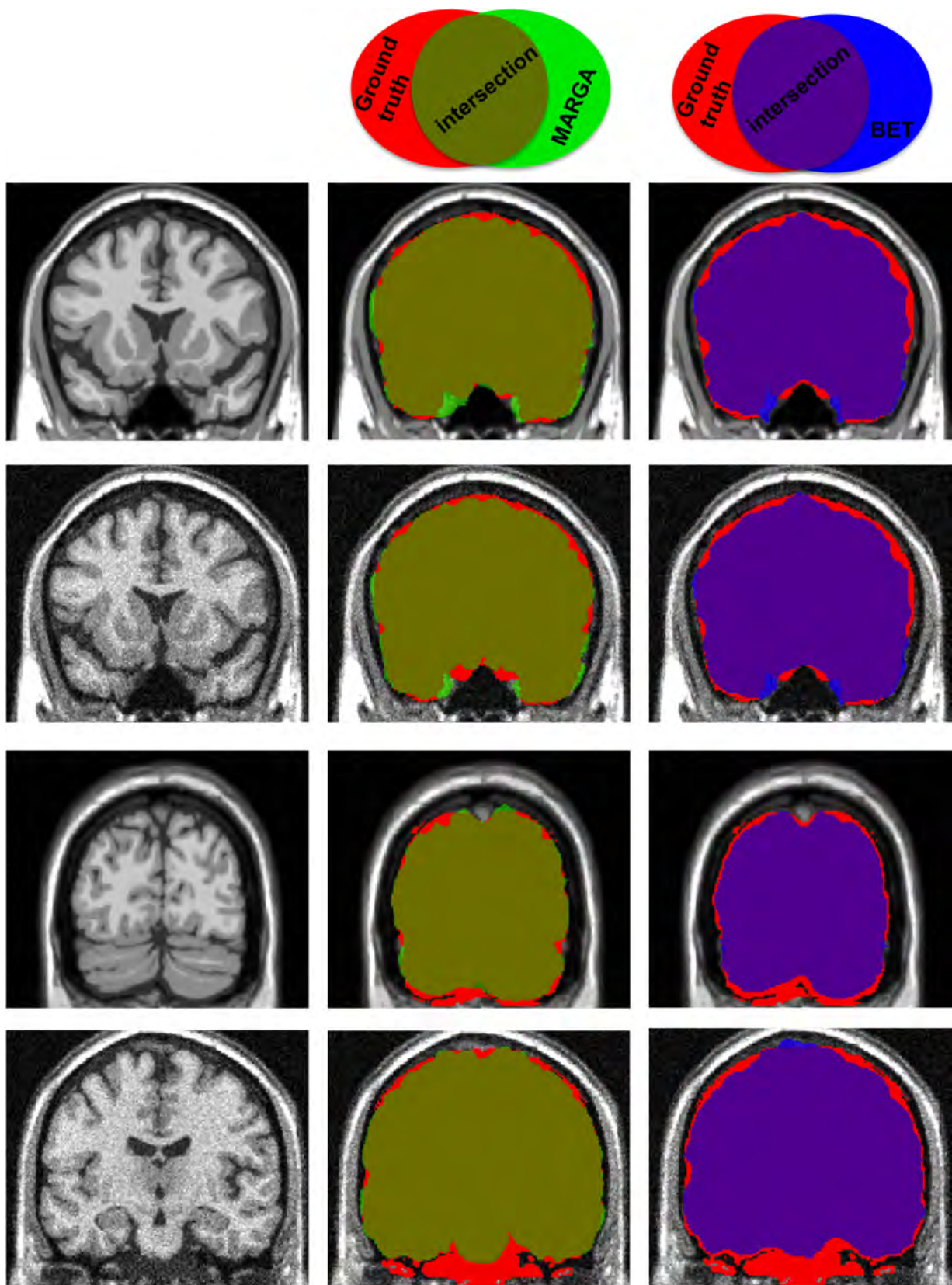


Fig. 9 – Brain extraction results obtained over the BrainWeb database with 1% noise and 0% intensity inhomogeneity (first and third rows) and also with 9% noise and 40% intensity inhomogeneity (second and fourth rows). First column shows the original data, second column the ground truth mask (red) and MARGA mask (green), and the third column ground truth (red) and BET mask (blue). Dark green and purple belongs to the intersection of BET and RG with the ground truth, respectively. (For interpretation of the references to color in this figure legend, the reader is referred to the web version of the article.)

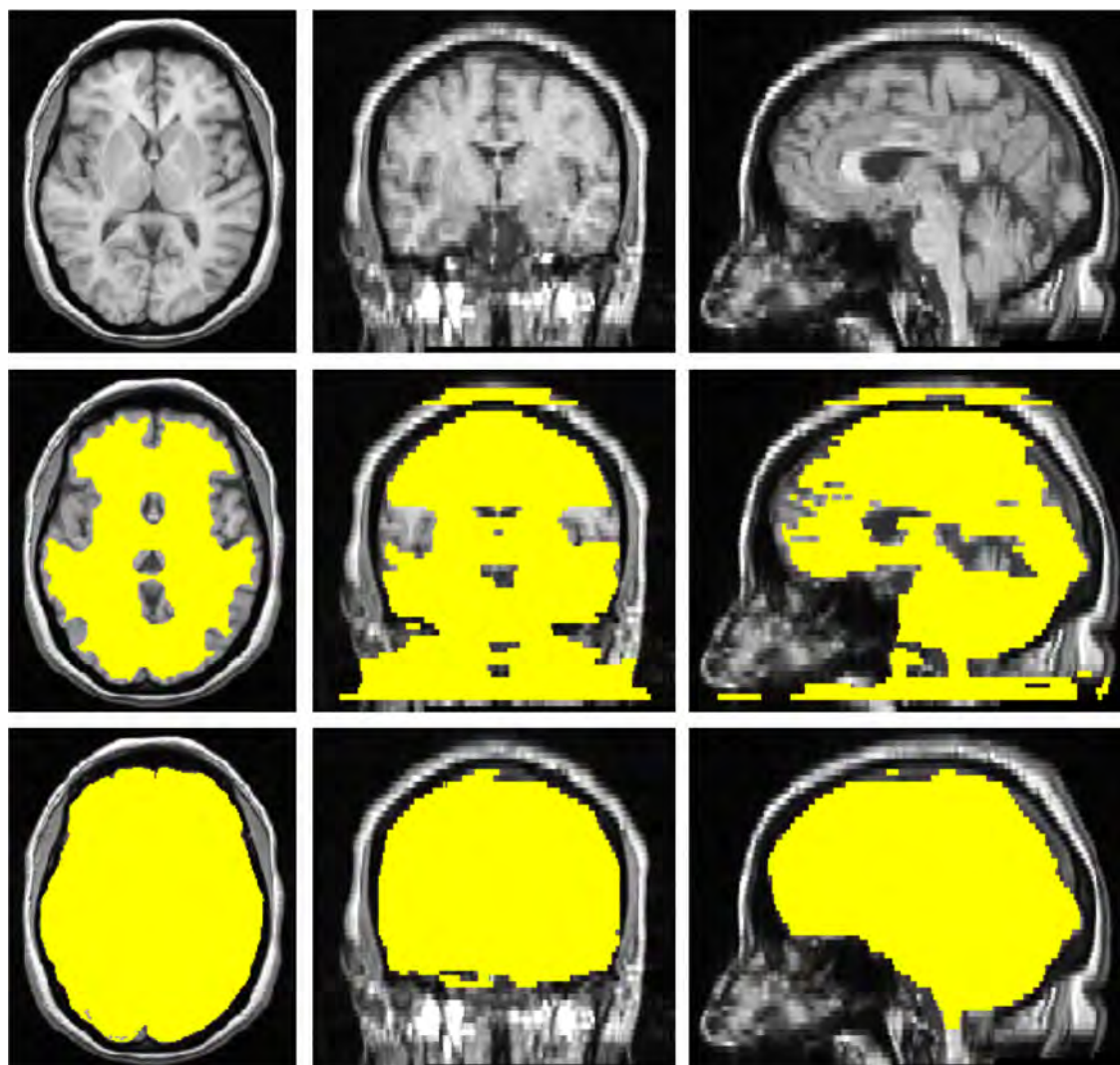


Fig. 10 – Example of bad brain segmentations with the original RG approach. From left to right: axial, coronal, sagittal views. First row shows the original image, second row illustrates the result of the RG approach, while third shows the improvement of MARGA.

specially in T1w images since the obtained results for T2w images complement the ones of T1w (see example of Fig. 8).

The second part of the NAMIC database is composed by 5 scans acquired with a different protocol than the first one. Table 2 summarizes the obtained results from all the methods. The mean DSC is slightly lower for MARGA (0.952 ± 0.006), BET (0.935 ± 0.019) and SPM (0.850 ± 0.008) while decreases considerably for BSE (0.575 ± 0.036). Note that the algorithms have performed differently on these cases which are highly affected by the low range of intensities in the provided images. The statistical significance has been tested as in the previous data set, although the few number of cases prevent us to extract significant conclusions. The tests concluded that, in this case, only SPM and BSE have DSC means significantly lower than MARGA while BET and MARGA are not significantly different, even though as shown in Table 2 the DSC mean is clearly higher for MARGA.

Furthermore, we have also analyzed the results for MARGA when using T1w and T2w separately. We observed that better

DSC percentage was obtained when using T2w (0.898 ± 0.037) than when using T1w (0.846 ± 0.020). The results with this data set follow the same behavior than the previous one, having both T1w and T2w values lower than those obtained with the combined used of T1w and T2w images (0.952 ± 0.006).

3.3.2. SALEM database

The SALEM database is composed by scans of 1.5T, where ground truth is not available. With the aim to provide also a quantitative analysis using this database, we compared the overlap of the masks obtained by the four algorithms MARGA, BET, BSE and SPM. This allows to assess how similar among them were the performances of these techniques. The results are summarized in Table 3, obtaining a mean overlap in DSC between MARGA and BET, MARGA and BSE, and MARGA and SPM of 0.951 ± 0.009 , 0.943 ± 0.013 and 0.962 ± 0.008 , respectively. Therefore, in this database, SPM provided the most similar performance to MARGA, while the biggest differences were with BSE.

Table 1 – Performance of the our modified approach applied over the 3 T GE scans (10 normal controls and 10 schizophrenic patients) on axial orientation. Comparison with the DICE similarity measure of MARGA, BET, BSE and SPM tools [parameters: $T_{lower} = 0.35$; $T_{upper} = 0.8$; $MinSliceThr = 40$; $MaxSliceThr = 40$; $MinSlice = 25$; $MaxSlice = 20$].

3 T GE data set				
Pat. id	MARGA	BET	BSE	SPM
01019	0.964	0.920	0.891	0.926
01020	0.987	0.927	0.910	0.921
01025	0.977	0.951	0.917	0.937
01026	0.973	0.960	0.905	0.886
01029	0.943	0.926	0.903	0.903
01033	0.960	0.944	0.890	0.931
01034	0.970	0.918	0.917	0.932
01035	0.957	0.947	0.923	0.923
01041	0.933	0.946	0.914	0.921
01104	0.968	0.951	0.930	0.928
AVG.	0.960	0.937	0.904	0.925
SD.	0.014	0.015	0.029	0.020
01011	0.968	0.943	0.897	0.902
01015	0.968	0.923	0.918	0.937
01017	0.976	0.947	0.913	0.918
01018	0.962	0.943	0.924	0.947
01028	0.977	0.928	0.896	0.879
01039	0.974	0.921	0.909	0.934
01042	0.968	0.965	0.934	0.969
01044	0.947	0.923	0.832	0.911
01045	0.966	0.928	0.906	0.935
01073	0.967	0.917	0.912	0.906
AVG.	0.970	0.936	0.910	0.920
SD.	0.009	0.015	0.011	0.022
TOTAL AVG.	0.965	0.936	0.907	0.922
SD.	0.012	0.015	0.021	0.021

Fig. 13 qualitatively illustrates the performance of the algorithms using two examples of this database. Although both initial images are fairly similar, the outcome result shows interesting differences to highlight. In concrete, we

Table 2 – Performance of the our modified approach applied over the 3 T Siemens scans (5 lupus patients). Comparison with the DICE similarity measure of MARGA, BET, BSE and SPM tools [T1w parameters: $T_{lower} = 0.45$; $T_{upper} = 0.8$; $MinSliceThr = 100$; $MaxSliceThr = 80$; $MinSlice = 89$; $MaxSlice = 58$. T2w parameters: $T_{lower} = 0.45$; $T_{upper} = 0.8$; $MinSliceThr = 120$; $MaxSliceThr = 80$; $MinSlice = 80$; $MaxSlice = 62$].

3 T Siemens data set				
Pat. id	MARGA	BET	BSE	SPM
00001	0.951	0.933	0.561	0.842
00002	0.958	0.904	0.547	0.854
00003	0.946	0.944	0.567	0.849
00004	0.957	0.955	0.640	0.863
00005	0.946	0.941	0.561	0.844
AVG.	0.952	0.935	0.575	0.850
SD	0.006	0.019	0.036	0.008

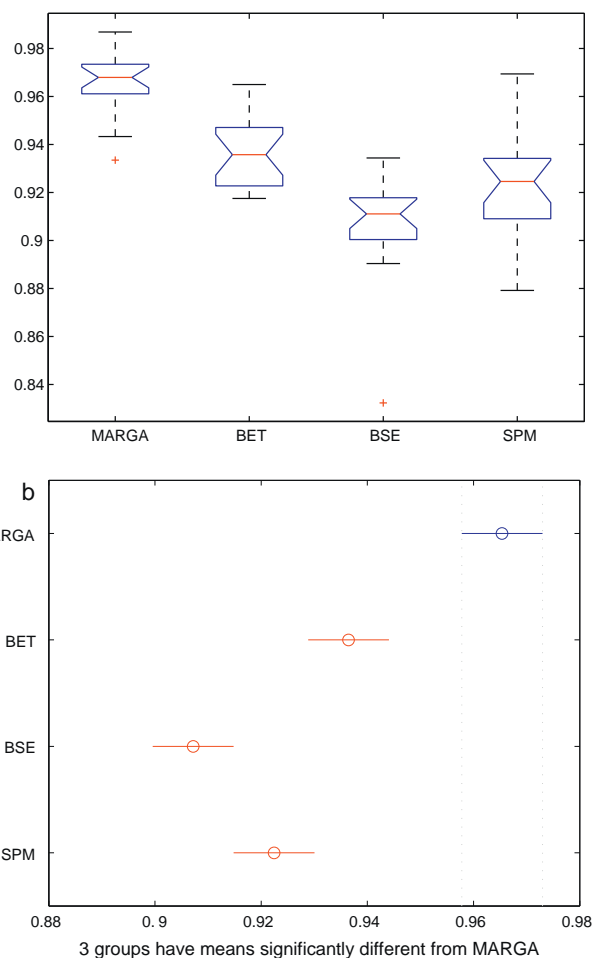


Fig. 11 – Significance test of the performance of MARGA for the first NAMIC database. Mean boxplots are shown on the left and Bonferroni output on the right.

have chosen the cases with larger differences among them where our approach successfully segments the brain or vice versa. The upper part of the figure shows a case where MARGA fails to exclude the eyes (only in three slices), while other techniques are able to distinguish them as non-brain. This is probably due to the low resolution (1.5 T) of the images that implies that sometimes is difficult to distinguish and separate some of the parts of the brain with the non-brain. Note that in this case, the rest of algorithms also had problems to segment some of these parts. On the other hand, the bottom part of Fig. 13 illustrates a case where MARGA works better than the rest of algorithms. For instance, in this case the BET algorithm included the eyes and other non-brain regions into the final mask. Observe also that MARGA is able to segment the front of this subject while BET and BSE failed to this purpose. Besides, this case of study shows that SPM has a performance similar to the one of our approach.

4. Discussion

In this paper we tested the skull stripping algorithm proposed by Park and Lee [1] in a new scenario. The results obtained

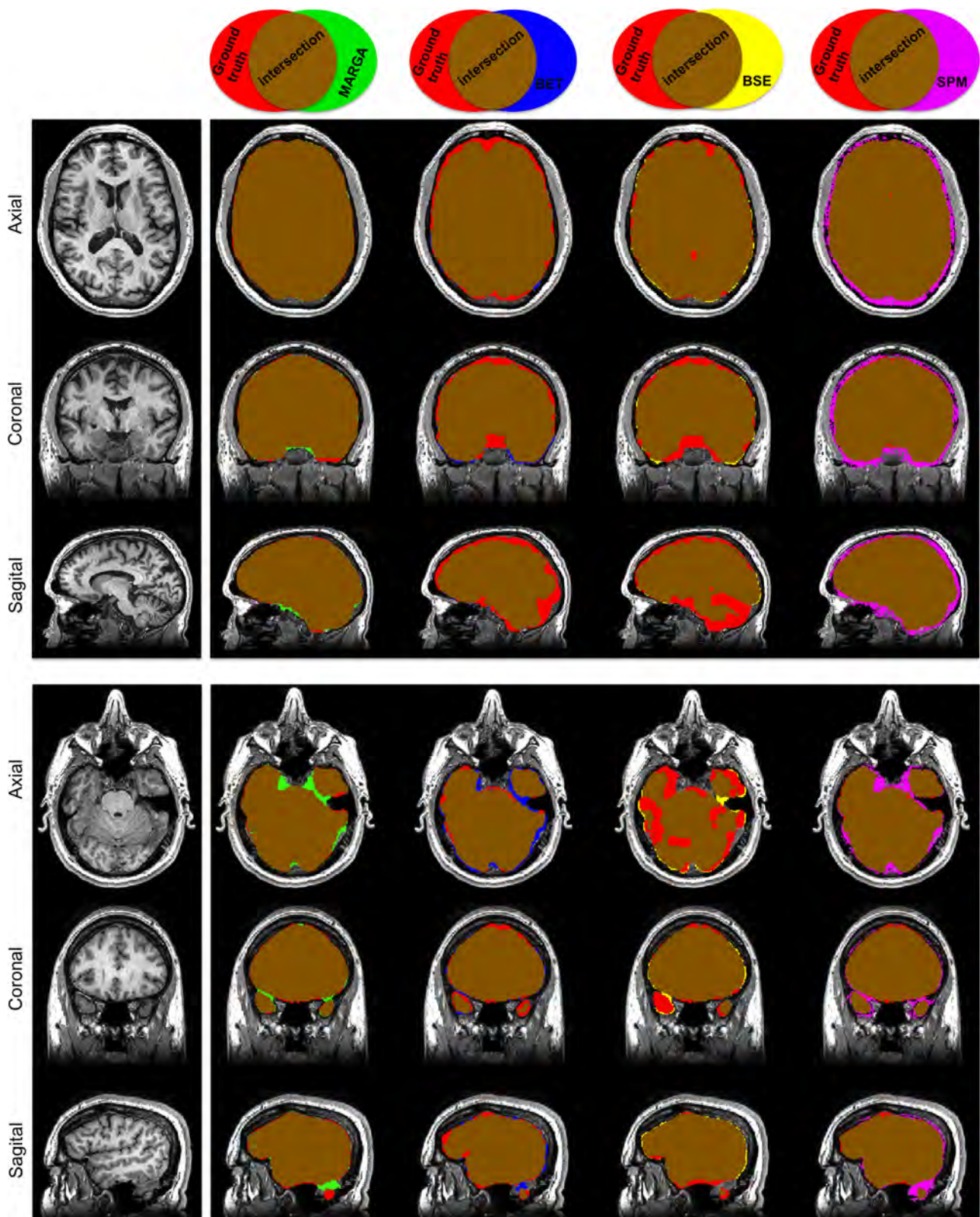


Fig. 12 – Qualitative comparison of the performance of the MARGA (green), BET (blue), BSE (yellow) and SPM (purple) algorithms using two examples of the NAMIC database, which contained an annotated ground-truth (red). The intersection of the automatic algorithms and the ground truth is shown in brown. Subject numbers 1020 and 1042, respectively. (For interpretation of the references to color in this figure legend, the reader is referred to the web version of the article.)

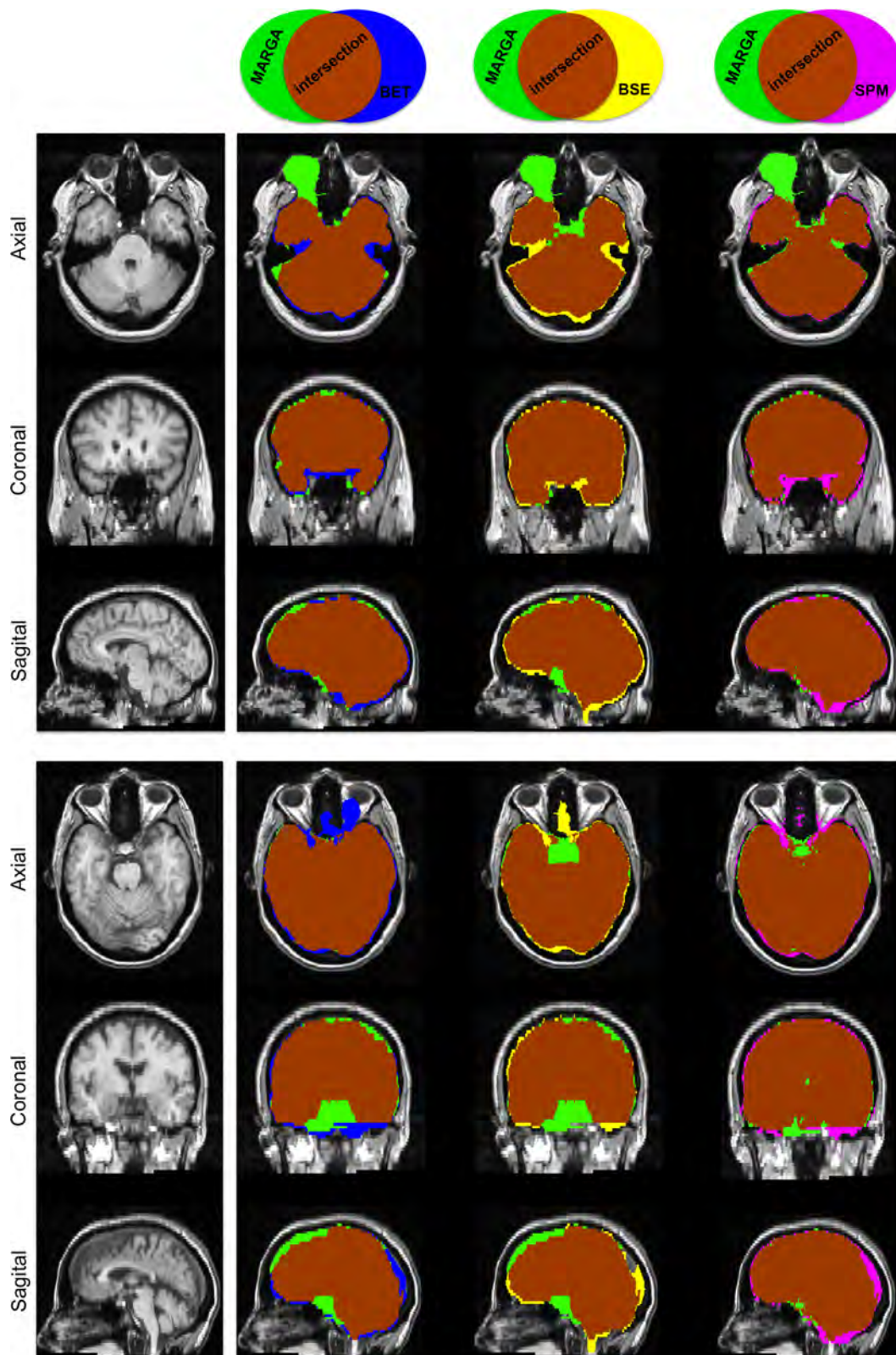


Fig. 13 – Qualitative comparison of the performance of MARGA (green) when compared to BET (blue), BSE (yellow), and SPM (purple) skull stripping algorithms. The intersection between MARGA and rest of algorithms is shown in brown. The subjects shown are 001 and 010, respectively. (For interpretation of the references to color in this figure legend, the reader is referred to the web version of the article.)

Table 3 – Performance of the our modified approach applied over the 1.5 T scans on axial orientation. Comparison with the DICE similarity measure of MARGA against BET, BSE and SPM tools [parameters: $T_{lower} = 0.35$; $T_{upper} = 0.8$; $MinSliceThr = 20$; $MaxSliceThr = 16$; $MinSlice = 18$; $MaxSlice = 10$].

1.5 T data set						
Pat. id	MARGAvsBET	MARGAvsBSE	MARGAvsSPM	BETvsBSE	BETvsSPM	BSEvsSPM
001	0.953	0.948	0.958	0.971	0.969	0.963
002	0.957	0.951	0.968	0.972	0.966	0.960
003	0.958	0.952	0.970	0.969	0.960	0.953
004	0.958	0.954	0.969	0.972	0.970	0.963
005	0.951	0.915	0.960	0.936	0.969	0.930
006	0.931	0.924	0.945	0.954	0.943	0.930
007	0.957	0.947	0.964	0.968	0.969	0.963
008	0.955	0.947	0.955	0.959	0.956	0.947
009	0.955	0.949	0.969	0.976	0.970	0.966
010	0.937	0.943	0.957	0.955	0.949	0.943
AVG.	0.951	0.943	0.962	0.963	0.962	0.952
SD	0.009	0.013	0.008	0.012	0.010	0.014

were not satisfactory, and this fact drove us to extend this proposal. Two main issues were identified to understand the poor performance of the original approach. Firstly, the fact that we were dealing with axial oriented brains instead of coronal ones affects the intensity distribution of the slices, mainly in the ones corresponding to the top and bottom extremes of the head, where the brain is a small part of the image surrounded by many different tissues and structures. On the other hand, the approach also failed when using lower resolution images acquired with 1.5 T scanners. This issue was more noticeable at the extremes of the head, where the intensity of the brain and non-brain tissues is even more similar.

To solve these issues two main contributions have been proposed in the MARGA approach. Firstly, we divided the volume in three different parts, since the intensity distribution on the middle slices is very different to those containing the extremes of the brain. Therefore, the proposed partition is driven by the contrast variation, and it allows to dynamically modify the range of intensities that take place in the segmentation. This way, the obtained 2D masks are smaller in these slices, avoiding oversegmentation in the cortex of the brain. Secondly, we proposed to use multispectral information coming from T1w and T2w images, since both images provide complementary information that helps the segmentation algorithm. Specifically, T1w images enhance the white matter tissue, while T2w images enhance gray and CSF tissues, fact that allows the method to segment the inner tissues with T1w images and the cortex of the brain in T2w images. The use of both sequences did not need any additional medical resource, since both modalities are commonly used in brain imaging protocols of clinical practice.

We tested the performance of MARGA with a synthetic MRI volume and two different databases of patients, comparing the obtained results with three well-known skull stripping algorithms: BET, BSE and SPM. Our approach has provided better results than those techniques for the databases presented, both quantitatively and qualitatively. In conclusion, our improved algorithm is stable and permits to obtain satisfactory skull stripping results when dealing with axial oriented MRI images acquired at 1.5 T or 3 T.

Conflict of interest statement

All authors in this paper have no potential conflict of interests.

Acknowledgements

This work has been supported by the Instituto de Salud Carlos III Grant PI09/91018, Grant VALTEC09-1-0025 from the Generalitat de Catalunya, and Grant CEM-Cat 2011 from the Fundació Esclerosi Múltiple. E. Roura holds a BR-UdG2013 grant.

REFERENCES

- [1] J.G. Park, C. Lee, Skull stripping based on region growing for magnetic resonance brain images, *NeuroImage* 47 (4) (2009) 1394–1407.
- [2] J. Ashburner, K.J. Friston, Unified segmentation, *NeuroImage* 26 (3) (2005) 839–851.
- [3] M. Cabezas, A. Oliver, X. Lladó, J. Freixenet, M. Bach Cuadra, A review of atlas-based segmentation for magnetic resonance brain images, *Computer Methods and Programs in Biomedicine* 104 (3) (2011) e158–e177.
- [4] D. Škerl, B. Likar, F. Pernuš, A protocol for evaluation of similarity measures for non-rigid registration, *Medical Image Analysis* 12 (1) (2008) 42–54.
- [5] M. Modat, G.R. Ridgway, Z.A. Taylor, M. Lehmann, J. Barnes, D.J. Hawkes, N.C. Fox, S. Ourselin, Fast free-form deformation using graphics processing units, *Computer Methods and Programs in Biomedicine* 98 (3) (2010) 278–284.
- [6] S. Klein, M. Staring, K. Murphy, M. Viergever, J. Pluim, elastix: a toolbox for intensity-based medical image registration, *IEEE Transactions on Medical Imaging* 29 (1) (2010) 196–205.
- [7] E. Roura, T. Schneider, M. Modat, P. Daga, N. Muhlert, D. Chard, S. Ourselin, X. Lladó, C.A.M. Wheeler-Kingshott, Evaluating a multi-channel registration approach of FA and T1w on MS patients with simulated atrophy, in: *International Society for Magnetic Resonance in Medicine*, 2013.
- [8] S. Saha, S. Bandyopadhyay, Automatic MR brain image segmentation using a multiseed based multiobjective clustering approach, *Applied Intelligence* 35 (3) (2011) 411–427.

- [9] X. Lladó, A. Oliver, M. Cabezas, J. Freixenet, J.C. Vilanova, A. Quiles, L. Valls, L. Ramió-Torrentà, A. Rovira, Segmentation of multiple sclerosis lesions in brain MRI: a review of automated approaches, *Information Sciences* 186 (1) (2012) 164–185.
- [10] X. Lladó, O. Ganiler, A. Oliver, R. Martí, J. Freixenet, L. Valls, J.C. Vilanova, L. Ramió-Torrentà, A. Rovira, Automated detection of multiple sclerosis lesions in serial brain MRI, *Neuroradiology* 54 (8) (2012) 787–807.
- [11] K. Li, L. Guo, C. Faraco, D. Zhu, H. Chen, Y. Yuan, J. Lv, F. Deng, X. Jiang, T. Zhang, X. Hu, D. Zhang, L.S. Miller, T. Liu, Visual analytics of brain networks, *NeuroImage* 61 (1) (2012) 82–97.
- [12] D.S. Bassett, B.G. Nelson, B.A. Mueller, J. Camchong, K.O. Lim, Altered resting state complexity in schizophrenia, *NeuroImage* 59 (3) (2012) 2196–2207.
- [13] E. Hodneland, M. Ystad, J. Haasz, A. Munthe-Kaas, A. Lundervold, Automated approaches for analysis of multimodal MRI acquisitions in a study of cognitive aging, *Computer Methods and Programs in Biomedicine* 106 (3) (2012) 328–341.
- [14] S.M. Smith, Fast robust automated brain extraction, *Human Brain Mapping* 17 (3) (2002) 143–155.
- [15] D.W. Shattuck, S.R. Sandor-Leahy, K.A. Schaper, D.A. Rottenberg, R.M. Leahy, Magnetic resonance image tissue classification using a partial volume model, *NeuroImage* 13 (5) (2001) 856–876.
- [16] K. Somasundaram, T. Kalaiselvi, Fully automatic brain extraction algorithm for axial T2-weighted magnetic resonance images, *Computers in Biology and Medicine* 40 (10) (2010) 811–822.
- [17] A.G.R. Balan, A.J.M. Traina, M.X. Ribeiro, P.M.A. Marques, C. Traina Jr, Smart histogram analysis applied to the skull-stripping problem in T1-weighted MRI, *Computers in Biology and Medicine* 42 (5) (2012) 509–522.
- [18] D. Marr, E. Hildreth, Theory of edge detection, *Proceedings of the Royal Society of London. Series B, Biological Sciences* 207 (1167) (1980) 187–217.
- [19] E.H. Kale, E.U. Mumcuoglu, S. Hamcan, Automatic segmentation of human facial tissue by MRI-CT fusion: a feasibility study, *Computer Methods and Programs in Biomedicine* 108 (3) (2012) 1106–1120.
- [20] C. Köse, U. Sevik, C. İkibaş, H. Erdöl, Simple methods for segmentation and measurement of diabetic retinopathy lesions in retinal fundus images, *Computer Methods and Programs in Biomedicine* 107 (2) (2012) 274–293.
- [21] T. Berber, A. Alpkocak, P. Balci, O. Dicle, Breast mass contour segmentation algorithm in digital mammograms, *Computer Methods and Programs in Biomedicine* 110 (2) (2013) 150–159.
- [22] C. Fennema-Notestine, I.B. Ozyurt, C.P. Clark, S. Morris, A. Bischoff-Grethe, M.W. Bondi, T.L. Jernigan, B. Fischl, F. Segonne, D.W. Shattuck, R.M. Leahy, D.E. Rex, A.W. Toga, K.H. Zou, G.G. Brown, Quantitative evaluation of automated skull-stripping methods applied to contemporary and legacy images: effects of diagnosis, bias correction, and slice location, *Human Brain Mapping* 27 (2) (2006) 99–113.
- [23] A.H. Zhuang, D.J. Valentino, A.W. Toga, Skull-stripping magnetic resonance brain images using a model-based level set, *NeuroImage* 32 (1) (2006) 79–92.
- [24] S. Hartley, A. Scher, E. Korf, L. White, L. Launer, Analysis and validation of automated skull stripping tools: a validation study based on 296 MR images from the Honolulu Asia aging study, *NeuroImage* 30 (4) (2006) 1179–1186.
- [25] J.-M. Lee, U. Yoon, S.H. Nam, J.-H. Kim, I.-Y. Kim, S.I. Kim, Evaluation of automated and semi-automated skull-stripping algorithms using similarity index and segmentation error, *Computers in Biology and Medicine* 33 (6) (2003) 495–507.
- [26] Q. Hu, Z. Hou, W. Nowinski, Supervised range-constrained thresholding, *IEEE Transactions on Image Processing* 15 (1) (2006) 228–240.
- [27] R. Beare, Histogram-based thresholding – some missing methods, *The Insight Journal* (2011).
- [28] L. Vincent, Morphological transformations of binary images with arbitrary structuring elements, *Signal Processing* 22 (1) (1991) 3–23.
- [29] N. Nikopoulos, I. Pitas, An efficient algorithm for 3D binary morphological transformations with 3D structuring elements of arbitrary size and shape, in: *IEEE Workshop on Nonlinear Signal and Image Processing*, 1997.
- [30] K. Boesen, K. Rehm, K. Schaper, S. Stoltzner, R. Woods, E. Lüders, D. Rottenberg, Quantitative comparison of four brain extraction algorithms, *NeuroImage* 22 (3) (2004) 1255–1261.
- [31] S. Holm, A simple sequentially rejective multiple test procedure, *Scandinavian Journal of Statistics* 6 (2) (1979) 65–70.
- [32] T.J. Sarén-Koivuniemi, A.M. Yli-Hankala, M.J. van Gils, Increased variation of the response index of nociception during noxious stimulation in patients during general anaesthesia, *Computer Methods and Programs in Biomedicine* 104 (2) (2011) 154–160.
- [33] S. Chen, J. Epps, Automatic classification of eye activity for cognitive load measurement with emotion interference, *Computer Methods and Programs in Biomedicine* 110 (2) (2013) 111–124.
- [34] R.N. Khushaba, S. Kodagoda, D. Liu, G. Dissanayake, Muscle computer interfaces for driver distraction reduction, *Computer Methods and Programs in Biomedicine* 110 (2) (2013) 137–149.

Multi-channel registration of FA and T1w images in the presence of atrophy: application to Multiple Sclerosis

In this chapter, we present a new pipeline for the co-registration of structural T1-weighted (T1w) scans and diffusion tensor imaging (DTI) derived fractional anisotropy (FA) maps to a common space. We test the performance of a MC registration approach applied to T1w and FA data using simulated brain atrophy images. Experimental results are compared with a standard single-channel (SC) registration approach.

The proposed method has been published in the following paper:

Paper published in Functional Neurology

Volume: 30, Issue: 4, Pages: 645-656. Published: December 2015.

DOI: 10.11138/FNeur/2015.30.4.245

JCR N IF 1.855, Q3(187/252)

Multi-channel registration of fractional anisotropy and T1-weighted images in the presence of atrophy: application to multiple sclerosis

Eloy Roura, MD^a
Torben Schneider, PhD^b
Marc Modat, PhD^c
Pankaj Daga, PhD^c
Nils Muhlert, PhD^b
Declan Chard, PhD^{b,d}
Sebastien Ourselin, PhD^c
Xavier Lladó, PhD^a
Claudia Gandini Wheeler-Kingshott, PhD^{b,e}

^a Computer Vision and Robotics Group, Department of Computer Architecture and Technology, University of Girona, Spain.

^b NMR Research Unit, Queen Square MS Centre, Department of Neuroinflammation, UCL Institute of Neurology, London, United Kingdom.

^c Centre for Medical Image Computing, Department of Medical Physics and Bioengineering, University College London, United Kingdom.

^d National Institute for Health Research (NIHR) University College London Hospitals (UCLH) Biomedical Research Centre, London, United Kingdom.

^e Brain MRI 3T Mondino Research Center, C. Mondino National Neurological Institute, Pavia, Italy.

Correspondence to: Eloy Roura
E-mail: eloyroura@eia.udg.edu

Summary

Co-registration of structural T1-weighted (T1w) scans and diffusion tensor imaging (DTI)-derived fractional anisotropy (FA) maps to a common space is of particular interest in neuroimaging, as T1w scans can be used for brain segmentation while DTI can provide microstructural tissue information. While the effect of lesions on registration has been tackled and solutions are available, the issue of atrophy is still open to discussion. Multi-channel (MC) registration algorithms have the advantage of maintaining anatomical correspondence between different contrast images after registration to any target space. In this work, we test the performance of an MC registration approach applied to T1w and FA data using simulated brain atrophy images. Experimental results are compared with a standard single-channel registration approach.

Both qualitative and quantitative evaluations are presented, showing that the MC approach provides better alignment with the target while maintaining better T1w and FA co-alignment.

KEY WORDS: neuroimaging, registration, multiple sclerosis, atrophy.

Introduction

Nowadays, research studies in multiple sclerosis (MS) (Ashtari et al., 2014) involve the use of both conventional magnetic resonance imaging (MRI) (Goroku et al., 2011) and quantitative MRI methods such as diffusion-weighted (DW) imaging (DWI); these new MRI techniques are also used in other diseases affecting the brain (Baglieri et al., 2013). A key challenge in quantitative MRI analysis is the registration of scans to structural images that can be used to segment gray matter (GM), white matter (WM) and lesions. However, both lesions and tissue atrophy can adversely affect registration. While in this study we focus on MS, this can also be seen in other neurological conditions, particularly in older cohorts where age-related or vascular lesions are seen in combination with disease-related tissue atrophy, for example in subjects with Alzheimer's disease. The effects of lesions on registration and tissue segmentation have already been assessed on T1-weighted (T1w) volumetric scans, and techniques for minimizing them developed (Sdika et al. 2009; Chard et al., 2010; Battaglini et al., 2012; Ceccarelli et al., 2012). However, MS-associated atrophy (as shown in Fig. 1) is also a substantial issue, making registration inaccurate. This is particularly apparent when the target is a template based on healthy control data and the source scan is from a person with progressive MS, where ventricular enlargement may be prominent (as shown in Fig. 2) (Derakhshan et al., 2010). In such a situation very large deformations are required to bring the ventricles into alignment, and methods developed to work with healthy controls may fail.

In the case of multi-contrast regional studies a registration step is often also required to align several subjects to a template space while maintaining intra-subject alignment of images with different contrasts such as T1w scans and diffusion MRI-derived indices. Registration of multi-spectral MRI data is usually undertaken either independently for each modality or

using transformations determined by registering T1w structural scans. However, diffusion MRI metrics, such as fractional anisotropy (FA), also contain structural information complementary to that of T1w scans, and so using both simultaneously to guide image registration may improve alignment in multi-modal analysis (Park et al., 2003; Geng et al., 2012). Several registration strategies have been proposed over the last few years:

1. Single-channel (SC), where individual different contrast datasets are deformed independently. In situations where source and target images belong to different modalities, e.g., T1w, T2-weighted (T2w), DW, dif-

fusion tensor (DT), the registration is considered multi-modal (Wells et al., 1996; Ourselin et al., 2000; Guimond et al., 2001; Archip et al., 2007; Studholme, 2008; Klein et al., 2010; Walimuni et al., 2011), while if source and target images correspond to the same image modality the registration is mono-modal (Thirion, 1996, 1998; Rueckert et al., 1999, 2003; Studholme et al., 2004; Vercauteren et al., 2007, 2008; Modat et al., 2010a). In this work, a multi-modal strategy is used when intra-subject registration is performed, and a mono-modal one when we perform SC inter-subject registrations.

2. Single modality-based approaches, where only one dataset is used to estimate the deformations and the other datasets are deformed according to the first. In this work, we based the deformations on the T1w sequence (T1w-based).

3. Multi-channel (MC) registration processes where each space contains more than one modality to compute the deformation. A previous co-alignment between the images in each space (source and target) is needed. The MC approach performs a simultaneous registration of two different modalities to a specific target (Park et al., 2003; Miller et al., 1993; Guimond et al., 2002; Avants et al., 2007), exploiting the complementary information in images of different modalities. This solution was previously developed by Studholme (2008), who combined structural and full DT information into the same registration process. More recently, Daga et al. (2011) proposed a normalised mutual information (NMI) expression able to perform this MC registration in a more computationally efficient manner, although only using the FA information rather than the full tensor. The latter approach (Daga et al., 2011) is the one used in this work.

Registration of MRI images affected by lesions and atrophy to a healthy target space is challenging, but can be improved by taking care of some of the problems. There exist freely available algorithms that include lesion filling, e.g. at the websites of FSL (http://fsl.fmrib.ox.ac.uk/fsl/fslwiki/lesion_filling), SPM-LST (<http://www.applied-statistics.de/lst.html>), and SPM-SLF (<http://eia.udg.edu/salem/slfToolbox/software.html>), which allow lesion inpainting of T1w images in order to minimize biases in image intensity distributions. However, such algorithms have not yet been developed for other modalities, in particular for DT imaging (DTI)-derived indices. Fewer studies have proposed solutions to the issue of registering multiple images of different contrast also affected by severe atrophy to a common space. In this study we tackle the specific issue of improving alignment between T1w and FA data for a single subject after registration to a common space. This is a particular concern when dealing with MS subjects because of the differences in the extent of atrophy across subjects, who sometimes also show large ventricular enlargement (Fig. 2). In such cases, the substantial anatomical structural difference between the source and target images requires very large deformations. Furthermore, in MS, both MS lesions and atrophy affect the different MRI process-

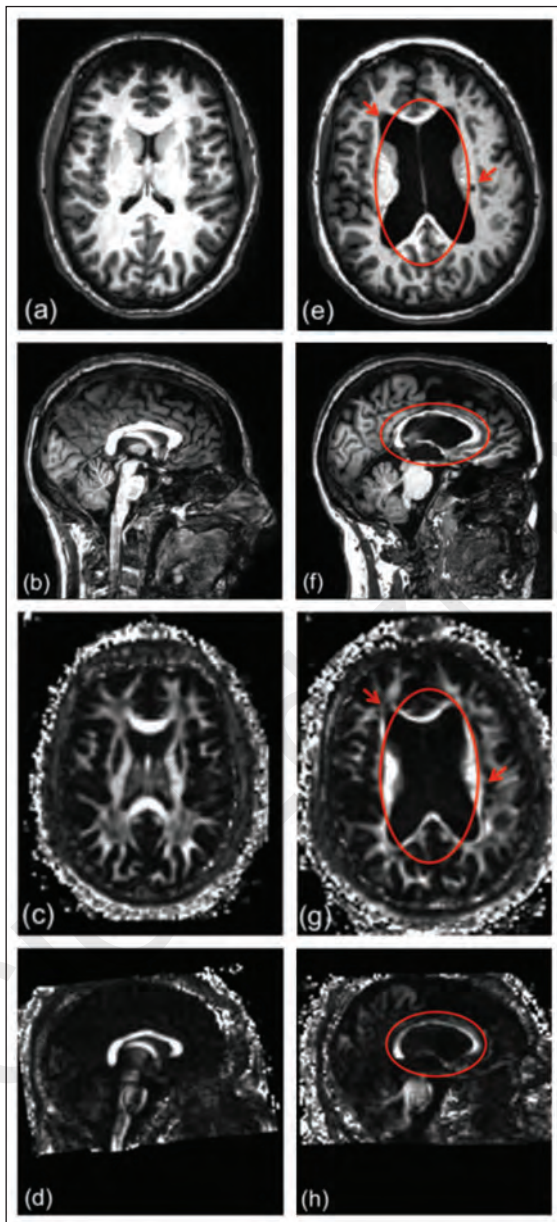


Figure 1 - Images in a healthy subject (on the left) and in an MS patient with ventricular enlargement and lesions (on the right). a,e) T1w axial images; b,f) T1w sagittal images; c,g) FA axial images; d,h) FA sagittal images. The lesions are circled in red.

ing tasks. However, as shown elsewhere (Battaglini et al., 2012; Roura et al., 2012), the presence of lesions does not significantly affect the quality of the registration process, while atrophy may introduce large segmentations and registration errors. Hence, in this work we will focus on the effects of atrophy on registration and propose techniques to limit this.

Multi-channel approaches may help by maintaining anatomical correspondence between T1w and FA images of each subject, after registration to any target space (e.g. to a healthy subject from the same study or to a common standard space). This is true even when large-scale deformations are necessary to match patient data to healthy targets. However, the specific registration of T1w and FA maps within the subject's space is not a simple task since the tissue contrast of these images is very different. In addition, these two modalities are often affected by different levels of partial volume effects due to differences in voxel sizes, as well as by sequence-specific image distortions.

The aim of our study is two-fold: first to demonstrate the validity of the MC registration approach for the registration of T1w and FA images to a target space, and second, to test whether the results obtained from the MC approach outperform those obtained with mono-modal SC registration or with the T1w-based approach. We therefore developed a new pipeline that includes a co-registration step between T1w and FA images followed by MC registration to a standard space. In order to achieve a good co-registration of T1w and FA images in the subject's space, T2w and non-DW (b0) images are also used.

In line with the work of Modat et al. (2010b), we propose to generate simulated brain atrophy images by using healthy control scans deformed to match scans from MS patients. This approach enables us to evaluate different registration approaches by registering these simulated images back to the unaltered healthy control scans. Previous studies have outlined a number of different algorithms that can be used to simulate atrophy for different specific applications (Camara et al., 2006; Karaçali and Davatzikos, 2006). However, there is no established method for simulating MS lesions on both T1w and FA images. In this study, therefore, we propose a simple method in which MS brains are simulated using Demons registration (DReg) of healthy subjects to MS subjects (Thirion, 1998; Vercauteren et al., 2008), whose images contain both MS lesions and atrophy, and an independent method is then used to test the registration of each atrophied dataset back to its original healthy subject. To evaluate the registration pipeline we performed both qualitative and quantitative analysis of the registration results, comparing the MC approach with standard SC registrations back to the original healthy subject images. In our study, 10 healthy subjects and 10 MS patients were used to generate 100 brain atrophy simulations. A qualitative evaluation using checkerboards and difference images as well as a quantitative analysis using the mean intensity difference are included in this work. Furthermore, in order to evaluate the impact of the lesions in the MS subjects, we also analyzed registration results when the MS lesions on T1w had been filled prior to the atrophy simulation.

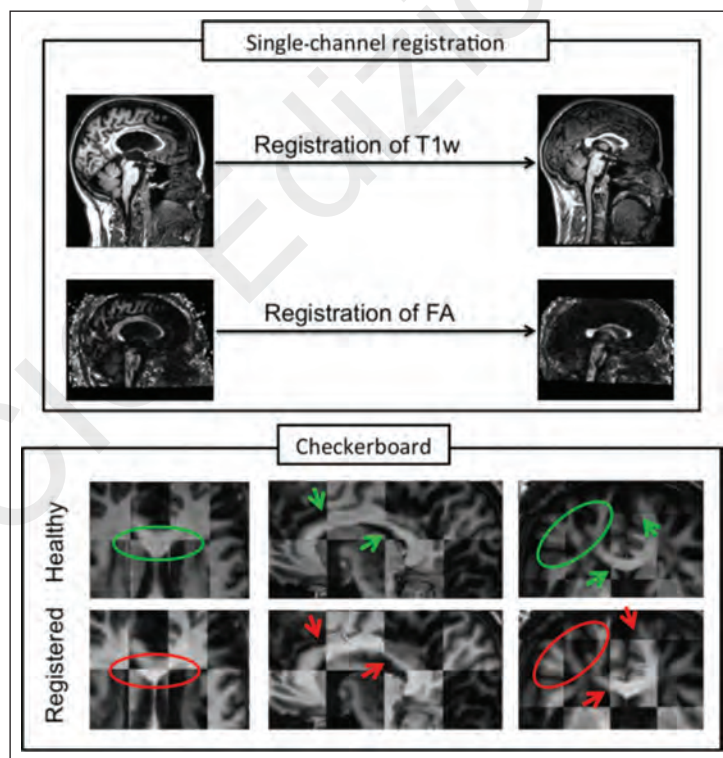


Figure 2 - Misalignment between T1w and FA brain images of an MS patient after registration to a healthy subject.

The box at the top shows the input images (original MS patient on the left and target healthy subject on the right). The box at the bottom shows: the checkerboard between T1w and FA of the original healthy subject (top row) and the checkerboard between the two output images of the single-channel registration (bottom row).

Methods

MRI data

SUBJECTS

Ten healthy subjects (mean age: 41.8 years, 4 males and 6 females) and 10 patients with MS (6 relapsing-remitting, 3 secondary progressive, 1 primary progressive, mean age: 41.6 years, 3 males and 7 females, mean disease duration: 13.2 years, median Expanded Disability Status Scale score = 2.5) were scanned on a 3T Philips Achieva scanner (Philips, Best, The Netherlands), with a 32-channel head coil.

MRI PROTOCOL

i) Dual echo proton density T2w scan: voxel size = 1 x 1 x 3 mm, TR = 3500 ms, TE = 19/85 ms; ii) three-dimensional (3D) fast-field echo T1w structural scan: voxel size = 1 x 1 x 1 mm, TR = 6.9 ms, TE = 3.1 ms, inversion time TI = 824 ms, field of view 256 x 256 x 180 sagittal slices; iii) DTI acquisition: cardiac-gated SE-EPI, TR \cong 24 s (depending on the subject's heart rate), TE = 68 ms, number of DW directions = 61 ($b = 1200 \text{ s/mm}^2$), number of non-DW (b_0) scans = 7, voxel size = 2 x 2 x 2 mm, SENSE acceleration factor = 3.1.

ATROPHY SIMULATIONS

From the 10 healthy subjects we generated a total of 100 simulations of atrophied brains. This was done by deforming the 10 healthy subjects into the native space of each of the 10 patients in order to introduce different rates of MS atrophy; for this purpose we used DReg. To generate the data for the testing purposes, T1w, FA, T2w and b_0 images were used, although here we evaluate only the performance of the registrations done using the T1w and FA images. Furthermore, another set of 100 simulations was generated after first filling the MS lesions (Chard et al.,

2010) on the T1w images, prior to performing the atrophy simulation.

Image processing

The image processing strategy presented in this work consists of three parts: i) pre-processing steps; ii) registration of T1w and FA images to a target space; and iii) evaluation of different registration pipelines (SC, MC and T1w-based).

PRE-PROCESSING

Pre-processing involves calculation of the DT maps, including FA maps, from the DW images (*DTI processing*), and the creation of MC datasets for each subject (*intra-subject registration*) to be used in the creation of the simulated atrophy data (*simulated atrophy data*).

DTI processing. The DTI dataset was first corrected for eddy current distortions using the eddy_correct command from the FMRIB Software Library (<http://www.fmrib.ox.ac.uk/fsl>), assuming a linear co-registration between all the 3D volumes, with the first b_0 image being taken as the reference image. The free open-source toolkit Camino (<http://www.camino.org.uk>) was then used to fit the DT and compute the FA in each voxel in the space of the first b_0 image. For anatomical reference and registration purposes, we also computed the average b_0 image, after the co-registration step, from seven non-DW b_0 images acquired as part of the DTI dataset.

Intra-subject registration. To perform the registration of T1w and FA images to a common space, it is essential to first align these images in the subject's native space. We registered the FA images to the T1w data in native space in order to retain the information from the higher resolution of these scans.

Figure 3 shows the overall scheme for co-registering T1w and FA images. For each of the 10 healthy subjects and 10 MS patients' datasets we performed the following steps:

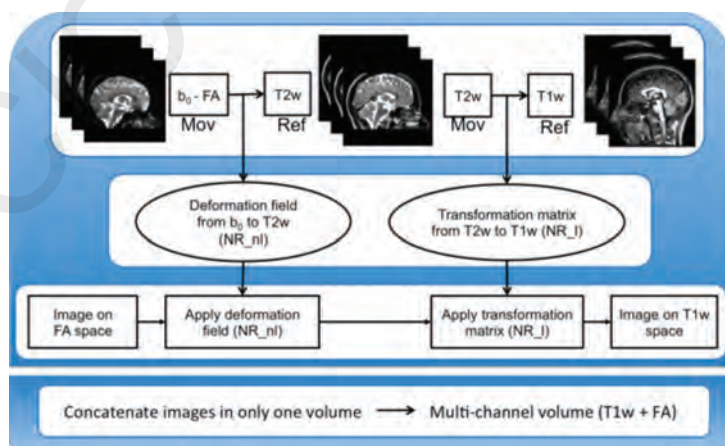


Figure 3 - Pipeline for the generation of the multi-channel data (T1w + FA).

Ref = reference image; Mov = moving image; NR_l = NiftyReg linear; NR_nl = NiftyReg non-linear.

1. The average b0 volume was aligned to the corresponding anatomical T2w using a non-rigid registration method from NiftyReg (<http://cmic.cs.ucl.ac.uk/home/software>) (Modat et al., 2010a) to correct for EPI-induced distortions in the DW data (Muhlert et al., 2013).
2. The T2w images were then aligned with the T1w images via affine registration with NiftyReg (Ourselin et al., 2000, 2001, 2002).
3. The composition of the deformation field (b0 to T2w, computed at step 1) and the transformation matrix (T2w to T1w, computed at step 2) allows us to transform images from the DTI space to the T1w space (and vice versa). This transformation was then applied to FA maps to obtain FA co-registered to T1w data in native space. The co-registered images (FA and T1w) obtained in this step were used as target images in the SC and T1w-based registration strategies of the simulated atrophy datasets, and concatenated to generate the MC data of T1w and DW images in native space, needed as the input for the MC registration.

Once the MC data had been created, we had all the data needed to test the registration of T1w and FA images to a target space using either an MC or an SC registration method. We always combined subsequent transformations in order to apply a single interpolation to the data and avoid interpolation-related biases and errors.

Simulated atrophy data. The strategy used to generate these simulations consists of three steps (Fig. 4):

1. Deformation of each T1w image from a healthy subject space to each MS patient space. This registration uses the NiftyReg software (Ourselin et al., 2000, 2001, 2002; Modat et al., 2010a) for rigid and affine registration and DReg (Vercauteren et al., 2008) for the deformation process.
2. Transportation of each healthy subject's FA map into the same subject's T1w space using the intra-subject registration pipeline as detailed above (Fig. 3).
3. Application of atrophy deformation, obtained in step 1 using the T1w image, to the aligned FA map resulting from step 2.

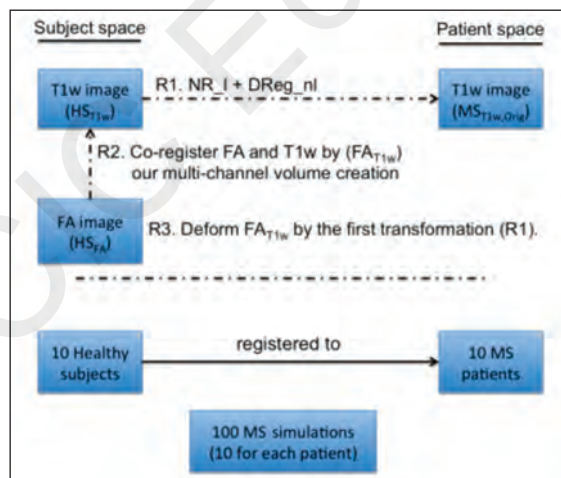


Figure 4 - Pipeline used to simulate atrophy in healthy subjects. NR_I = NiftyReg linear registration (rigid+affine); DReg = Demons registration. R1, R2, and R3 refer to the three registration steps performed in this pipeline.

These three steps were performed for each of the 10 healthy subjects to match them to each of the 10 MS patients (Fig. 4) in such a way that we obtained 100 simulated atrophy datasets, derived from original MS subjects and also containing MS lesions. This set of data was used for evaluating the registration performance. Henceforth we will refer to the 10 healthy subjects' dataset as HS_{T1w} , HS_{FA} and HS_{MC} . The original 10 MS subjects' datasets will be referred to as $MS_{T1w,Orig}$, $MS_{FA,Orig}$ (an MC dataset from the original MS patients was not created as they were used only as the targets to simulate atrophy). The 100 datasets deformed to simulate MS will be the input of the registrations and will be referred to as $MS_{T1w,Sim}$, $MS_{FA,Sim}$ and $MS_{MC,Sim}$. Note that first subindex refers to the image modality and the second to the specific subset.

It is important to note that DReg is a symmetric log-domain diffeomorphic registration algorithm that deforms the input source image ($I_{source}(x,y,z)$) into the target image ($I_{target}(x,y,z)$) returning both the deformation field T and the inverse deformation field T^{-1} (both consisting of a vector field where each vector is applied to each voxel). Those two deformations allow transformation of either the input $I_{source}(x,y,z)$ into the resultant image ($R_D(x,y,z)$) by T , or the inverse by T^{-1} . The inverse transformation of the atrophy generation provides us with the ground truth that is needed to evaluate how well our registration approach can recover the simulated atrophy.

To summarize, *DReg* receives $I_{source}(x,y,z)$ and $I_{target}(x,y,z)$ and outputs:

$$DReg(I_{source}(x,y,z), I_{target}(x,y,z)) \rightarrow [R_D(x,y,z), T_D, T_D^{-1}]; \quad [1]$$

where $R_D(x,y,z)$, T_D and T_D^{-1} are the output image and the transformations T mentioned earlier. Here I_{source} , I_{target} and R_D are HS_{T1w} , $MS_{T1w,Orig}$ and $MS_{T1w,Sim}$ respectively. The non-linear registration method used in this step of atrophy generation was performed using the Symmetric Log-Domain Diffeomorphic Demons Algorithm (Vercauteren et al., 2008), which has the advantage over previous Demons algorithms of providing the inverse of the spatial transformation. Demons is an iterative optimization procedure, which tries to minimize the cost function based on the sum of squared differences of the two images (I_{source} and I_{target}) plus the regularization of a Gaussian kernel by a second order optimization method.

Using this atrophy simulation procedure we also created another set of 100 simulations in which, in accordance with the approach of Chard et al. (2010), the lesions on $MS_{T1w,Regj}$ (with $j = SC, T1w$ -based and MC) images were filled before performing the registration of the HS_{T1w} to each MS patient space (step 1).

Registration

In this section we focus on the main purpose of this work, which is to use an MC approach based on the work of Daga et al. (2011), which, in turn, is based on the Free Form Deformation (FFD) algorithm of

Rueckert et al. (1999), and to compare it with classical SC approaches. The three different strategies evaluated in this study and explained here below all start from the co-registered $MS_{T1w,Sim}$ and $MS_{FA,Sim}$ images, and the $MS_{MC,Sim}$ obtained from the data preparation in the pre-processing step, as well as the HS_{T1w} , the HS_{FA} and the HS_{MC} . Note that Demons is based on a non-parametric approach that includes a Gaussian smoothing kernel, while FFD is a parametric model that uses B-Splines. Therefore, the two transformation models are independent, and recovering simulated deformation created with the Demons using FFD is appropriate and unbiased.

The FFD algorithm consists of the same main registration steps, i.e. the optimization of a cost function, transformation of the moving image and interpolation function. The similarity measure used by Modat et al. (2010b) is based on the NMI. This measure is regularized by adding a penalty term (bending energy) computed at the control point positions in order to smooth the transformation. This cost function is optimized by the conjugate gradient ascent. The transformation model locally deforms the moving image using cubic B-Splines. Moreover, as stated by Daga et al. (2011), when the MC approach is used a reformulation of the NMI is needed.

Therefore, after deforming the original healthy subject images ($I_{source}(x,y,z)$) into simulated atrophy images ($R_D(x,y,z)$) by registering them to the MS patients ($I_{target}(x,y,z)$) we recovered the simulated atrophy with the NiftyReg software, *NReg*, by registering the $R_D(x,y,z)$ images back to the original subject data ($I_{source}(x,y,z)$). *NReg* receives $R_D(x,y,z)$ and $I_{source}(x,y,z)$ and outputs:

$$NReg(R_D(x,y,z), I_{source}(x,y,z)) \rightarrow [R_N(x,y,z), T_N]; \quad [2]$$

The result of this registration, where $R_N(x,y,z)$ is the warped image and T_N is the deformation field, is compared with the original image, I_{source} , where an ideal registration should give:

$$T_N(R_D(x,y,z)) = T_D^{-1}(R_D(x,y,z)); \quad [3]$$

where $R_D = MS_{i,Sim}$, $I_{source} = HS_j$ and $R_N = MS_{i,Reg}$, with $i = T1w, FA, MC$ and $j = SC, T1w$ -based, MC respectively. The process explained above is used to compare the performance of the three different registration strategies, when registering the 100 simulations to the original healthy subjects:

1. *Mono-modal single-channel registration.* Each specific modality, $MS_{T1w,Sim}$ and $MS_{FA,Sim}$ is registered to its corresponding target modality, HS_{T1w} and HS_{FA} respectively, as schematically shown in figure 5a. We use the registration of Modat et al. (2010a). The output of these registrations are noted as $MS_{T1w,RegSC}$ and $MS_{FA,RegSC}$ respectively.

2. *T1w-based registration.* In this registration approach the deformation of one modality is used as a transformation model for all the source images. We refer to this strategy as a one modality-based SC

approach, which in our experiments applies the transformations from $MS_{T1w,Sim}$ to HS_{T1w} also to transform $MS_{FA,Sim}$ into the target space, HS_{FA} . This strategy is schematically represented in figure 5b. The output of this registration will be $MS_{T1w,RegT1w-based}$ and $MS_{FA,RegT1w-based}$.

3. *Multi-channel registration.* Conversely to the SC approaches 1) and 2), here the different modalities are merged into one MC dataset for both source, $MS_{MC,Sim}$, and target, HS_{MC} images. This approach is based on the work presented by Daga et al. (2011) where the NMI similarity measure from Modat et al. (2010a) was re-edited to share the information of different modalities during registration. Figure 5c illustrates the MC approach, where the images are simultaneously registered to the target. The output of this registration will be $MS_{T1w,RegMC}$ and $MS_{FA,RegMC}$.

Evaluation

We evaluate the performance of the registration in two ways using simulated atrophy and its recovery: i) using a qualitative analysis based on a checkerboard image (visual agreement); ii) calculating the mean intensity of the absolute value of the difference images.

CHECKERBOARD IMAGE

The checkerboard between the registered T1w and FA images allows visual inspection of alignment accuracy

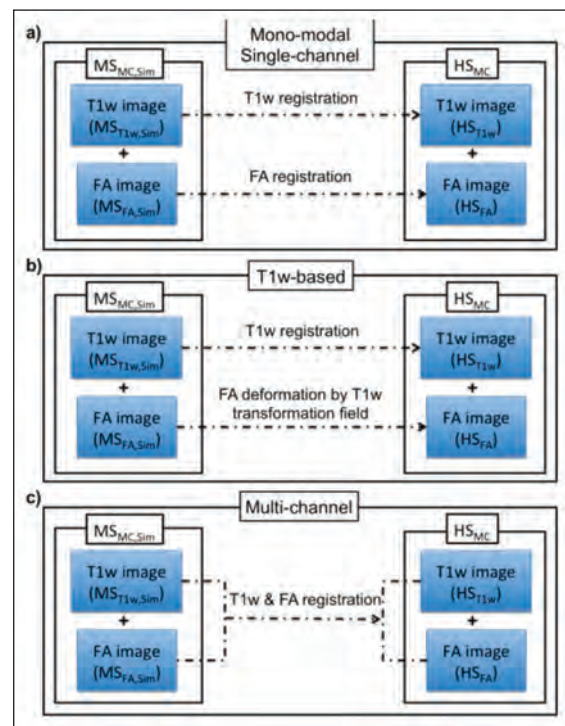


Figure 5 - Three different registration strategies compared in the analysis of the experimental results.

based on the continuity of structural features and it shows: i) how well the registration process works in terms of matching the source image to the target image; ii) how well different source image modalities, e.g. T1w and FA, are aligned to each other in the target space.

DIFFERENCE IMAGE

Here the registration performance is assessed within each modality using a global rather than a local index. A difference image $D(x,y,z)$ is calculated using the target ($I_{\text{target}}(x,y,z)$) and the registered image ($R_n(x,y,z)$) of the same modality (e.g. HS_{FA} and $MS_{FA,Regj}$ respectively, or HS_{T1w} and $MS_{T1w,Regj}$ with $j = SC, T1w\text{-based}, MC$), and it is assumed that better registration corresponds to a lower overall mean value.

These difference images have been used in previous applications, i.e. to help localize MS lesion changes in longitudinal studies (Lladó et al., 2012) or to detect anatomical structures in medical images (Diez et al., 2011). For each registration method (Fig. 5) we computed $D(x,y,z)$, performing a voxel-wise subtraction between the original subject (target in each registration) and the registration result. To compute $D(x,y,z)$, the results of each registration method were normalized due to the vastly different intensities that may appear in the T1w images. We chose to normalize to the CSF, because WM and GM may differ in T1w images from healthy and from MS subjects. Therefore, we considered the ratio: intensity voxel divided by mean of the CSF. Furthermore, we quantified the mean of $D(x,y,z)$, $Mean_D$, which provides a quantitative measure of the goodness of the registration methods, where the smaller $Mean_D$ is, the more accurate the registration. Note that to compute the difference we always used the absolute values.

In order to assess the registration performance at tissue-class level, $Mean_D$ was computed for the whole brain as well as for WM and GM masks. The whole brain mask was obtained using the Brain Extraction Tool (<http://fsl.fmrib.ox.ac.uk/fsl/fslwiki/BET>) (Smith, 2002) while the tissue class segmentation was performed using the SPM8 toolbox (<http://www.fil.ion.ucl.ac.uk/spm>) (Ashburner and Friston, 2005). However, as the result of the segmentation is a probability map per tissue type, we performed a maximum likelihood operation to identify voxels belonging to masks of GM and WM, which were computed by assigning each voxel the class of maximum likelihood (probability threshold 0.5).

To assess whether $Mean_D$ values were significantly different when calculated for each registration method, the Bonferroni correction test (Holm, 1979) was performed to counteract multiple comparisons. To analyze the statistical significance of these comparisons, we carried out a one-way ANOVA to compare the performance of the different methods, considering as a null hypothesis (H_0) that the means are equal with a 5% confidence level ($\alpha = 0.05$).

Results

Data processed in the pre-processing section were then used for all the registration experiments, with original healthy subjects (10 cases) as target and simulated MS subjects (100 cases) as source. We repeated these experiments with the MS subjects in which lesions had first been filled, before simulation. Figure 6 shows an example of the images through the various steps for SC registration (original, simulated and registered).

Checkerboard evaluation

The first assessment was based on qualitative analyses using the checkerboard images to compare how the structures were aligned with each other for each combination of images: i) T1w result vs T1w target; ii) FA result vs FA target; and iii) T1w result vs FA result. This was performed for SC, MC and T1w-based registrations (as summarized in figure 4). In this stage, as well as comparing against the target, we checked whether the registration process kept the original alignment between T1w and FA for each registration approach.

In particular, we carefully inspected the alignment of the corpus callosum, which is very close to the ventricles, and can therefore be affected by their large enlargement, and can undergo thinning as a result of pathology but also of large image processing deformations, especially when registered to a healthy brain. Also, we assessed the cortical regions because their low FA values make them challenging to register properly with T1w. Figure 7 provides an illustration of the combined results for each registration strategy and each modality for one of the simulated MS datasets, with large deformations due to severe simulated atrophy.

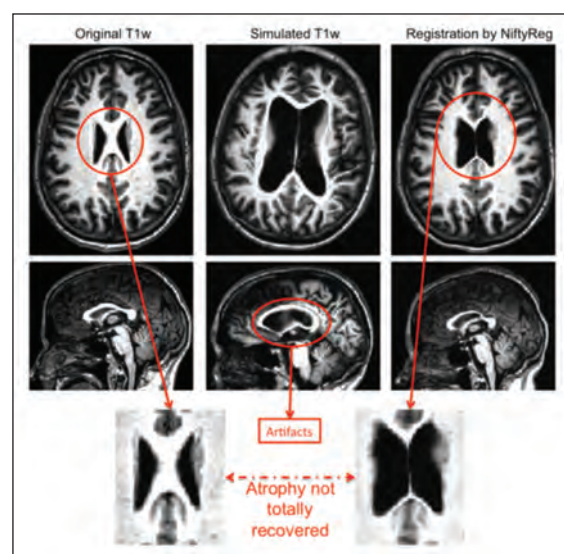


Figure 6 - Original atrophied and registered T1w images. The bottom row illustrates the problem of the registration back to the original healthy subject, using a single-channel registration pipeline, where the software is not able to recover the ventricles.

On visual inspection we observed that:

1. When employing the SC approach in the presence of a high level of atrophy the registration cannot recover structures like the corpus callosum and therefore the alignment with the target image is not accurate. Moreover, poor structure alignment is also observed when comparing the co-alignment of $MS_{T1w,RegSC}$ and $MS_{FA,RegSC}$ in the target space, e.g. the FA WM structures do not match the WM structures on the T1w image.
2. When employing the T1w-based registration approach, similar results are noticeable when comparing the results of the registration between the same modality source and target images, e.g. $MS_{FA,RegT1w-based}$ and HS_{FA} or $MS_{T1w,RegT1w-based}$. As expected, though, the co-alignment of T1w and FA images in the target

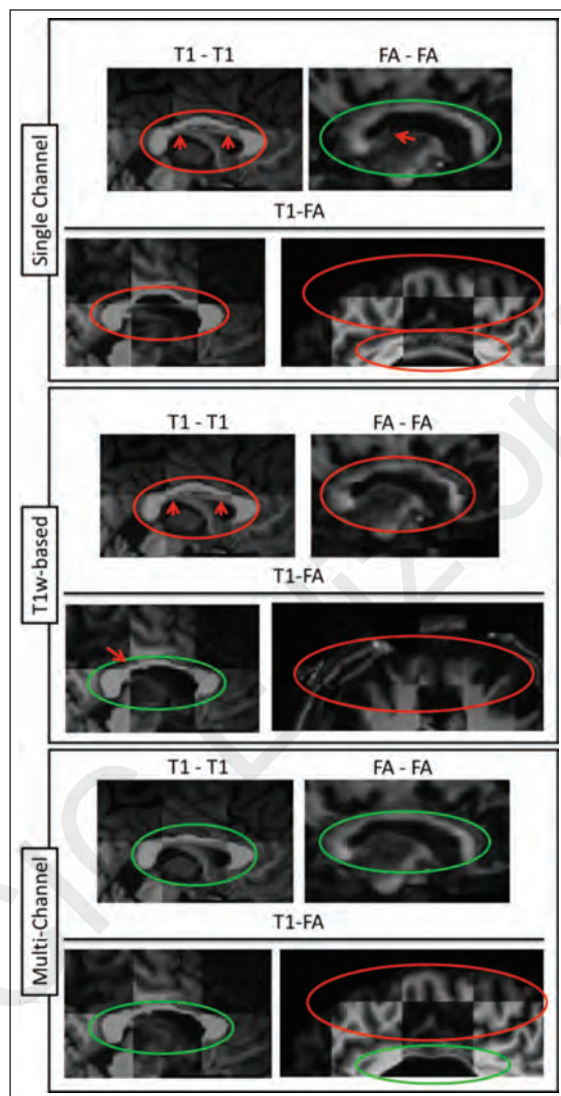


Figure 7 - Checkerboard images of all the combinations for the three strategies (SC, T1w-based and MC). The top row of each strategy corresponds to T1w-T1w and FA-FA comparisons separately while the second row corresponds to comparison of T1w-FA results. Orange circles show regions of poor registration, whereas green circles show regions of accurate registration.

space, e.g. of $MS_{FA,RegT1w-based}$ with $MS_{T1w,RegT1w-based}$ is better due to their initial co-registration.

3. Finally, when employing the MC approach the corpus callosum of the registered images, $MS_{FA,RegMC}$ and $MS_{T1w,RegMC}$, is better aligned with the corresponding target images, HS_{FA} and HS_{T1w} , compared to what is observed with the SC method, for both T1w and FA data. Due to the inherent co-registration of $MS_{FA,RegMC}$ and $MS_{T1w,RegMC}$, structures are well matched even across modalities.

Difference image evaluation

The difference image between $MS_{T1w,Regj}$ and HS_{T1w} was computed for all simulated data and for $j = SC, MC$ (Fig. 8), while the difference image for FA was computed for $j = SC, T1w-based, MC$ (Fig. 8).

On visual inspection, SC registration was associated with higher intensity differences between registered and target T1w images in the corpus callosum and periventricular areas. T1w-based registration was associated with higher intensity differences for FA images. The MC approach provided the lowest intensity differences for both T1w and FA images. This was confirmed in all the simulated data and registration tests.

To corroborate the visual results, we compared the $Mean_D$ image between the different registration methods shown in figure 9. SC and MC registrations produced similar results on T1w over the whole brain or the GM mask. No consistent pattern was observed on the T1w registrations of the WM mask. For registration of FA images, the MC approach presented lower mean difference values for all cases (whole brain, WM mask and GM mask; Fig. 9).

Last, we assessed whether the $Mean_D$ scores differed between the SC and MC registrations. Analyzing the Bonferroni test, we observed that for T1w images, SC and MC approaches showed no significant differences. Instead, for FA images, the MC approach led to significantly lower $Mean_D$ for whole brain, GM and WM masks ($p < 0.01$). This can be explained by the fact that the T1w image provides information for example in GM regions where FA presents very low contrast. We conclude that MC registration provides better alignment to a target as well as better T1w and FA co-alignment in target space.

Simulated images with lesions filled

Similarly to the results presented before, the registration strategies for both T1w and FA images followed a similar trend when registering the simulated images with the MS lesions-filled T1w dataset, obtaining better FA and T1w image alignment with MC. We performed statistical analysis using the Bonferroni test obtaining significant differences between strategies ($p < 0.01$). On the other hand, we also performed a balanced one-way ANOVA analysis individually for each registration strategy (SC, T1w-based and MC)

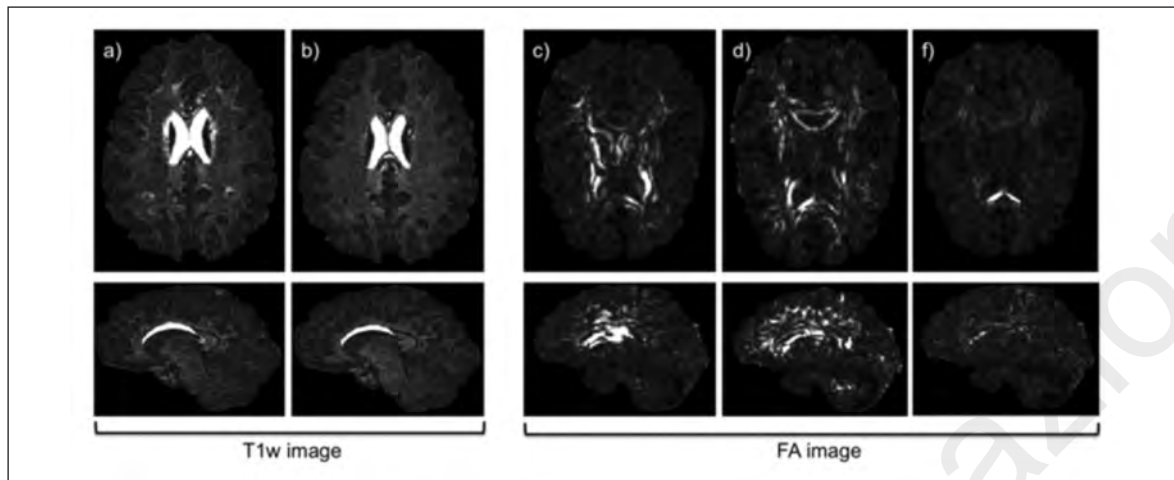


Figure 8 - Difference image of T1w and FA from SC, MC and T1w-based approach. Difference of T1w images from a) SC and b) MC results. Difference between FA images for c) SC registration, d) T1w-based approach, and e) MC registration. The brighter the voxels the greater the differences. All the images are from the same subject at the same location where first row are axial and second row are sagittal image orientations. The range of intensities has been optimized for better visualization of the differences (voxel values range in all the images from 0 to 1).



Figure 9 - Bar plot of the mean intensity of the difference image for the T1w images on the left and FA images on the right. Values for each patient (319, 342, ... 739) are the mean of the 10 MS simulations; the error bar illustrates the standard deviation.

between simulated images with lesions and simulated images with lesions filled. The p-values obtained in all cases did not suggest to reject the null hypothesis ($p \gg 0.05$), confirming that the effect of the MS lesions was not significant in the proposed atrophy simulation. Figure 10 illustrates the results obtained for the $MS_{FA, RegMC}$ when using both the original and lesion-filled simulations.

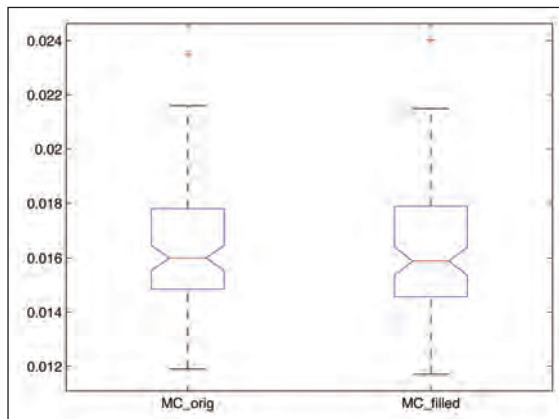


Figure 10 - Boxplot of the MC registration results when using the original and lesion-filled simulations.

Differences are computed between the $MS_{FA, RegMC}$ result image and the original HS_{FA} .

Discussion

Registration of the individual T1w images to the target space showed similar performances between the mono-modal SC, T1w-based and MC approaches. This may relate to the well-defined tissue contrast between GM and WM on these images, but could also be due to preserved signal in GM, allowing the SC approach to perform well. On the FA maps, however, both qualitative and quantitative evaluations demonstrated significantly better registration when the MC approach was used. This was apparent on whole brain, GM and WM alignment. It was also reflected in the alignment of FA with T1w data after registration, which provided substantially greater accuracy when using the MC strategy. We also demonstrated that MC, compared to SC and T1w-based, offers improved results of T1w and FA co-registration in common space; even though both MC and T1w-based strategies rely on initial co-registration of FA and T1w in native space, the final direct alignment, i.e. T1w and FA alignment, in common space was significantly better for MC techniques.

An important point to consider in this experimental analysis is that the SC approach provided good co-registration between the input image and the target space. This may not be the case in real patient data, where it is well known that WM and GM contain lesions, causing localized and sometimes diffuse intensity changes across the whole brain. In our simulations we evaluated the effect of atrophy, but not focal

intensity changes, such as the WM lesions that are characteristic of MS. The rationale for our choice to concentrate on atrophy was highlighted in the introduction and rested on the fact that the influence of WM lesions on registration outcomes is limited when it comes to the whole brain (Roura et al., 2012). This was also shown when repeating the experiments using simulations created using previously lesion-filled T1w images from MS subjects. Moreover, strategies to cope with lesions, such as inpainting, have been proposed and validated only for the T1w modality (Sdika and Pelletier, 2009; Chard et al., 2010; Battaglini et al., 2012), while they still need to be developed for DTI-derived indices such as FA where local properties of signal intensities are far from uniform even within a specific tissue type. Furthermore, it is important to consider standard target spaces such as the MNI atlas or a group-specific atlas built with MS patient data, which could simplify registration of patient scans.

Despite the clear improvements presented in this work, there are some limitations that should be addressed in future studies. For instance, we generated simulated atrophy by registering T1w images of healthy controls to T1w images of MS patients and then we applied the same transformation to FA images of the same subjects. This procedure ensured that the FA and T1w images were deformed equally, but it did not accurately reproduce the presence of MS lesions. Previous evaluations, though, confirmed that lesions have minimal effect on MC (T1w and FA) registration to a common space (Battaglini et al., 2012; Roura et al., 2012), therefore justifying the use of the proposed strategy as a simple means of atrophy generation without having to explicitly consider MS lesions. Following previous work presented by Daga et al. (2011), we focused on the evaluation of an MC pipeline applied to T1w and FA images. However, it is well known that other indices from the DTI matrix or even other imaging modalities could provide complementary information and could also be used for the MC registration pipeline.

In conclusion, this paper has presented an MC registration approach for moving T1w and FA images to a healthy control target space. The registration pipeline was tested in people with MS with atrophy and marked ventricular enlargement. For the experimental evaluation, we proposed our own atrophy generation framework based on deforming healthy subjects by registering them to real MS patients with MS lesions and atrophy. We created 100 simulated atrophy images from original healthy subjects who were registered to the patients. A comparison between SC and MC registration with qualitative and quantitative analysis has been presented. We have shown that for FA, more than for T1w images, MC registration offers significant improvements in alignment accuracy over SC or T1w approaches. Studies registering FA maps to common space should consider using MC registrations in preference to SC or T1w-based pipelines.

Acknowledgments

E. Roura holds a UdG BR-GR13 grant. The International Federation of MS (Du Pré Grant 2012) granted E. Roura a research stay in IoN/UCL. Declan Chard has received research support from the MS Society of Great Britain and Northern Ireland, and the UCLH/UCL NIHR Biomedical Research Centre. This work has also been partially supported by “La Fundació la Marató de TV3” and by Retos de Investigación TIN2014-55710-R.

References

- Archip N, Clatz O, Whalen S, et al (2007). Non-rigid alignment of pre-operative MRI, fMRI, and DT-MRI with intra-operative MRI for enhanced visualization and navigation in image-guided neurosurgery. *Neuroimage* 35:609-624.
- Ashburner J, Friston KJ (2005). Unified segmentation. *Neuroimage* 26:839-851.
- Ashtari F, Bahreini SA, Zahendasab H (2014). Co-occurrence of multiple sclerosis and Thomsen’s myotonia: a report of two cases. *Funct Neurol* 29:269-271.
- Avants BB, Duda JT, Zhang H, et al (2007). Multivariate normalization with symmetric diffeomorphisms for multivariate studies. *Med Image Comput Comput Assist Interv* 10:359-366.
- Baglieri A, Marino MA, Morabito R, et al (2013). Differences between conventional and non-conventional MRI techniques in Parkinson’s disease. *Funct Neurol* 28:73-82.
- Battaglini M, Jenkinson M, De Stefano N (2012). Evaluating and reducing the impact of white matter lesions on brain volume measurements. *Hum Brain Mapp* 33:2062-2071.
- Camara O, Schweiger M, Scahill RI, et al (2006). Phenomenological model of diffuse global and regional atrophy using finite-element methods. *IEEE Trans Med Imaging* 25:1417-1430.
- Ceccarelli A, Jackson JS, Tauhid S, et al (2012). The impact of lesion in-painting and registration methods on voxel-based morphometry in detecting regional cerebral gray matter atrophy in multiple sclerosis. *AJNR Am J Neuroradiol* 33:1579-1585.
- Chard DT, Jackson JS, Miller DH, et al (2010). Reducing the impact of white matter lesions on automated measures of brain gray and white matter volumes. *J Magn Reson Imaging* 32:223-228.
- Daga P, Winston G, Modat M, et al (2011). Integrating structural and diffusion MR information for optic radiation localisation in focal epilepsy patients. *Proc IEEE Int Symp Biomed Imaging* 2011: 353-356.
- Derakhshan M, Caramanos Z, Giacomini PS, et al (2010). Evaluation of automated techniques for the quantification of grey matter atrophy in patients with multiple sclerosis. *Neuroimage* 52:1261-1267.
- Díez Y, Oliver A, Lladó X, et al (2011). Revisiting intensity-based image registration applied to mammography. *IEEE Trans Inf Technol Biomed* 15:716-725.
- Geng X, Styner M, Gupta A, et al (2012). Multi-contrast diffusion tensor image registration with structural MRI. *Proc IEEE Int Symp Biomed Imaging* 2012: 684-687.
- Goruku Y, Albayram S, Balci B, et al (2011). Cerebrospinal fluid flow dynamics in patients with multiple sclerosis: a phase contrast magnetic resonance study. *Funct Neurol* 26:215-222.
- Guimond A, Guttmann CRG, Warfield SK, et al (2002). Deformable registration of DT-MRI data based on transformation invariant tensor characteristics. *Proc IEEE Int Symp Biomed Imaging* 2002:1-4.
- Guimond A, Roche A, Ayache N, et al (2001). Three-dimensional multimodal brain warping using the demons algorithm and adaptive intensity corrections. *IEEE Trans Med Imaging* 20:58-69.
- Holm S (1979). A Simple Sequentially Rejective Multiple Test Procedure. *Scand Stat Theory Appl* 6:65-70.
- Karaçali B, Davatzikos C (2006). Simulation of tissue atrophy using a topology preserving transformation model. *IEEE Trans Med Imaging* 25:649-652.
- Klein S, Staring M, Murphy K, et al (2010). Elastix: a toolbox for intensity-based medical image registration. *IEEE Trans Med Imaging* 29:196-205.
- Lladó X, Ganiler O, Oliver A, et al (2012). Automated detection of multiple sclerosis lesions in serial brain MRI. *Neuroradiology* 54:787-807.
- Miller MI, Christensen GE, Amit Y, et al (1993). A mathematical textbook of deformable neuroanatomies. *Proc Natl Acad Sci USA* 90:11944-11948.
- Modat M, Ridgway G, Hawkes D, et al (2010a). Nonrigid registration with differential bias correction using normalised mutual information. *Proc IEEE Int Symp Biomed Imaging* 2010:356-359.
- Modat M, Ridgway GR, Taylor ZA, et al (2010b). Fast free-form deformation using graphics processing units. *Computer Methods Programs Biomed* 98:278-284.
- Muhlert N, Sethi V, Schneider T, et al (2013). Diffusion MRI-based cortical complexity alterations associated with executive function in multiple sclerosis. *J Magn Reson Imaging* 38:54-63.
- Ourselin S, Stefanescu R, Pennec X (2002). Robust registration of multi-modal images: towards real-time clinical applications. In: Dohi T, Kikinis R (Eds.) *Medical Image Computing and Computer-Assisted Intervention – MICCAI 2002*, Berlin Heidelberg, Springer, pp 140-147.
- Ourselin S, Roche A, Subsol G, et al (2001). Reconstructing a 3D structure from serial histological sections. *Image and Vision Computing* 19:25-31.
- Ourselin S, Roche A, Prima, S, et al (2000). Block matching: a general framework to improve robustness of rigid registration of medical images. In: Delp SL, DiGioia AM, Jaramaz B (Eds.) *Medical Image Computing and Computer-Assisted Intervention – MICCAI 2000*, Berlin Heidelberg, Springer, pp. 557-566.
- Park HJ, Kubicki M, Shenton ME, et al (2003). Spatial normalization of diffusion tensor MRI using multiple channels. *Neuroimage* 20:1995-2009.
- Roura E, Schneider T, Daga P, et al (2012). Multi-channel registration of FA and T1-weighted images to standard space: patients with multiple sclerosis. *ISMRM (abstract 2525)* (<http://discovery.ucl.ac.uk/1410585>)
- Rueckert D, Frangi AF, Schnabel JA (2003). Automatic construction of 3-D statistical deformation models using non-rigid registration. *IEEE Trans Med Imaging* 22:1014-1025.
- Rueckert D, Sonoda LI, Hayes C, et al (1999). Nonrigid registration using free-form deformations: application to breast MR images. *IEEE Trans Med Imaging* 18:712-721.
- Sdika M, Pelletier D (2009). Nonrigid registration of multiple sclerosis brain images using lesion inpainting for morphometry or lesion mapping. *Hum Brain Mapp* 30:1060-1067.
- Smith SM (2002). Fast robust automated brain extraction. *Hum Brain Mapp* 17:143-155.
- Studholme C (2008). Dense feature deformation morphometry: incorporating DTI data into conventional MRI morphometry. *Med Image Anal* 12:742-751.

- Studholme C, Cardenas V, Song E, et al (2004). Accurate template-based correction of brain mri intensity distortion with application to dementia and aging. *IEEE Trans Med Imaging* 23:99-110.
- Thirion JP (1998). Image matching as a diffusion process: an analogy with Maxwell's demons. *Med Image Anal* 2:243-260.
- Thirion JP (1996). Non-rigid matching using demons. *Proceedings of the 1996 Conference on Computer Vision and Pattern Recognition*: 245-251. Doi: 10.1109/CVPR.1996.517081
- Vercauteren T, Pennec X, Perchant A, et al (2008). Symmetric log-domain diffeomorphic Registration: a demons-based approach. *Med Image Comput Comput Assist Interv* 11:754-761.
- Vercauteren T, Pennec X, Perchant A, et al (2007). Non-parametric diffeomorphic image registration with the demons algorithm. *Med Image Comput Comput Assist Interv* 10:319-326.
- Walimuni IS, Abid H, Hasan KM (2011). A computational framework to quantify tissue microstructural integrity using conventional MRI macrostructural volumetry. *Comput Biol Med* 41:1073-1081.
- Wells WM, Viola P, Atsumi H, et al (1996). Multi-modal volume registration by maximization of mutual information. *Med Image Anal* 1:35-51.

A toolbox for multiple sclerosis lesion segmentation

In this chapter, we present a new toolbox to segment WML of MS patients. This method is based on the outlier thresholding of GM brain tissue on the FLAIR images followed by a set of FP reduction rules. To prove the robustness of the method, we have evaluated its performance with more than 100 MRI scans of different nature, including data from the MICCAI Challenge 2008, where we have submitted our results.

The proposed method has been published in the following paper:

Paper published in *Neuroradiology*

Volume: 57, Issue: 10, Pages: 1031-1043. Published: October 2015.

DOI: 10.1007/s00234-015-1552-2

JCR RNMMI IF 2.485, Q2(41/125)

Eloy Roura, Arnau Oliver, Mariano Cabezas, Sergi Valverde, Deborah Pareto, Joan Carles Vilanova, Lluís Ramillo-Torrent, Àlex Rovira and Xavier Lladó. "A toolbox for multiple sclerosis lesion segmentation". *Neuroradiology*. Vol. 57, Issue 10 (2015) : 1031-1043

<http://dx.doi.org/10.1007/s00234-015-1552-2>

<http://link.springer.com/article/10.1007%2Fs00234-015-1552-2>

Received: 26 February 2015 / Accepted: 16 June 2015 / Published online: 31 July 2015

Introduction

Lesion segmentation plays an important role in the diagnosis and follow-up of multiple sclerosis (MS). This task is very time-consuming and subject to intra- and inter-rater variability. In this paper, we present a new tool for automated MS lesion segmentation using T1w and fluid-attenuated inversion recovery (FLAIR) images.

Methods

Our approach is based on two main steps, initial brain tissue segmentation according to the gray matter (GM), white matter (WM), and cerebrospinal fluid (CSF) performed in T1w images, followed by a second step where the lesions are segmented as outliers to the normal apparent GM brain tissue on the FLAIR image.

Results

The tool has been validated using data from more than 100 MS patients acquired with different scanners and at different magnetic field strengths. Quantitative evaluation provided a better performance in terms of precision while maintaining similar results on sensitivity and Dice similarity measures compared with those of other approaches.

Conclusion

Our tool is implemented as a publicly available SPM8/12 extension that can be used by both the medical and research communities.

Keywords

Multiple sclerosis, Magnetic resonance images, Lesion detection, Lesion segmentation, Automated tool

Automated detection of Lupus white matter lesions in MRI images

In this chapter, we present a new approach based on the proposal presented in the previous chapter to automatically segment WML on Lupus patients. We incorporate context information from an in-house group-wise atlas to reduce FP detections from the posterior fossa. This proposal has been evaluated in 20 patients, which have been labeled semiautomatically to be used as a gold standard segmentation.

The proposed method has been published in the following paper:

Paper submitted to *Frontiers in Human Neuroscience*

Currently in revision

JCR PS IF 3.626, Q1(13/76)

Automated detection of Lupus white matter lesions in MRI images

Eloy Roura^{a,*}, Nicolae Sarbu^b, Arnau Oliver^a, Sergi Valverde^a, Sandra González^a, Ricard Cervera^c, Nuria Bargalló^{b,d}, Xavier Lladó^a

^a*Department of Computer Architecture and Technology, University of Girona, Girona, Catalonia, Spain*

^b*Centre de diagnòstic per la Imatge (CDIC), Hospital Clínic, Barcelona, Catalonia, Spain.*

^c*Department of Autoimmune Diseases, Hospital Clínic-Institut d'Investigació Biomèdica August Pi i Sunyer (IDIBAPS), Barcelona, Catalonia, Spain.*

^d*Magnetic Resonance Imaging Core facility, Institut d'Investigació Biomèdica August Pi i Sunyer (IDIBAPS), Barcelona, Catalonia, Spain.*

Abstract

Brain magnetic resonance imaging provides detailed information which can be used to detect and segment white matter lesions (WML). In this work we propose an approach to automatically segment WML in Lupus patients by using T1w and fluid-attenuated inversion recovery (FLAIR) images. Lupus WML appear as small focal abnormal tissue observed as hyperintensities in the FLAIR images. The quantification of these WML is a key factor for the stratification of lupus patients and therefore both lesion detection and segmentation play an important role. In our approach, the T1w image is first used to classify the three main tissues of the brain, white matter (WM), gray matter (GM) and cerebrospinal fluid (CSF), while the FLAIR image is then used to detect focal WML as outliers of its GM distribution. A set of post-processing steps based on lesion size, tissue neighbourhood, and location are used to refine the lesion candidates. The proposal is evaluated on 20 patients, presenting qualitative and quantitative results in terms of precision and sensitivity of lesion detection (True Positive Rate (62%) and Positive Prediction Value (80%) respectively) as well as segmentation accuracy (Dice Similarity Coefficient (72%)). Obtained results illustrate the validity of the approach to automatically detect and segment lupus lesions. Besides, our approach is publicly available as a SPM8/12 toolbox extension with a simple parameter configuration.

Keywords: Magnetic resonance images, Lupus disease, Image analysis, Automatic lesion detection and segmentation.

1. Introduction

Several brain diseases present abnormalities in the white matter tissue, usually denoted as white matter lesions (WML). Segmenting these WML is important to diagnose and better understand these diseases as well as monitoring its progression. However, performing this task manually is tedious and very time consuming. Hence, several works have been proposed to tackle automatically this lesion segmentation problem. For instance, several works have been presented in multiple sclerosis lesion segmentation [1, 2, 3, 4, 5, 6, 7, 8], stroke [9], vascular dementia [10, 11] and other diseases [12, 13]. Instead, few attempts have been done on semiautomatic or automatic segmentation of Lupus lesions [14, 15, 16, 17], which are few and isolated, and have the particularity of being very small and focal WML.

Magnetic resonance imaging (MRI) is the gold standard technique for studying the brain in lupus [18]. The neuroimaging findings are classified as small or large vessel

disease, and inflammatory-type lesions [19]. Small vessel disease is represented by white-matter hyperintensities/lesions, recent small subcortical infarcts, lacunes, microbleeds, and brain atrophy [20]. WML are the most common findings of small vessel disease seen in lupus, and represent small T2-hyperintensities following the distribution of the white matter (periventricular, deep, subcortical), and including also the white matter at the basal ganglia, and cerebellum [18, 19]. Over the recent years, WML have been shown to function as an independent predictor for the neuro-lupus activity and injury, and quantitative methods are increasingly proposed for the quantification and follow-up of the WML in neuro-lupus.

Previous approaches, such as the automated one of Scully et al [17], have used a supervised strategy to deal with the lupus WML segmentation problem. In their work, local morphometric features extracted from multiple sequences, including T1w, T2w, and fluid-attenuated inversion recovery (FLAIR) images, were used to train a supervised classifier that takes advantage of a different subset of the features to segment lesion voxels. With a different viewpoint, in our work we present an unsupervised approach to automatically segment WML in Lupus patients by using only T1w and FLAIR images. This work

*Corresponding Author. E. Roura (eloyroua@eia.udg.edu)
University of Girona, Campus Montilivi, Ed. P-IV
17071, Girona (Spain).
Phone: +34 972418878; Fax: +34 972 418259

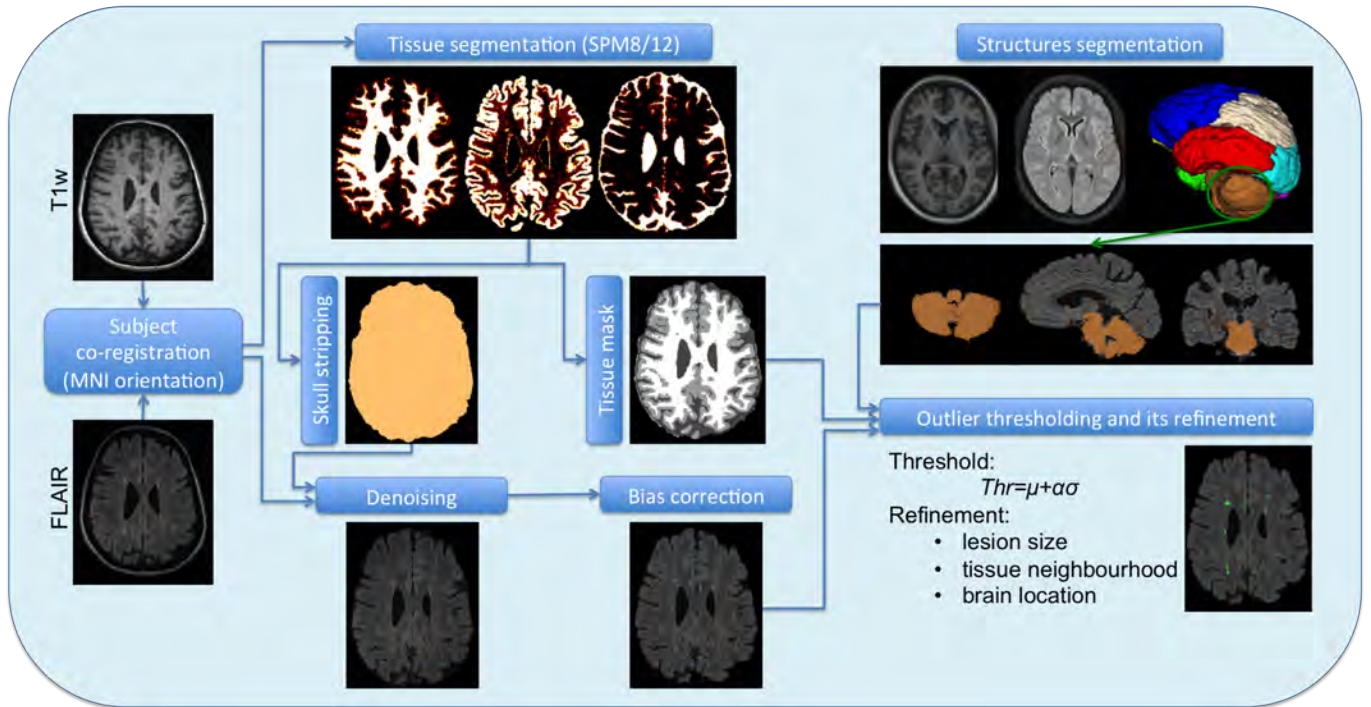


Figure 1: Scheme of the full lesion segmentation process.

can be seen as an extension of the tool recently presented by Roura et al. [8], in which the focus was the segmentation of multiple sclerosis lesions. The whole pipeline can be considered as a two main step process: pre-processing and WML segmentation. The first step is focused on the image enhancement by performing different intensity corrections on the brain and co-aligning all the image modalities. The second one, performs the lesion segmentation by detecting outliers to the normal apparent gray matter brain tissue on the FLAIR image as was previously done by Souplet et al. [21] and Roura et al. [8]. Given the specific properties of the Lupus WML, we introduce a set of post-processing steps to reduce possible false positive (FP) detections which are based on lesion size, lesion tissue neighbourhood and lesion location. The last one aims to eliminate the FP detections usually found in the posterior fossa due to frequent scanner artefacts, yet this is an uncommon location for WML in neurolyupus (up to 7% of patients versus 40-60% in frontal lobes) [19].

We introduced this constraint in the segmentation by using an in-house atlas created with the unbiased template creation algorithm proposed by Fonov et al. [22], which was then segmented into 12 brain structures including the posterior fossa using the Computational Morphometry Toolkit software ¹.

The evaluation of the Lupus WML segmentation has been done on a dataset of 20 patients comparing quantitatively the results obtained by our tool with the ones

performed manually by an expert radiologist. This ground truth (GT) has been used to compute quantitative measures in terms of detection, such as True Positive Rate (TPR) and Positive Prediction Value (PPV), and in terms of segmentation accuracy by using the Dice Similarity Coefficient (DSC). Both detection and segmentation results show the ability of the approach to automatically detect and segment focal WML in Lupus patients. The code of our approach is publicly available as a Statistical Parametric Mapping (SPM8/12) toolbox extension with a simple parameter configuration ².

2. Materials and methods

2.1. Data

This study included 20 Lupus patients. The brain MRIs were performed between 2014 and 2015 at Hospital Clinic, University of Barcelona, the main national referral institution for lupus. All scans were performed at 3 Tesla Siemens MAGNETOM TIM Trio scanner, using a 32-channel head coil, with the same protocol including 3D T1 and 3D FLAIR, with a voxel size = $1 \times 1 \times 1 \text{ mm}^3$. The lesions were semiautomatically annotated on FLAIR images by neuroimaging experts. They present a lesion volume variation (mean±standard deviation) and range (min-max) per patient of $0.217 \pm 0.325 [0.011 - 1.459]$ ml.

²<http://atc.udg.edu/salem/slsToolbox/index.html>

¹<http://www.nitrc.org/projects/cmtk/>

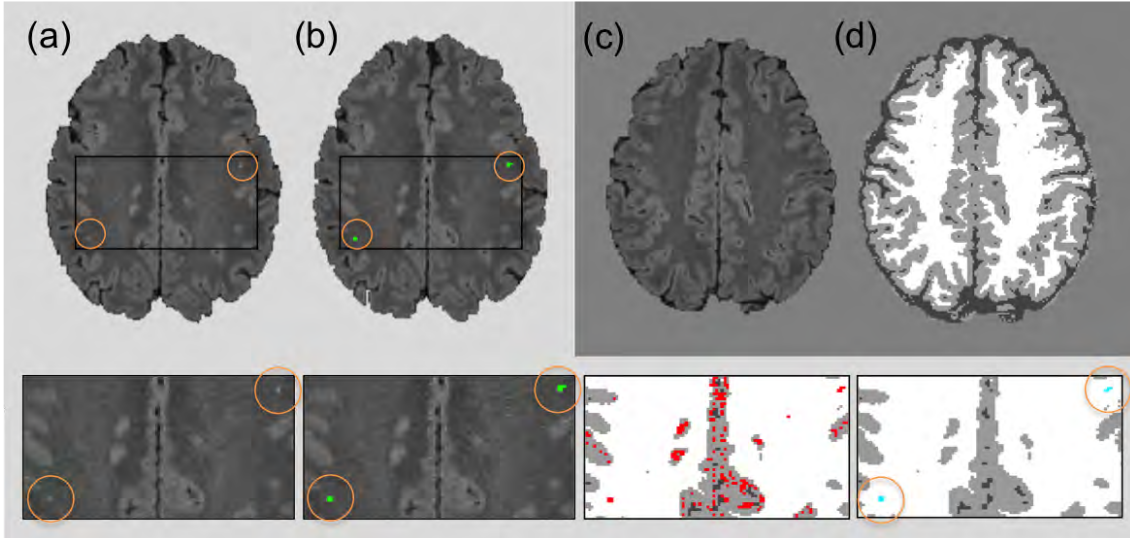


Figure 2: FLAIR 2D axial slice (a) showing 2 lesions (in green) of 4 voxels each (b), both completely surrounded by white matter. Original image and tissue segmentation result of two slices forward are shown in (c) and (d). The bottom row shows four zooms of the original image, ground truth (green), candidates regions (red) and final lesion segmentation (blue).

2.2. MRI pre-processing

To deal with the Lupus WML segmentation, several pre-processing steps (see Figure 1) are required to optimise the overall performance, as seen in previous works [4, 5, 6, 23, 8, 7]. Since our aim is to provide a publicly available Lupus segmentation tool as an extension of the SPM8/12 all the required steps are performed within the Matlab environment.

The first step of the pre-processing consists in the intra-subject registration. For this, we follow a similar procedure than the one used in Roura et al. [8]. In this case, we register FLAIR to the T1w image, where the target space used (corresponding to the Montreal Neurological Institute (MNI) [24]) as well as the co-registration software are provided by the SPM toolbox.

One of the most common pre-processing step is the skull stripping process [25, 26, 27, 28], which we incorporate into our pipeline using the SPM tissue segmentation algorithm [29], avoiding therefore the use of external libraries such as BET [26] or BSE [25]. Given that this process provides the probability map of the three main brain tissues (white matter (WM), gray matter (GM), and cerebrospinal fluid (CSF)), we performed a maximum likelihood thresholded at 0.5 to determine directly the brain mask [30, 28]. This process is performed on the T1w image, although the brain mask is applied on the FLAIR image where the rest of the pre-processing will be carried out, since intensity corrections of the T1w image are handled by the SPM tissue segmentation process itself.

It is well known that MRI images obtained directly from the scanner present noise and undesired artefacts (movement, high signal value, blood, flow artefacts, etc) [31]. These abnormalities may be corrected during the scanning procedure while others such as inhomogeneities in the

magnetic field [32] must be attenuated by post-scanning processes. We first apply the anisotropic diffusion filter of Perona and Malik [33] in order to enhance the image by smoothing its histogram with the 3D Matlab implementation³ of this algorithm. Given the reduced size of the lesions, we have carefully run this method over all the patients with a restrictive parameter configuration (1 iteration, $K = 50$, and option=1), reducing the iterations and gradient modulus, and focusing on contrast instead of region size.

To correct the bias field we used the Matlab method proposed by Thode et al. [34], which is based on an expectation maximisation model (EM) that relies on the same generative models and bias field estimation computations of the well-known non-parametric, non-uniform intensity normalisation (N3) method [35]. This approach requires to mask out the low intensity voxels, thus the brain mask obtained from T1w image is used when correcting the FLAIR image.

2.3. Lupus lesion segmentation

Lupus lesions, similarly to other WML such as multiple sclerosis lesions, are characterised by being hyperintense regions in the FLAIR images. Due to the fact that the GM is the highest intensity tissue in this image modality, we used its histogram distribution to identify the hyperintense outliers. In order to obtain the GM distribution, we used the same SPM tissue segmentation [29] applied in the skull stripping process. At this point the lesion detection can be performed as a thresholding process, commonly computed by $\mu + \alpha\sigma$, where the standard deviation

³<http://www.mathworks.com/matlabcentral/fileexchange/14995-anisotropic-diffusion--perona---malik->

(σ) is determined using the full width at half maximum (FWHM) of the main peak (μ). We can then adjust the number of detected candidate lesions via the α parameter, observing a good trade off when setting this parameter to 2.5, assuming more than 98% of the histogram belonging to GM.

Afterwards, we apply a set of post-processing steps to remove FP lesions that remained after thresholding the FLAIR image: 1) Lesion size: we constraint the minimum size of the lupus lesion to be $3mm^3$. Therefore, we eliminate hyperintense voxels or a group of voxels smaller than this size. 2) Lesion tissue neighbourhood: because the lupus lesions should appear in the WM, the surrounding voxels must strictly belong to WM. Therefore, we introduce a parameter to limit the proportion of the WM over GM and CSF in the lesion neighbourhood. We observed in our tests that the best trade off was obtained when using the ratio 0.7. Looking at Figure 2, one can see how the neighbours of the two higher hyperintense regions marked in green in Figure 2 (b), all belong to WM in the tissue segmentation, while other candidate regions seen in the centre (marked in red) are not considered lesions because the neighbours voxels belong to GM. This neighbourhood operation is applied in 3D. Figure 2(c)(d) shows the original image and the tissue segmentation result of two slices forward, where the candidates marked in red are attached to GM and therefore eliminated with the neighbourhood constraint. 3) Lesion location: since Lupus lesions are rarely present in the posterior fossa [18, 19], and this particular area is highly prone to present hyperintense artefacts, we have decided to exclude this region when looking for possible lesion candidates. This is done automatically by registering an atlas with the corresponding structure segmentation to the T1w image. In particular, we use an in-house 3T template created over healthy subjects using the unbiased template creation approach proposed by Fonov et al. [22]. This procedure, as stated by the authors, converges after 20 iterations, meaning that 20 non-rigid registrations must be performed for each subject of the population. The nonlinear registration process relies on the Automatic Nonlinear Image Matching and Anatomical Labeling (ANIMAL) of Collins et al. [36]. In order to obtain the structure segmentation of the healthy template, we have re-arranged the 83 labels of the T1w atlas from Hammers et al. [37] into 12 regions⁴. Subsequently, our template was segmented into these 12 regions using the Computational Morphometry Toolkit (CMTK)⁵. To register the in-house template T1w image to each patient we used the SPM registration module, similarly to the intra-subject registration process. Finally, using the deformation field obtained by the non-rigid registration, we are able to bring the structure corresponding to the posterior fossa to each of the patient’s space and therefore remove

FP in this area caused by artefacts. A summary of the full pipeline is illustrated in Figure 1.

3. Experimental results

We have quantitatively analysed the obtained results evaluating three different measures, TPR and PPV for lesion detection, sensitivity and precision respectively, and DSC in terms of segmentation accuracy. Figure 3 shows the obtained results per patient. We have stratified the population according to three different groups depending on the number of GT lesions per patient: 1) low lesion burden (< 5 lesions); 2) medium lesion burden (between $5 - 25$ lesions); 3) high lesion burden > 25 lesions.

Regarding the obtained results, both group and total averages of all the measures are over 50%, specially highlighting the group with more than 25 lesions, where we obtain a $TPR = 81\% \pm 14$, a $PPV = 96\%$ and a $DSC = 95\% \pm 1$. When considering the whole dataset, these values are: $TPR = 62\% \pm 19$, $PPV = 80\% \pm 25$, and $DSC = 72\% \pm 22$; this is due to the lower performance obtained in the first group, where a small error represents a big percentage in the total measure.

To better understand the results, we also show two correlation plots, one with the number of lesions and one with the lesion volume (see Figure 4). We have fitted a linear polynomial curve and showing also the expected fit, which is basically the ideal correlation. Looking at the number of lesions correlation, the model lies under the expected fit meaning that the approach underestimates the number of lesions. However, we obtained a very high Pearson’s coefficient ($r = 0.93$), i.e. the whole dataset can be linearly explained because all the samples follow the same trend, except one outlier which also has a correct stratification. Besides, one can see how the stratification results fit for most of the patients with the expected groups, except for two cases which are close to the group limit.

Regarding the lesion volume correlation, the model fitting shows also a very good correlation, with only one sample out of the confidence level. The model coincides almost perfectly with the expected fit and Pearson’s coefficient is also high with $r = 0.96$. Notice that this high fitting illustrates in terms of total affected tissue volume that the FP and FN are not significant compared to the TP.

Some samples of qualitative results are shown in Figure 5, where we compare the results of our automated tool with the GT annotations. We have chosen different samples to illustrate the performance in patients with different lesion load. Notice that the total lesion volume is very small in all of them, but the automatic detection provides a good performance in terms of TP while having a reduced number of FP and FN. When illustrating the whole 3D volume in the figure, those FP and FN are inappreciable because they are smaller than 0.01ml. However, we show some FP and FN examples on the 2D slices for the second

⁴<http://www.pmod.com/files/download/v35/doc/pneuro/5674.htm>

⁵<https://www.nitrc.org/projects/cmtk/>

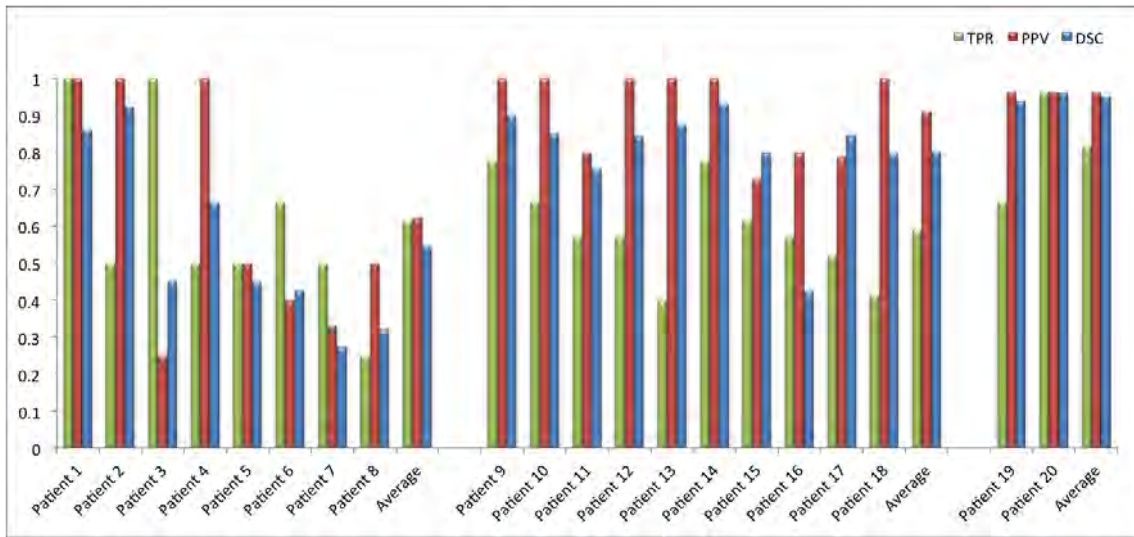


Figure 3: Bar plots of each patient representing the DSC, TPR and PPV values. The population is stratified in four groups depending on the GT number of lesions, from left to right: < 5; [5 – 25]; > 25].

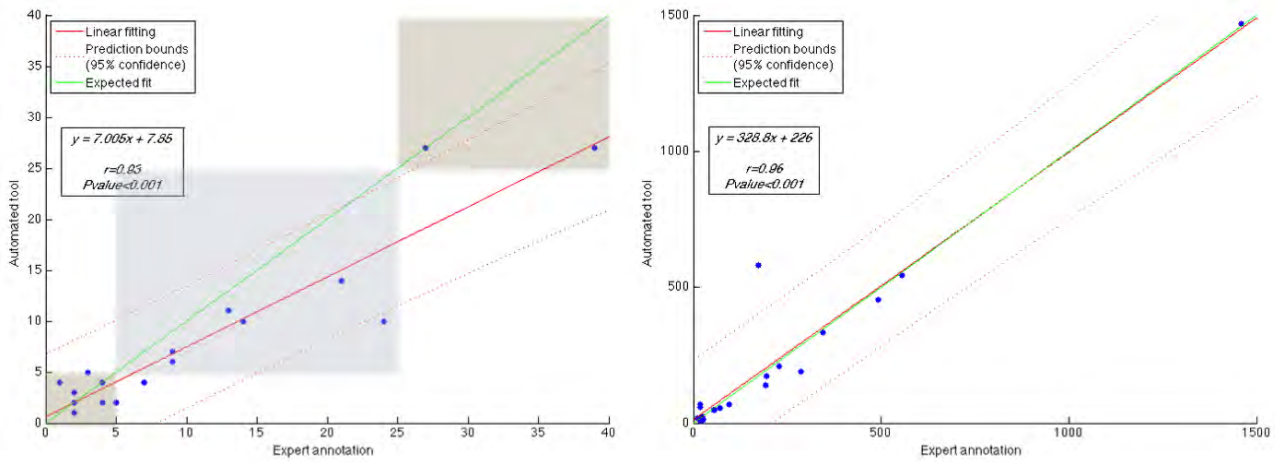


Figure 4: Correlation with number of lesions (stratified by the three groups) on the left and lesion volume, in terms of voxels, on the right.

and third group, zooming also into these regions in the first group.

4. Discussion

WML are the most common radiological finding in neurolupus. They are non-specific findings, being frequently observed in older age groups, migraine, chronic diseases, heart diseases, diabetes, high-blood pressure, dyslipidemia and other vascular risk factors, although they are also present in asymptomatic subjects without known diseases [18]. However, WML are found in 40-60% of neurolupus patients, even at the onset of the disease, and many previous reports showed a higher frequency of WML in neurolupus when compared with lupus without neurolupus and general population [18, 19, 20, 38].

The pathogenesis of WM hyperintensity is attributed to chronic small vessel disease, which is supported by a study with radiologic-pathologic correlation in patients with neurolupus [39]. The underlying mechanisms for small vessel disease in neurolupus are not well understood, although multiple factors are incriminated, including accelerated atherosclerosis, direct immune mediated alterations, microembolisms, intimal hyperplasia, erythrocytes extravasation, fibrin thrombi and coagulopathy [18, 40, 41].

In neurolupus, WML involve preferentially the frontal and parietal regions, different from primary autoimmune demyelinating diseases such as multiple sclerosis. WML were repeatedly correlated with lupus duration, cognitive dysfunction, cerebrovascular syndrome, seizures, antiphospholipid antibody and low complement (C3, C4, CH50) levels [15, 42, 43]. A quantitative WML analysis in lupus patients demonstrated that age, duration of neuropsychiatric manifestations and total corticosteroid dosage were independent predictors for WML [15]. Importantly, there was demonstrated a positive association between the lesion burden and the score of lupus activity (Systemic Lupus Erythematosus Disease Activity Index-SLEDAI) and injury (Systemic Lupus International Collaborating Clinic-SLICCC). This means that WML are an independent predictor for lupus activity and injury, and suggests that the quantification of WML (either by number or, maybe better, by volumetric methods) and their follow-up, could be used for monitoring the disease progression and response to therapy [14, 15, 18].

We have proposed in this work an automated tool which presents a good correlation in both number of lesions and lesion volume, as seen in Figure 4. Even though the obtained results tend to underestimate the lesion detections, the number of lesions detected have shown a good correlation with the stratified population into three groups. Notice that the FN rate has a weak influence on the final lesion volume, since Lupus WML are small focal lesions, characteristic of this particular disease. Nevertheless, FN rate could be improved by decreasing the minimum lesion size, but this could lead to misclassification of scanner artefacts (more FP detections). Besides, in order to reduce this

FP detection rate introduced by the artefacts of the scanner, we have set a high lesion neighbourhood restriction to belong to WM.

The parameter configuration has been set up with an exhaustive analysis over both α and lesion tissue neighbourhood parameters, testing values from 1 to 3 each 0.1 and from 0 to 1 each 0.05 respectively. The analysis showed that the optimal configuration was with the α of 2.5 and tissue neighbourhood ratio of 0.7. We want to remark this will be the default configuration of the tool, however, other configurations provided very similar results.

Even though this study has been evaluated with a dataset of 20 patients, we observed promising results in both lesion detection and segmentation, highly comparable to the state of the art approach of Scully et al. [17]. We believe that the benefits of an unsupervised approach, which allows to avoid the training stage and therefore having manually annotated cases by experts, will help to the community to quantify WML on Lupus patients, specially considering that we provide a public tool which is straightforward to use in SPM8/12.

5. Conclusions

In this work we have presented an approach to perform WML segmentation on Lupus patients. We have maintained the same pre-processing pipeline applied in [8], but now implemented in MATLAB code, fact that facilitates the integration to SPM8/12, the installation and execution. The lesion segmentation process has been modified specially on the application of the refinement constraints due to the difference on the lesion features. Results shown in this manuscript demonstrate the good performance of the approach. The correlation results in both number of lesions and lesion volume, illustrates the validity of the approach as a tool for clinicians when diagnosing Lupus patients or evaluating the disease evolution in patients treated with different therapies.

Acknowledgements

E. Roura holds a BR-UdG2013 PhD grant. Sergi Valverde holds a FI-DGR2013 PhD grant. This work has been partially supported by “La Fundació la Marató de TV3” and by Retos de Investigación TIN2014-55710-R.

References

- [1] Van Leemput K., Maes F., Vandermeulen D., Colchester A., Suetens P. Automated segmentation of multiple sclerosis lesions by model outlier detection *Medical Imaging, IEEE Transactions on*. 2001;20:677–688.
- [2] Lladó X., Oliver A., Cabezas M., et al. Segmentation of multiple sclerosis lesions in brain MRI: a review of automated approaches *Information Sciences*. 2012;186:164–185.
- [3] Lladó X., Ganiler O., Oliver A., et al. Automated detection of multiple sclerosis lesions in serial brain MRI *Neuroradiology*. 2012;54:787–807.

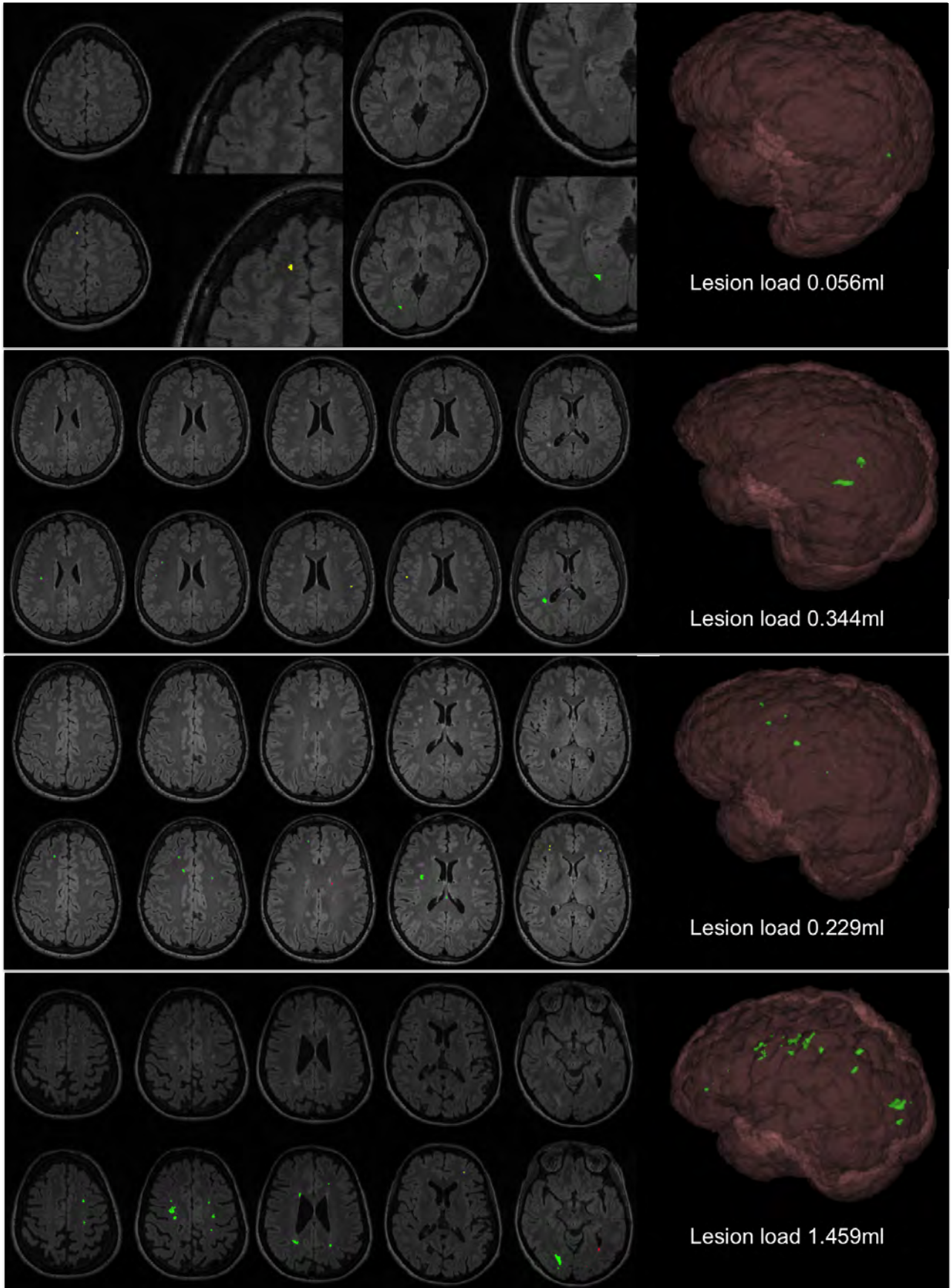


Figure 5: Qualitative results of the approach. First row of each patient shows the original FLAIR image and second row shows the automatic segmentation (green=TP, red=FP, and yellow=FN).

- [4] Schmidt Paul, Gaser Christian, Arsic Milan, et al. An automated tool for detection of FLAIR-hyperintense white-matter lesions in Multiple Sclerosis *NeuroImage*. 2012;59:3774–3783.
- [5] Cabezas M., Oliver A., Roura E., et al. Automatic multiple sclerosis lesion detection in brain MRI by FLAIR thresholding *Computer Methods and Programs in Biomedicine*. 2014;115:147–161.
- [6] Cabezas M., Oliver A., Valverde S., et al. BOOST: a supervised approach for multiple sclerosis lesion segmentation *Journal of Neuroscience Methods*. 2014;237:108 – 117.
- [7] Guizard N., Coupé P., Fonov V., Manjón J., Arnold D.L., Collins L.. Rotation-invariant multi-contrast non-local means for {MS} lesion segmentation *NeuroImage: Clinical*. 2015;8:376 – 389.
- [8] Roura E., Oliver A., Cabezas M., et al. A toolbox for multiple sclerosis lesion segmentation *Neuroradiology*. 2015:1-13.
- [9] Mitsias P.D., Jacobs M.A., Hammoud R., et al. Multiparametric MRI ISODATA ischemic lesion analysis: correlation with the clinical neurological deficit and single-parameter MRI techniques *Stroke*. 2002;33:2839–2844.
- [10] Mohamed F.B., Vinitiski S., González C.F., et al. Increased differentiation of intracranial white matter lesions by multispectral 3D-tissue segmentation: preliminary results *Magnetic Resonance Imaging*. 2001;19:207 – 218.
- [11] Yamashita Y., Arimura H., Tsuchiya K.. Computer-aided Detection of Ischemic Lesions Related to Subcortical Vascular Dementia on Magnetic Resonance Images *Academic Radiology*. 2008;15:978 – 985.
- [12] Kruggel F., Paul J.S., Gertz H.. Texture-based segmentation of diffuse lesions of the brain as white matter *NeuroImage*. 2008;39:987 – 996.
- [13] Schwarz C., Fletcher E., DeCarli C., Carmichael O.. Fully-Automated White Matter Hyperintensity Detection with Anatomical Prior Knowledge and without FLAIR in *Information Processing in Medical Imaging* (Prince JerryL., Pham DzungL., Myers KyleJ., eds.);5636 of *Lecture Notes in Computer Science*:239-251Springer Berlin Heidelberg 2009.
- [14] Appenzeller S, Pike GB, Clarke A. Magnetic Resonance Imaging in the Evaluation of Central Nervous System Manifestations in Systemic Lupus Erythematosus *Clinical Reviews in Allergy & Immunology*. 2008;34:361-366.
- [15] Appenzeller S, Vasconcelos Faria A, Li LM, Costallat LTL, Cendes F. Quantitative magnetic resonance imaging analyses and clinical significance of hyperintense white matter lesions in systemic lupus erythematosus patients *Annals of Neurology*. 2008;64:635–643.
- [16] Petri M, Naqibuddin M, Carson KA, et al. Brain magnetic resonance imaging in newly diagnosed systemic lupus erythematosus *J Rheumatol*. 2008;35:2348–2354.
- [17] Scully M., Anderson B., Lane T., et al. An Automated Method for Segmenting White Matter Lesions through Multi-level Morphometric Feature Classification with Application to Lupus *Frontiers in Human Neuroscience*. 2010;4.
- [18] Sarbu N, Bargalló N, Cervera R. Advanced and Conventional Magnetic Resonance Imaging in Neuropsychiatric Lupus *F1000Research*. 2015;4.
- [19] Sarbu Nicolae, Alobeidi Farah, Toledano Pilar, et al. Brain abnormalities in newly diagnosed neuropsychiatric lupus: Systematic MRI approach and correlation with clinical and laboratory data in a large multicenter cohort *Autoimmunity Reviews*. 2015;14:153 – 159.
- [20] Wardlaw JM, Smith EE, Biessels GJ, et al. Neuroimaging standards for research into small vessel disease and its contribution to ageing and neurodegeneration *The Lancet Neurology*. 2013;12:822 – 838.
- [21] Souplet J.C., Lebrun C., Ayache N., Malandain G.. An Automatic Segmentation of T2-FLAIR Multiple Sclerosis Lesions in *Multiple Sclerosis Lesion Segmentation Challenge Workshop (MICCAI-2008)*(New York, NY, USA, United States):1–8 2008.
- [22] Fonov V., Evans A., Botteron K., Almlri R., McKinstry R., Collins L.. Unbiased average age-appropriate atlases for pediatric studies *NeuroImage*. 2011;54:313 – 327.
- [23] Valverde S., Oliver A., Lladó X.. A white matter lesion-filling approach to improve brain tissue volume measurements *NeuroImage: Clinical*. 2014;6:86 – 92.
- [24] Mazziotta J. C., Toga A. W., Evans A., Fox P., Lancaster J.. A Probabilistic Atlas of the Human Brain: Theory and Rationale for Its Development *NeuroImage*. 1995;2:89–101.
- [25] Shattuck D.W., Sandor-Leahy S.R., Schaper K.A., Rottenberg D.A., Leahy R.M.. Magnetic Resonance Image Tissue Classification Using a Partial Volume Model *NeuroImage*. 2001;13:856 – 876.
- [26] Smith S.M.. Fast robust automated brain extraction *Human Brain Mapping*. 2002;17:143–155.
- [27] Park J.G., Lee C.. Skull stripping based on region growing for magnetic resonance brain images *NeuroImage*. 2009;47:1394–1407.
- [28] Roura E., Oliver A., Cabezas M., et al. MARGA: Multispectral Adaptive Region Growing Algorithm for brain extraction on axial MRI *Computer Methods and Programs in Biomedicine*. 2014;113:655–673.
- [29] Ashburner J., Friston K. J.. Unified segmentation *NeuroImage*. 2005;26:839 – 851.
- [30] Boesen K., Rehm K., Schaper K., et al. Quantitative comparison of four brain extraction algorithms *NeuroImage*. 2004;22:1255–1261.
- [31] Lemieux L., Wieshmann N., Moran N., Fish D., Shorvon S.. The detection and significance of subtle changes in mixed-signal brain lesions by serial MRI scan matching and spatial normalization *Medical Image Analysis*. 1998;2:227-242.
- [32] Sha D., Sutton J.P.. Towards automated enhancement, segmentation and classification of digital brain images using networks of networks *Information Sciences*. 2001;138:45–77.
- [33] Perona P., Malik J.. Scale-space and edge detection using anisotropic diffusion *Pattern Analysis and Machine Intelligence, IEEE Transactions on*. 1990;12:629–639.
- [34] Larsen C.T., Iglesias J.E., Van Leemput K.. N3 Bias Field Correction Explained as a Bayesian Modeling Method in *Bayesian and graphical Models for Biomedical Imaging*;8677 of *Lecture Notes in Computer Science*:1–12Springer International Publishing 2014.
- [35] Sled J.G., Zijdenbos A.P., Evans A.C.. A nonparametric method for automatic correction of intensity nonuniformity in MRI data *IEEE Transactions on Medical Imaging*. 1998;17:87–97.
- [36] Collins L., Holmes C. J., Peters T. M., Evans A. C.. Automatic 3-D model-based neuroanatomical segmentation *Human Brain Mapping*. 1995;3:190–208.
- [37] Hammers A., Allom R., Koeppe M.J., et al. Three-dimensional maximum probability atlas of the human brain, with particular reference to the temporal lobe *Human Brain Mapping*. 2003;19:224–247.
- [38] Castellino G., Govoni M., Giacuzzo S., Trotta F.. Optimizing clinical monitoring of central nervous system involvement in SLE *Autoimmunity Reviews*. 2008;7:297 – 304.
- [39] Sibbitt WL Jr, Brooks WM, Kornfeld M, Hart BL, Bankhurst AD, Roldan C. Magnetic Resonance Imaging And Brain Histopathology In Neuropsychiatric Systemic Lupus Erythematosus *Semin Arthritis Rheum*. 2010;40:35–52.
- [40] Joseph FG, Scolding NJ. Neurolupus *Pract Neurol*. 2009;10:4–15.
- [41] Sarbu MI, Salman-Monte TC, Rubio Muoz P, Lisbona MP, Bernabé MA, Carbonell J. Differences between clinical and laboratory findings in patients with recent diagnosis of SLE according to the positivity of anti-dsDNA by the Crithidia luciliae method. *Lupus*. 2015;24:1198-1203.
- [42] Aimiala H., Dastidar P., Loukkola J., et al. Cerebral MRI abnormalities and their association with neuropsychiatric manifestations in SLE: a population-based study *Scandinavian Journal of Rheumatology*. 2005;34:376–382.
- [43] Toledano P, Sarbu N, Espinosa G, Bargalló N, Cervera R. Neuropsychiatric systemic lupus erythematosus: magnetic resonance imaging findings and correlation with clinical and im-

munological features *Autoimmun Rev.* 2013;12:1166–1170.

Main results and discussion

This chapter outlines the main results and discussions derived from this thesis. Although we present our contributions related to the various papers, all of them target the same final goal, i.e. to develop automated tools to help in the analysis of Brain MRI images, with the main focus on the detection and segmentation of WML (see Section 1.4). We divided the outcomes of this thesis according to the different pre-processing contributions:

1. **Skull-stripping (MARGA):** As stated in previous work and in this thesis, when trying to segment the brain, sometimes standard tools that are used worldwide (BET, BSE), do not properly remove the non-brain tissues. With the aim of improving these cases, we have based our approach on the work of Park and Lee [34] and contributed new strategies. On the one hand, in terms of implementation, we took into account the contrast variation throughout the whole brain when processing the axial orientation. On the other hand, in terms of image modalities, we used multispectral information obtained from T1w and T2w. These two sequences provide complementary information that enhanced the segmentation process. We improved the accuracy of WM segmentation by using T1w, while GM and CSF was better segmented on T2w. Besides, the common protocol in daily clinical practice includes these two modalities, therefore no extra resources are required. The robustness of our algorithm has been tested with both synthetic and real MRI data outperforming the state-of-the-art in some datasets. Qualitative and quantitative evaluations have proved the good performance of this approach.
2. **Multi-channel registration:** The use of complementary information provided by different MRI modalities allows us to build a greater understanding of the human body. This is also true when dealing with computer vision algorithms, whose performance depends on the information received. In this thesis, we also tackled the

issue of co-registration of conventional and diffusion MRI when registering it in a common space. Note that we did not evaluate the effect of WML but of the MS atrophy, because WML has a reduced impact on the registration of the whole brain. This fact was highlighted in Roura et al. [132], an issue covered in the Master Thesis [133], where we analysed our pipeline simulating atrophy patients after the WML were inpainted [94, 134–136]. This process was carried out with three different strategies, single-channel and T1w approaches being commonly used in the current literature, while multi-channel has been recently proposed by several authors. The results obtained from the MC registration showed significant improvement over the SC and T1w approaches.

3. **Exhaustive analysis of the pre-processing:** Skull-stripping and registration are two of the several steps covered in this complex topic of image pre-processing where the image enhancement is the basic aim. Image noise and intensity inhomogeneities are usually present in all acquisitions. These aspects, as well as those mentioned above, have been extensively analysed in this thesis, considering all the standard methods in the state-of-the-art for each of the pre-processing steps (skull-stripping, image denoising, intensity inhomogeneities correction, and registration). We have come up with a standard pipeline used in all our experiments, but especially in the WML segmentation tool that we have presented in this thesis. Besides, all these experiments have been tested on a wide variety of images with different resolutions in both 1.5T and 3T scanners.

The second part of the main results refers to the WML segmentation applications:

1. **Multiple Sclerosis:** Segmentation and detection of WML in MS is of particular interest when diagnosing and assessing the evolution of the disease, which indeed is a tedious task for radiologists. In this thesis, we have presented a new tool to help doctors perform this task, allowing them to quantify the number of lesions and the lesion burden. We introduced an iterative strategy, which increases the performance specially when dealing with 3T data, while the 1.5T dataset used here did not allow us to prove the same improvement, mainly due to the difference on the lesion burden as one can read in the discussion of the paper in Chapter 5. This method was tested over more than 100 patient images from three different databases (see dataset description in Chapter 5) with different properties and acquired at different magnetic field strengths (3T and 1.5T). The good performance shown in all the experimental

results, especially when evaluating the results with the MICCAI Grand Challenge 2008 algorithms for both training and testing data, proves the robustness of this tool. We were able to maintain a regular and reduced FP rate while TP rate was similar to the state-of-the-art methods. Although in the manuscript describing the tool, we stated that pre-processing must be done beforehand and we recommended strictly following the pipeline, the final version of our tool incorporates all these steps, insuring the same performance in a user-friendly GUI to be used straightaway.

2. **Lupus:** The same core of the WML segmentation tool was tested over a database of Lupus patients. This disease also presents WML, whose quantification is a good predictor for Lupus activity and injury. There is a lot of literature on automated WML segmentation for MS and other neurological diseases, but it has seldom been explored in Lupus. In order to adapt the tool to this end, we included an atlas registration to segment the posterior fossa, where WML are rarely present and because this area is also prone to FP detections due to hyperintensities induced by the artefacts from the scanner. Also, another post-processing step was used to test 20 Lupus patients, obtaining highly satisfactory results when comparing a manual ground truth with the outcomes of the tool.

In this regard, we have avoided the adaptation of the pre-processing approaches presented earlier in this thesis, such as MARGA for the skull stripping procedure. This task is currently performed by masking the output of the inner SPM tissue segmentation, which allows to reduce the computational cost of this process. Regarding the co-registration step, we have also used the inner process of the SPM, since good results have been obtained and no extra compilation is needed.

Related collaborations:

In neurological diseases, tissue measurements are also a key step when measuring atrophy. Automatic tissue segmentation methods do not take into account the possible lesions appearing in the WM, and this fact highly affects their measurements. In collaboration with another thesis carried out in this group, we studied the impact of WML on tissue measurements [103, 104], where we contributed by automatically segmenting WML with the tool presented here. In this study, we showed how the % of error in the total normal-appearing WM volume was lower when the lesions were segmented and filled before the tissue segmentation. As this work highlights the importance of refilling WML, the necessity of WML segmentation is also reflected.

The WML segmentation tool includes a previous image pre-processing before the lesion segmentation is done. Although pre-processing involves both skull-stripping and co-registration, none of the above mentioned have been adapted for the WML segmentation toolbox. Our skull-stripping has been implemented in C++ and its adaption to the tool would need a new implementation in MATLAB by using the GPU core. This requirement is especially needed to improve the computational time, and remains as an open line for future collaborations or PhD theses. Therefore, we have decided to use the SPM itself for this purpose. Regarding the multi-channel approach, it is not possible at the moment since none of our database provides DTI data. However, the in-house atlas used for the structure segmentation consists of T1w and FLAIR images, thus a new multi-channel registration pipeline considering these two modalities might be used to enhance the structure segmentation.

Conclusions

We have satisfactorily covered all the goals proposed in this thesis. We have been very active during the four years invested in this thesis, as proven by the number of publications in both international conferences and journals. We have also been on several research stays in some of the most relevant research centres in the field.

We believe that the results and contributions produced in this thesis will have a high impact on the community and will achieve the main goal of helping the community of brain MRI analysis, and especially for the diagnosis and monitoring of neurological diseases.

8.1 Research stays

During this PhD thesis, Eloy Roura had the opportunity of going on the following research stays:

- 4 months in the Biomedical Image Computing Group in the University of Washington under the supervision of Dr. Colin Studholme. In this center, we had to deal with MRI of neonates where the biggest challenge was the rapid tissue evolution. This fact makes common approaches used in adults unsuitable for such a scenario. In premature infants, one can sometimes appreciate intraventricular hemorrhages, a type of bleeding that looks hyperintense in T1w images. Our goal here was to improve the current automatic segmentation of these lesions with novel methods that have produced a journal paper (submitted to *NeuroImage: Clinical*).
- 3 months in the Montreal Neurological Institute in McGill University under the supervision of Dr. Arnold Douglas, Dr. Sridar Narayanan and Dr. Parya Momayyez. This project consisted of the hypothesis of finding a correlation between the visual

system connectivity and its acuity tests on paediatric MS patients. This was a preliminary study during which we strongly confirmed our knowledge in the field and produced an internal technical report.

- 5 months in the Institute of Neurology in the University College London under the supervision of Dr. Claudia AM Wheeler-Kingshott and Dr. Torben Schneider. During this research stay, we worked on the Master Thesis, work that has contributed to the MC pipeline presented in this thesis.

8.2 Contributions

The results of this thesis led to the following contributions to both the scientific and medical communities:

- Experimental tests have been carried out with several datasets of different characteristics: a) 1.5T data with 45 MS patients manually annotated by experts to obtain the GT lesion segmentation; b) 3T data with 10 Lupus patients and 10 schizophrenic patients from the public NAMIC database. c) 3T simulated data with 10 brain cases from the BrainWeb; d) 3T DTI data with 10 MS patients and 100 simulations of MS atrophy; e) 3T data with 70 MS patients with different lesion loads from the Hospital Vall d’Hebron. These cases were also manually annotated by experts; f) 3T dataset with 20 Lupus patients with different lesion loads from the Hospital Clínic, University of Barcelona.
- A novel method for isolating the brain from the rest of the head, obtaining promising results compared to the state-of-the-art. This method has been tested with simulated and real MS patients. We have shown that this algorithm is stable and permits us to obtain satisfactory skull stripping results when dealing with axial oriented MRI images acquired at 1.5T or 3T. This method has produced a conference abstract (ECTRIMS 2013) and a journal paper (Computer Methods and Programs in Biomedicine 2014).
- A novel MC registration approach to move T1w and FA images to a healthy control target space. The registration pipeline has been tested on people with MS with atrophy and marked ventricular enlargement. We proposed our own atrophy generation framework for an experimental evaluation. We have shown that MC registration

offers significant improvements in alignment accuracy compared to SC or T1w approaches. This work has produced two conference abstracts (ISMRM 2012, ISMRM 2013) and a journal paper (Functional Neurology 2015).

- An exhaustive analysis of the impact of pre-processing methods with special focus on WML segmentation. We have developed our skull-stripping method and compared its performance with the BET, BSE and SPM. We have tested several configurations for both image denoising [46] and intensity inhomogeneity correction with SPM [47] and N3 [48]. Finally, we have also compared different pipelines in terms of flux execution, aiming to propose a standard pipeline for this purpose.
- A novel method to segment WML using T1w and FLAIR images. Our tool is publicly available as an SPM8/12 extension toolbox [<http://atc.udg.edu/salem/slsToolbox>], which is easily adaptable and has a default configuration to be used straightaway. We have provided a user-friendly GUI for doctors to interact with. The tool has been tested with different parameter configuration on both MS and Lupus patients. From this approach, we published a conference abstract (ECTRIMS 2015), a conference paper (SPIE 2016), and two journal papers (Neuroradiology 2015 for MS and Frontiers in Human Neuroscience 2016 for Lupus)

8.3 Future work

Several aspects have to be taken into account in MRI analysis, especially from the computer science point of view. In this thesis, we have exhaustively covered some of them but there is still room for improvement on both the pre-processing and lesion segmentation processes. Besides, our collaborations in other projects listed in the publications can be considered in order to enhance the current online tool.

The skull-stripping method presented in this thesis has been developed in a non-optimised c++ code. However, our WML segmentation tool was implemented in MATLAB as an SPM8/12 toolbox since it is commonly used in the clinical community. Therefore, an efficient MATLAB implementation of this method, which handles computer resources accurately, would allow us to include this skull-stripping algorithm in the final version of the tool. Techniques such as OPENCL and GPU programming may help to enhance the computational cost.

Despite the clear improvements presented with the MC pipeline approach, the analysis of other registration approaches, such as SyN or ANTs that use different mathematical

models, in the three strategies presented in this work would be useful to reinforce our findings.. Besides, there are some limitations that should be addressed in future studies. For instance, we generated simulated atrophy by registering T1w images of healthy controls to T1w images of MS patients and then applied the same transformation to FA images of the same subject. This procedure ensured that the FA and T1w images were equally deformed, but it did not accurately reproduce the presence of MS lesions. Previous evaluations, though, confirmed that lesions have a minimal effect on MC (T1w and FA) registration to a common space [132, 136], therefore, justifying the use of the proposed strategy as a simple way for atrophy generation without having to explicitly consider MS lesions. Following the previous work presented by Daga et al. [71], we focused on the evaluation of an MC pipeline applied to T1w and FA images. However, it is well-known that other indices from the DTI matrix or even other imaging modalities could provide complementary information and could also be used in the MC registration pipeline.

In the latest publications, we have started to use structure information from an in-house atlas, a fact that allows us to treat the parts of the brain differently. A more exhaustive analysis on the behaviour of each of the structures could help in the lesion refinement. One of the issues when labelling the brain in different structures lies in the registration process with an atlas, thus, the use of our MC pipeline could enhance this alignment. Even though our MC pipeline was optimised for the alignment of conventional and diffusion MRI, this same pipeline could be adapted for other image modalities (T1w and FLAIR). At the moment, we are using T1w and FLAIR images because the other modalities (PDw and T2w) in the studied database did not provide valuable information to our segmentation approach. On the other hand, we could consider using DTI information to improve the detection and segmentation of WML. Another issue that can be studied to optimise the WML segmentation toolbox is to standardise a uniform threshold and automated parameters configuration. We believe that a proper image normalisation obtaining similar histogram distributions for the different tissues could help to uniform the set-up of the tool.

Finally, we would like to include all the topics we have tackled in this thesis in the online tool. In parallel, other projects related to the MS field have been carried out and the main author of this thesis has taken part in them. The combination of all the projects, performing some steps iteratively, like tissue segmentation and lesion segmentation and correcting errors at each step for both methods, may lead to better results and improvements in the automated processes. Besides, with this global tool, new biomarkers could be used to describe the disease, e.g. measures of atrophy, lesion volumes classified per

tissues, structures or regions, evolution of both lesions and atrophy, etc. Follow-up studies have an important interest in monitoring the disease's evolution. We did not tackle this scenario in this thesis, but our group has previous knowledge in this field. To incorporate all the methods in one online tool would also be a huge contribution to the daily clinical practices of radiologists and neurologists in order to obtain quantitative reports covering different aspects: number of lesions, volume of lesions, atrophy volume, matter loss, region affected, etc.

Bibliography

- [1] J. Love, “Demyelinating diseases,” *Journal of Clinical pathology*, vol. 59, no. 11, pp. 1151–1159, 2006.
- [2] M. Crow, “Systemic lupus erythematosu,” in *Goldman’s Cecil Medicin*, 24th ed., L. Goldman and A. Schafer, Eds. Elsevier Saunders, 2011, ch. 274.
- [3] M. Crow, “Etiology and pathogenesis of systemic lupus erythematosus,” in *Kelley’s Textbook of Rheumatology*, 9th ed., G. Firestein, R. Budd, and S. e. a. Gabriel, Eds. Elsevier Saunders, 2012, ch. 79.
- [4] G. Pons-Estel, G. Alarcón, L. Scofield, L. Reinlib, and G. Cooper, “Understanding the epidemiology and progression of systemic lupus erythematosus,” *Seminars in arthritis and rheumatism*, vol. 39, no. 4, p. 257, 2010.
- [5] R. Cervera, M. A. Khamashta, J. Font, G. D. Sebastiani, A. Gil, P. Lavilla, J. C. Mejia, A. O. Aydintug, H. Chwalinska-Sadowska, E. de Ramon, A. Fernandez-Nebro, M. Galeazzi, M. Valen, A. Mathieu, F. Houssiau, N. Caro, P. Alba, M. Ramos-Casals, M. Ingelmo, G. R. Hughes, and E. W. P. on Systemic Lupus Erythematosus, “Mor-bidity and mortality in systemic lupus erythematosus during a 10-year period: A comparison of early and late manifestations in a cohort of 1,000 patients,” *Medicine*, vol. 82, no. 5, pp. 299–308, 2003.
- [6] S. O’Neill and R. Cervera, “Systemic lupus,” *Best Practice & Research Clinical Rheumatology*, vol. 24, no. 6, pp. 841–855, 2010.
- [7] P. Chiewthanakul, K. Sawanyawisuth, C. Foocharoen, and S. Tiamkao, “Clinical features and predictive factors in neuropsychiatric lupus,” *Asian Pac J Allergy Im-munol*, vol. 30, no. 1, pp. 55–60, 2012.

- [8] E. Zirkzee, T. Huizinga, E. Bollen, M. van Buchem, H. Middelkoop, N. van der Wee, S. le Cessie, and G. Steup-Beekman, “Mortality in neuropsychiatric systemic lupus erythematosus (npsle),” *Lupus*, vol. 23, no. 1, pp. 31–38, 2014.
- [9] W. R. Hendee and C. J. Morgan, “Magnetic resonance imaging part i-physical principles,” *Western Journal of Medicine*, vol. 141, no. 4, pp. 491–500, 1984.
- [10] A. L. Scherzinger, “Basic principles of magnetic resonance imaging-an update,” *Western Journal of Medicine*, vol. 143, no. 6, pp. 782–792, 1985.
- [11] D. Miller, R. Grossman, S. Reingold, and H. McFarland, “The role of magnetic resonance techniques in understanding and managing multiple sclerosis: Consensus report of the white matter study group,” *Brain*, vol. 121, no. 1, pp. 3–24, 1998.
- [12] F. Fazekas, F. Barkhof, M. Filippi, R. Grossman, D. Li, W. McDonald, H. McFarland, D. Paty, J. Simon, J. Wolinsky, and D. Miller, “The contribution of magnetic resonance imaging to the diagnosis of multiple sclerosis,” *Neurology*, vol. 53, no. 3, pp. 448–456, 1999.
- [13] M. Filippi, V. Dousset, H. McFarland, D. Miller, and R. Grossman, “Role of magnetic resonance imaging in the diagnosis and monitoring of multiple sclerosis: Consensus report of the white matter study group,” *Journal of Magnetic Resonance Imaging*, vol. 15, no. 5, pp. 499–504, 2002.
- [14] P. Brex, O. Ciccarelli, J. O’Riordan, M. Sailer, A. Thompson, and D. Miller, “A longitudinal study of abnormalities on mri and disability from multiple sclerosis,” *The New England Journal of Medicine*, vol. 346, no. 3, pp. 158–164, 2002.
- [15] W. McDonald, A. Compston, G. Edan, D. Goodkin, H. Hartung, F. Lublin, H. McFarland, D. Paty, C. Polman, S. Reingold, M. Sandberg-Wollheim, W. Sibley, A. Thompson, S. van den Noort, B. Weinshenker, and J. Wolinsky, “Recommended diagnostic criteria for multiple sclerosis: guidelines from the international panel on the diagnosis of multiple sclerosis,” *Annals of Neurology*, vol. 50, no. 1, pp. 121–127, 2001.
- [16] C. H. Polman, S. C. Reingold, G. Edan, M. Filippi, H.-P. Hartung, L. Kappos, F. D. Lublin, L. M. Metz, H. F. McFarland, P. W. O’Connor, M. Sandberg-Wollheim, A. J. Thompson, B. G. Weinshenker, and J. S. Wolinsky, “Diagnostic criteria for multiple sclerosis: 2005 revisions to the mcdonald criteria,” *Annals of Neurology*, vol. 58, no. 6, pp. 840–846, 2005.

- [17] C. H. Polman, S. C. Reingold, B. Banwell, M. Clanet, J. A. Cohen, M. Filippi, K. Fujihara, E. Havrdova, M. Hutchinson, L. Kappos, F. D. Lublin, X. Montalban, P. O'Connor, M. Sandberg-Wollheim, A. J. Thompson, E. Waubant, B. Weinshenker, and J. S. Wolinsky, "Diagnostic criteria for multiple sclerosis: 2010 revisions to the mcdonald criteria," *Annals of Neurology*, vol. 69, no. 2, pp. 292–302, 2011.
- [18] Àlex Rovira, M. P. Wattjes, M. Tintoré, C. Tur, T. A. Yousry, M. P. Sormani, N. D. Stefano, M. Filippi, C. Auger, M. A. Rocca, F. Barkhof, F. Fazekas, L. Kappos, C. Polman, D. Miller, and X. M. on behalf of the MAGNIMS study group, "Evidence-based guidelines: Magnims consensus guidelines on the use of mri in multiple sclerosis - clinical implementation in the diagnostic process," *Nature Reviews Neurology*, vol. 11, no. 8, pp. 471–482, 2015.
- [19] L. Lemieux, N. Wieshmann, N. Moran, D. Fish, and S. Shorvon, "The detection and significance of subtle changes in mixed-signal brain lesions by serial mri scan matching and spatial normalization," *Medical Image Analysis*, vol. 2, no. 3, pp. 227–242, 1998.
- [20] W. I. Wells, P. Viola, H. Atsumi, S. Nakajima, and R. Kikinis, "Multi-modal volume registration by maximization of mutual information," *Medical Image Analysis*, vol. 1, no. 1, pp. 35–51, 1996.
- [21] S. Ourselin, A. Roche, S. Prima, and N. Ayache, "Block matching: A general framework to improve robustness of rigid registration of medical images," *Medical Image Computing and Computer-Assisted Intervention (MICCAI 2000)*, vol. 1935, pp. CH373–CH373, 2000.
- [22] R. Bitar, G. Leung, R. Perng, S. Tadros, A. R. Moody, J. Sarrazin, C. McGregor, M. Christakis, S. Symons, A. Nelson, and T. P. Roberts, "Mr pulse sequences: What every radiologist wants to know but is afraid to ask," *RadioGraphics*, vol. 26, no. 2, pp. 513–537, 2006.
- [23] A. Elster, "Gradient echo imaging: techniques and acronyms," *Radiology*, vol. 186, pp. 1–8, 1993.
- [24] M. Susumu and Z. Jiangyang, "Principles of diffusion tensor imaging and its applications to basic neuroscience research," *Neuron*, vol. 51, no. 5, pp. 527–539, 2006.
- [25] P. J. Basser, J. Mattiello, and D. LeBihan, "MR diffusion tensor spectroscopy and imaging," *Biophysical journal*, vol. 66, no. 1, pp. 259–267, 1994.

- [26] H. Johansen-Berg and T. E. Behrens, *Diffusion MRI: From Quantitative Measurement In vivo Neuroanatomy*. Elsevier, 2009.
- [27] C. Pierpaoli and P. J. Basser, “Toward a quantitative assessment of diffusion anisotropy,” *Magnetic Resonance in Medicine*, vol. 36, no. 6, pp. 893–906, 1996.
- [28] S. M. Smith, M. Jenkinson, H. Johansen-Berg, D. Rueckert, T. E. Nichols, C. E. Mackay, K. E. Watkins, O. Ciccarelli, M. Z. Cader, P. M. Matthews, and T. E. Behrens, “Tract-based spatial statistics: Voxelwise analysis of multi-subject diffusion data,” *NeuroImage*, vol. 31, no. 4, pp. 1487 – 1505, 2006.
- [29] T. Behrens, H. J. Berg, S. Jbabdi, M. Rushworth, and M. Woolrich, “Probabilistic diffusion tractography with multiple fibre orientations: What can we gain?” *NeuroImage*, vol. 34, no. 1, pp. 144 – 155, 2007.
- [30] M. Bomans, K.-H. Hohne, U. Tiede, and M. Riemer, “3-D segmentation of MR images of the head for 3-D display,” *IEEE Transactions on Medical Imaging*, vol. 9, no. 2, pp. 177 –183, 1990.
- [31] D. E. Rex, D. W. Shattuck, R. P. Woods, K. L. Narr, E. Luders, K. Rehm, S. E. Stolzner, D. A. Rottenberg, and A. W. Toga, “A meta-algorithm for brain extraction in MRI,” *NeuroImage*, vol. 23, no. 2, pp. 625–637, 2004.
- [32] M. Jenkinson, M. Pechaud, and S. Smith, “BET2 - MRI-based estimation of brain, skull and scalp surfaces,” *In Eleventh Annual Meeting of the Organization for Human Brain Mapping*, 2005.
- [33] A. H. Zhuang, D. J. Valentino, and A. W. Toga, “Skull-stripping magnetic resonance brain images using a model-based level set,” *NeuroImage*, vol. 32, no. 1, pp. 79 – 92, 2006.
- [34] J. G. Park and C. Lee, “Skull stripping based on region growing for magnetic resonance brain images,” *NeuroImage*, vol. 47, no. 4, pp. 1394–1407, 2009.
- [35] K. Somasundaram and T. Kalaiselvi, “Fully automatic brain extraction algorithm for axial T2-weighted magnetic resonance images,” *Computers in Biology and Medicine*, vol. 40, no. 10, pp. 811 – 822, 2010.
- [36] A. G. R. Balan, A. J. M. Traina, M. X. Ribeiro, P. M. A. Marques, and C. Traina Jr, “Smart histogram analysis applied to the skull-stripping problem in T1-weighted MRI,” *Computers in Biology and Medicine*, vol. 42, no. 5, pp. 509 – 522, 2012.

- [37] S. M. Smith, “Fast robust automated brain extraction,” *Human Brain Mapping*, vol. 17, no. 3, pp. 143–155, 2002.
- [38] D. W. Shattuck, S. R. Sandor-Leahy, K. A. Schaper, D. A. Rottenberg, and R. M. Leahy, “Magnetic resonance image tissue classification using a partial volume model,” *NeuroImage*, vol. 13, no. 5, pp. 856 – 876, 2001.
- [39] K. Boesen, K. Rehm, K. Schaper, S. Stoltzner, R. Woods, E. Lüders, and D. Rottenberg, “Quantitative comparison of four brain extraction algorithms,” *NeuroImage*, vol. 22, no. 3, pp. 1255–1261, 2004.
- [40] E. Roura, A. Oliver, M. Cabezas, J. Vilanova, A. Rovira, L. Ramió-Torrentà†, and X. Lladó, “MARGA: Multispectral Adaptive Region Growing Algorithm for brain extraction on axial MRI,” *Computer Methods and Programs in Biomedicine*, vol. 113, no. 2, pp. 655 – 673, 2014.
- [41] D. D. Sha and J. P. Sutton, “Towards automated enhancement, segmentation and classification of digital brain images using networks of networks,” *Information Sciences*, vol. 138, no. 1, pp. 45 – 77, 2001.
- [42] M. Cabezas, A. Oliver, E. Roura, J. Freixenet, J. C. Vilanova, L. Ramió-Torrentà, À. Rovira, and X. Lladó, “Automatic multiple sclerosis lesion detection in brain mri by flair thresholding,” *Computer Methods and Programs in Biomedicine*, vol. 115, no. 3, pp. 147–161, 2014.
- [43] Z. Hou, “A review on MRI image intensity inhomogeneity correction,” *International Journal of Biomedical Imaging*, pp. 1–11, 2006.
- [44] U. Vovk, F. Pernus, and B. Likar, “A Review of Methods for Correction of Intensity Inhomogeneity in MRI,” *IEEE Transactions on Medical Imaging*, vol. 26, no. 3, pp. 405–421, 2007.
- [45] M. A. Farooque and J. S. Rohankar, “Survey on various noises and techniques for denoising the color image,” *International Journal of Application or Innovation in Engineering & Management (IJAIEEM)*, vol. 2, no. 11, 2013.
- [46] P. Perona and J. Malik, “Scale-space and edge detection using anisotropic diffusion,” *Pattern Analysis and Machine Intelligence, IEEE Transactions on*, vol. 12, no. 7, pp. 629–639, Jul 1990.

- [47] J. Ashburner and K. J. Friston, "Voxel-Based Morphometry—The Methods," *NeuroImage*, vol. 11, no. 6, pp. 805–821, 2000.
- [48] J. Sled, A. Zijdenbos, and A. Evans, "A nonparametric method for automatic correction of intensity nonuniformity in MRI data," *IEEE Transactions on Medical Imaging*, vol. 17, no. 1, pp. 87–97, 1998.
- [49] R. G. Boyes, J. L. Gunter, C. Frost, A. L. Janke, T. Yeatman, D. L. Hill, M. A. Bernstein, P. M. Thompson, M. W. Weiner, N. Schuff, G. E. Alexander, R. J. Killiany, C. DeCarli, C. R. Jack, and N. C. Fox, "Intensity non-uniformity correction using N3 on 3-T scanners with multichannel phased array coils," *NeuroImage*, vol. 39, no. 4, pp. 1752 – 1762, 2008.
- [50] W. Zheng, M. W. Chee, and V. Zagorodnov, "Improvement of brain segmentation accuracy by optimizing non-uniformity correction using N3," *NeuroImage*, vol. 48, no. 1, pp. 73 – 83, 2009.
- [51] J. Rosenman, E. Miller, G. Tracton, and C. T.J., "Image registration: an essential part of radiation therapy treatment planning," *International Journal of Radiation Oncology, Biology and Physics*, vol. 40, no. 1, pp. 197–205, 1998.
- [52] P. Thompson, M. Mega, and A. Toga, "Mathematical/computational challenges in creating deformable and probabilistic atlases of the human brain," *Human Brain Mapping*, vol. 9, pp. 81–92, 2000.
- [53] A. Toga and P. Thompson, "The role of image registration in brain mapping," *Image and Vision Computing*, vol. 19, no. 1-2, pp. 3–24, 2001.
- [54] H. Brian F., B. Michael, T. Lennart, and Y. L. Dennys, "Image registration: an essential tool for nuclear medicine," *European Journal of Nuclear Medicine and Molecular Imaging*, vol. 29, pp. 559–577, 2002.
- [55] T. Makela, P. Clarysse, O. Sipila, N. Pauna, Q. C. Pham, T. Katila, and I. Magnin, "A review of cardiac image registration methods," *IEEE Transactions on Medical Imaging*, vol. 21, no. 9, pp. 1011–1021, 2002.
- [56] V. Fonov, A. C. Evans, K. Botteron, C. R. Almli, R. C. McKinstry, and D. L. Collins, "Unbiased average age-appropriate atlases for pediatric studies," *NeuroImage*, vol. 54, no. 1, pp. 313 – 327, 2011.

- [57] S. Klein, U. van der Heide, I. Lips, M. van Vulpen, M. Staring, and J. Pluim, “Automatic Segmentation of the Prostate in 3D MR Images by Atlas Matching using Localized Mutual Information,” *Medical Physics*, vol. 35, no. 4, pp. 1407–1417, 2008.
- [58] M. Cabezas, A. Oliver, X. Lladó, J. Freixenet, and M. B. Cuadra, “A review of atlas-based segmentation for magnetic resonance brain images,” *Computer Methods and Programs in Biomedicine*, vol. 104, no. 3, pp. e158–e177, 2011.
- [59] A. Gubern-Mérida, M. Kallenberg, R. Martí, and N. Karssemeijer, “Multi-class probabilistic atlas-based segmentation method in breast MRI,” *Proceedings of the 5th Iberian conference on Pattern recognition and image analysis*, vol. 5, pp. 660–667, 2011.
- [60] M. Cabezas, A. Oliver, S. Valverde, J. Freixenet, B. Beltran, J. C. Vilanova, L. Ramió-Torrentà, À. Rovira, and X. Lladó, “Boost: a supervised approach for multiple sclerosis lesion segmentation,” *Journal of Neuroscience Methods*, vol. 237, pp. 108 – 117, 2014.
- [61] N. Guizard, P. Coupé, V. S. Fonov, J. V. Manjón, D. L. Arnold, and D. L. Collins, “Rotation-invariant multi-contrast non-local means for {MS} lesion segmentation,” *NeuroImage: Clinical*, vol. 8, pp. 376 – 389, 2015.
- [62] R. Harmouche, N. Subbanna, D. Collins, D. Arnold, and T. Arbel, “Probabilistic multiple sclerosis lesion classification based on modeling regional intensity variability and local neighborhood information,” *Biomedical Engineering, IEEE Transactions on*, vol. 62, no. 5, pp. 1281–1292, 2015.
- [63] E. Roura, A. Oliver, M. Cabezas, S. Valverde, D. Pareto, J. Vilanova, L. Ramió-Torrentà, A. Rovira, and X. Lladó, “A toolbox for multiple sclerosis lesion segmentation,” *Neuroradiology*, vol. 57, no. 10, pp. 1031–1043, 2015.
- [64] S. Klein, M. Staring, K. Murphy, M. Viergever, and J. Pluim, “Elastix: A Toolbox for Intensity-Based Medical Image Registration,” *IEEE Transactions on Medical Imaging*, vol. 29, no. 1, pp. 196–205, 2010.
- [65] Y. Diez, A. Oliver, M. Cabezas, S. Valverde, R. Martí, J. Vilanova, L. Ramió-Torrentà, À. Rovira, and X. Lladó, “Intensity based methods for brain mri longitudinal registration. a study on multiple sclerosis patients,” *Neuroinformatics*, vol. 12, no. 3, pp. 365–379, 2014.

- [66] E. Roura, T. Schneider, M. Modat, P. Daga, N. Muhlert, D. Chard, S. Ourselin, X. Lladó, and C. A. M. Wheeler-Kingshott, “Multi-channel registration of fa and t1w images in the presence of atrophy: application to multiple sclerosis,” *Functional Neurology*, vol. 30, no. 4, 2015.
- [67] E. Roura, N. Sarbu, A. Oliver, S. Valverde, S. González, R. Cervera, N. Bargalló, and X. Lladó, “A toolbox for multiple sclerosis lesion segmentation,” *Frontiers*, 2016.
- [68] E. Roura, T. Schneider, M. Modat, P. Daga, N. Muhlert, D. Chard, S. Ourselin, X. Lladó, and C. A. M. Wheeler-Kingshott, “Evaluating a multi-channel registration approach of FA and T1w on MS patients with simulated atrophy,” in *International Society for Magnetic Resonance in Medicine (ISMRM 21st)*, 2013.
- [69] P. A. Viola, “Alignment by maximization of mutual information,” *5th International Conference of Computer Vision*, pp. 16–23, 1995.
- [70] J. Pluim, J. Maintz, and M. Viergever, “Mutual-information-based registration of medical images: A survey,” *IEEE Transactions on Medical Imaging*, vol. 22, no. 8, pp. 986–1004, 2003.
- [71] P. Daga, G. Winston, M. Modat, M. Cardoso, J. Stretton, M. Symms, A. McEvoy, D. Hawkes, J. Duncan, and S. Ourselin, “Integrating structural and diffusion mr information for optic radiation localisation in focal epilepsy patients,” in *Biomedical Imaging: From Nano to Macro, 2011 IEEE International Symposium on*, March 2011, pp. 353–356.
- [72] W. Pratt, *Digital Image Processing*, 2nd ed. Wiley, New York, 1991.
- [73] J.-P. Thirion, “Non-rigid matching using demons,” *Proceedings of the 1996 Conference on Computer Vision and Pattern Recognition (CVPR '96)*, p. 245, 1996.
- [74] J.-P. Thirion, “Image matching as a diffusion process: an analogy with Maxwell’s demons,” *Medical Image Analysis*, vol. 2, no. 3, pp. 243–260, 1998.
- [75] D. Rueckert, L. Sonoda, C. Hayes, D. Hill, M. Leach, and D. Hawkes, “Nonrigid registration using free-form deformations: application to breast MR images,” *IEEE Transactions on Medical Imaging*, vol. 18, no. 8, pp. 712–721, 1999.
- [76] T. Vercauteren, X. Pennec, A. Perchant, and N. Ayache, “Non-parametric Diffeomorphic Image Registration with the Demons Algorithm,” *Medical Image Computing and Computer-Assisted Intervention (MICCAI 2007)*, vol. 4792, pp. 319–326, 2007.

- [77] T. Vercauteren, X. Pennec, A. Perchant, and N. Ayache, “Symmetric Log-Domain Diffeomorphic Registration: A Demons-Based Approach,” *Medical Image Computing and Computer-Assisted Intervention (MICCAI 2008)*, vol. 5241, pp. 754–761, 2008.
- [78] L. G. Brown, “A survey of image registration techniques,” *ACM Computing Surveys*, vol. 24, no. 4, pp. 325–376, 1992.
- [79] J. Maintz and M. Viergever, “A survey of medical image registration,” *Medical Image Analysis*, vol. 2, no. 1, pp. 1–36, 1998.
- [80] B. Zitová and J. Flusser, “Image registration methods: A survey,” *Image and Vision Computing*, vol. 21, no. 11, pp. 977–1000, 2003.
- [81] A. Gholipour, N. Kehtarnavaz, R. Briggs, M. Devous, and K. Gopinath, “Brain functional localization: A survey of image registration techniques,” *IEEE Transactions on Medical Imaging*, vol. 26, no. 4, pp. 427–451, 2007.
- [82] M. Holden, “A review of geometric transformations for nonrigid body registration,” *IEEE Transactions on Medical Imaging*, vol. 27, no. 1, pp. 111–128, 2008.
- [83] R. D. Rabbitt, J. A. Weiss, G. E. Christensen, and M. I. Miller, “Mapping of hyperelastic deformable templates using the finite element method,” *SPIE*, vol. 2573, pp. 252–265, 1995.
- [84] G. E. Christensen, “Deformable shape models for anatomy,” Ph.D. dissertation, The University of Iowa, 1994.
- [85] G. E. Christensen, R. D. Rabbitt, and M. I. Miller, “Deformable templates using large deformation kinematics,” *IEEE Transactions on Image Processing*, vol. 5, no. 10, pp. 1435–1447, 1996.
- [86] J. Čížek, K. Herholz, S. Vollmar, R. Schrader, J. Klein, and W.-D. Heiss, “Fast and robust registration of pet and mr images of human brain,” *NeuroImage*, vol. 22, no. 1, pp. 434–442, 2004.
- [87] P. Hellier and C. Barillot, “A hierarchical parametric algorithm for deformable multimodal image registration,” *Computer Methods and Programs in Biomedicine*, vol. 75, no. 2, pp. 107–115, 2004.

- [88] V. Noblet, C. Heinrich, F. Heitz, and J. Paul Armspach, “3-d deformable image registration: A topology preservation scheme based on hierarchical deformation models and interval analysis optimization,” *IEEE Transactions on Image Processing*, vol. 14, pp. 553–566, 2005.
- [89] M. Modat, G. R. Ridgway, Z. A. Taylor, M. Lehmann, J. Barnes, D. J. Hawkes, N. C. Fox, and S. Ourselin, “Fast free-form deformation using graphics processing units,” *Computer Methods and Programs in Biomedicine*, vol. 98, no. 3, pp. 278–284, 2010.
- [90] C. Xu, D. Pham, M. Rettmann, D. Yu, and J. Prince, “Reconstruction of the human cerebral cortex from magnetic resonance images,” *Medical Imaging, IEEE Transactions on*, vol. 18, no. 6, pp. 467–480, 1999.
- [91] D. MacDonald, N. Kabani, D. Avis, and A. C. Evans, “Automated 3-d extraction of inner and outer surfaces of cerebral cortex from {MRI},” *NeuroImage*, vol. 12, no. 3, pp. 340 – 356, 2000.
- [92] J. de Bresser, M. P. Portegies, A. Leemans, G. J. Biessels, L. J. Kappelle, and M. A. Viergever, “A comparison of {MR} based segmentation methods for measuring brain atrophy progression,” *NeuroImage*, vol. 54, no. 2, pp. 760 – 768, 2011.
- [93] V. Popescu, N. Ran, F. Barkhof, D. Chard, C. Wheeler-Kingshott, and H. Vrenken, “Accurate {GM} atrophy quantification in {MS} using lesion-filling with co-registered 2d lesion masks,” *NeuroImage: Clinical*, vol. 4, pp. 366 – 373, 2014.
- [94] S. Valverde, A. Oliver, and X. Lladó, “A white matter lesion-filling approach to improve brain tissue volume measurements,” *NeuroImage: Clinical*, vol. 6, pp. 86 – 92, 2014.
- [95] N. Kovacevic, N. Lobaugh, M. Bronskill, B. Levine, A. Feinstein, and S. Black, “A robust method for extraction and automatic segmentation of brain images,” *NeuroImage*, vol. 17, no. 3, pp. 1087 – 1100, 2002.
- [96] B. Cherradi, M. Y. Omar Bouattane, and A. Raihani, “Brain extraction and fuzzy tissue segmentation in cerebral 2d t1-weighted magnetic resonance images,” *International Journal of Computer Science Issues*, vol. 8, no. 1, pp. 215–224, 2011.
- [97] P. Schmidt, C. Gaser, M. Arsic, D. Buck, A. Förschler, A. Berthele, M. Hoshi, R. Ilg, V. J. Schmid, C. Zimmer, B. Hemmer, and M. Mühlau, “An automated

- tool for detection of flair-hyperintense white-matter lesions in multiple sclerosis,” *NeuroImage*, vol. 59, no. 4, pp. 3774–3783, 2012.
- [98] Y. Zhang, M. Brady, and S. Smith, “Segmentation of brain mr images through a hidden markov random field model and the expectation-maximization algorithm,” *Medical Imaging, IEEE Transactions on*, vol. 20, no. 1, pp. 45–57, 2001.
- [99] J. Tohka, I. D. Dinov, D. W. Shattuck, and A. W. Toga, “Brain {MRI} tissue classification based on local markov random fields,” *Magnetic Resonance Imaging*, vol. 28, no. 4, pp. 557 – 573, 2010.
- [100] J. Ashburner and K. J. Friston, “Unified segmentation,” *NeuroImage*, vol. 26, no. 3, pp. 839 – 851, 2005.
- [101] D. Pham, “Robust fuzzy segmentation of magnetic resonance images,” in *Computer-Based Medical Systems, 2001. CBMS 2001. Proceedings. 14th IEEE Symposium on*, 2001, pp. 127–131.
- [102] R. de Boer, H. A. Vrooman, F. van der Lijn, M. W. Vernooij, M. A. Ikram, A. van der Lugt, M. M. Breteler, and W. J. Niessen, “White matter lesion extension to automatic brain tissue segmentation on {MRI},” *NeuroImage*, vol. 45, no. 4, pp. 1151 – 1161, 2009.
- [103] S. Valverde, A. Oliver, Y. Díez, M. Cabezas, J. Vilanova, L. Ramió-Torrentà†, A. Rovira, and X. Lladó, “Evaluating the effects of white matter multiple sclerosis lesions on the volume estimation of 6 brain tissue segmentation methods,” *American Journal of Neuroradiology*, vol. 36, no. 10, pp. 1109–1115, 2015.
- [104] S. Valverde, A. Oliver, E. Roura, D. Pareto, J. Vilanova, L. Ramió-Torrentà†, J. Sastre-Garriga, X. Montalban, A. Rovira, and X. Lladó, “Quantifying brain tissue volume in multiple sclerosis with automated lesion segmentation and filling,” *NeuroImage: Clinical*, 2015.
- [105] X. Lladó, A. Oliver, M. Cabezas, J. Freixenet, J. C. Vilanova, A. Quiles, L. Valls, L. Ramió-Torrentà, and A. Rovira, “Segmentation of multiple sclerosis lesions in brain MRI: a review of automated approaches,” *Information Sciences*, vol. 186, no. 1, pp. 164–185, 2012.
- [106] D. García-Lorenzo, S. Francis, S. Narayanan, D. L. Arnold, and D. L. Collins, “Review of automatic segmentation methods of multiple sclerosis white matter lesions on

- conventional magnetic resonance imaging,” *Medical Image Analysis*, vol. 17, no. 1, pp. 1 – 18, 2013.
- [107] J.-C. Souplet, C. Lebrun, N. Ayache, and G. Malandain, “An automatic segmentation of t2-flair multiple sclerosis lesions,” in *Multiple Sclerosis Lesion Segmentation Challenge Workshop (MICCAI-2008)*, New York, NY, USA, United States, 2008, pp. 1–8.
- [108] E. Geremia, B. Menze, O. Clatz, E. Konukoglu, A. Criminisi, and N. Ayache, “Spatial decision forests for MS lesion segmentation in multi-channel MR images,” *Lecture Notes in Computer Science*, vol. 6361, no. PART 1, pp. 111–118, 2010.
- [109] D. Goldberg-Zimring, A. Achiron, S. Miron, M. Faibel, and H. Azhari, “Automated detection and characterization of multiple sclerosis lesions in brain {MR} images,” *Magnetic Resonance Imaging*, vol. 16, no. 3, pp. 311 – 318, 1998.
- [110] P. Anbeek, K. L. Vincken, G. S. van Bochove, M. J. van Osch, and J. van der Grond, “Probabilistic segmentation of brain tissue in {MR} imaging,” *NeuroImage*, vol. 27, no. 4, pp. 795 – 804, 2005.
- [111] J. H. Morra, Z. Tu, A. W. Toga, and P. M. Thompson, “Automatic segmentation of ms lesions using a contextual model for the miccai grand challenge,” 2008.
- [112] M. Styner, J. Lee, B. Chin, M. Chin, O. Commowick, H. Tran, S. Markovic-Plese, V. Jewells, and S. Warfield, “3d segmentation in the clinic: A grand challenge ii: Ms lesion segmentation,” 2008.
- [113] J. Lecoecur, J.-C. Ferré, and C. Barillot, “Optimized supervised segmentation of MS lesions from multispectral MRIs,” in *MICCAI workshop on Medical Image Analysis on Multiple Sclerosis (validation and methodological issues)*, Londres, United Kingdom, 2009.
- [114] B. Bedell and N. P.A., “Automatic segmentation of gadolinium-enhanced multiple sclerosis lesions.” *Magnetic Resonance in Medicine*, vol. 39, no. 6, pp. 935–940, 1998.
- [115] A.-O. Boudraa, S. M. R. Dehak, Y.-M. Zhu, C. Pachai, Y.-G. Bao, and J. Grimaud, “Automated segmentation of multiple sclerosis lesions in multispectral {MR} imaging using fuzzy clustering,” *Computers in Biology and Medicine*, vol. 30, no. 1, pp. 23 – 40, 2000.

- [116] R. He and N. P.A., “Automatic delineation of gd enhancements on magnetic resonance images in multiple sclerosis,” *Medical Physics*, vol. 29, no. 7, pp. 1536–1546, 2002.
- [117] S. Datta, B. R. Sajja, R. He, R. K. Gupta, J. S. Wolinsky, and P. A. Narayana, “Segmentation of gadolinium-enhanced lesions on mri in multiple sclerosis,” *Journal of Magnetic Resonance Imaging*, vol. 25, no. 5, pp. 932–937, 2007.
- [118] S. Saha and S. Bandyopadhyay, “A new point symmetry based fuzzy genetic clustering technique for automatic evolution of clusters,” *Information Sciences*, vol. 179, no. 19, pp. 3230 – 3246, 2009.
- [119] K. Van Leemput, F. Maes, D. Vandermeulen, A. Colchester, and P. Suetens, “Automated segmentation of multiple sclerosis lesions by model outlier detection,” *Medical Imaging, IEEE Transactions on*, vol. 20, no. 8, pp. 677–688, 2001.
- [120] Y. Wu, S. K. Warfield, I. L. Tan, W. M. W. III, D. S. Meier, R. A. van Schijndel, F. Barkhof, and C. R. Guttmann, “Automated segmentation of multiple sclerosis lesion subtypes with multichannel {MRI},” *NeuroImage*, vol. 32, no. 3, pp. 1205 – 1215, 2006.
- [121] O. Freifeld, H. Greenspan, and J. Goldberger, “Lesion detection in noisy mr brain images using constrained gmm and active contours,” in *Biomedical Imaging: From Nano to Macro, 2007. ISBI 2007. 4th IEEE International Symposium on*, 2007, pp. 596–599.
- [122] R. Khayati, M. Vafadust, F. Towhidkhah, and M. Nabavi, “Fully automatic segmentation of multiple sclerosis lesions in brain {MR} {FLAIR} images using adaptive mixtures method and markov random field model,” *Computers in Biology and Medicine*, vol. 38, no. 3, pp. 379 – 390, 2008.
- [123] D. García-Lorenzo, S. Prima, L. Collins, D. Arnold, S. P. Morrissey, and C. Barillot, “Combining robust expectation maximization and mean shift algorithms for multiple sclerosis brain segmentation,” *In Work. Med. Image Anal. Mult. Scler*, vol. 30, no. 8, pp. 1455 – 1467, 2008.
- [124] D. García-Lorenzo, S. Prima, S. Prima, L. Parkes, J.-C. Ferré, S. P. Morrissey, and C. Barillot, “The impact of processing workflow in performance of automatic white matter lesion segmentation in multiple sclerosis,” *In Work. Med. Image Anal. Mult. Scler*, pp. 104 – 112, 2008.

- [125] D. García-Lorenzo, J. Lecoecur, D. Arnold, D. Collins, and C. Barillot, “Multiple sclerosis lesion segmentation using an automatic multimodal graph cuts,” in *Medical Image Computing and Computer-Assisted Intervention, MICCAI 2009*, ser. Lecture Notes in Computer Science, 2009, vol. 5762, pp. 584–591.
- [126] D. Garcia-Lorenzo, S. Prima, D. Arnold, D. Collins, and C. Barillot, “Trimmed-likelihood estimation for focal lesions and tissue segmentation in multisequence mri for multiple sclerosis,” *Medical Imaging, IEEE Transactions on*, vol. 30, no. 8, pp. 1455–1467, 2011.
- [127] S. Appenzeller, G. Pike, and A. Clarke, “Magnetic resonance imaging in the evaluation of central nervous system manifestations in systemic lupus erythematosus,” *Clinical Reviews in Allergy & Immunology*, vol. 34, no. 3, pp. 361–366, 2008.
- [128] S. Appenzeller, A. Vasconcelos Faria, L. Li, L. Costallat, and F. Cendes, “Quantitative magnetic resonance imaging analyses and clinical significance of hyperintense white matter lesions in systemic lupus erythematosus patients,” *Annals of Neurology*, vol. 64, no. 6, pp. 635–643, 2008.
- [129] M. Scully, B. Anderson, T. Lane, C. Gasparovic, V. Magnotta, W. Sibbitt, C. Roldan, R. Kikinis, and H. Bockholt, “An automated method for segmenting white matter lesions through multi-level morphometric feature classification with application to lupus,” *Frontiers in Human Neuroscience*, vol. 4, no. 27, 2010.
- [130] N. Sarbu, N. Bargalló, and R. Cervera, “Advanced and conventional magnetic resonance imaging in neuropsychiatric lupus,” *F1000Research*, vol. 4, no. 162, 2015.
- [131] N. Sarbu, F. Alobeidi, P. Toledano, G. Espinosa, I. Giles, A. Rahman, T. Yousry, S. Capurro, R. Jägger, R. Cervera, and N. Bargalló, “Brain abnormalities in newly diagnosed neuropsychiatric lupus: Systematic MRI approach and correlation with clinical and laboratory data in a large multicenter cohort,” *Autoimmunity Reviews*, vol. 14, no. 2, pp. 153 – 159, 2015.
- [132] E. Roura, T. Schneider, P. Daga, M. Modat, N. Muhlert, J. Freixenet, D. Chard, S. Ourselin, X. Lladó, and C. Wheeler-Kingshott, “Multi-channel registration of FA and T1-weighted images to standard space: patients with Multiple Sclerosis,” 2012.
- [133] E. Roura, “Multi-channel registration of conventional and diffusion MRI on MS patients,” Master’s thesis, University of Girona, Catalonia, Spain, 2012.

- [134] M. Sdika and D. Pelletier, “Nonrigid registration of multiple sclerosis brain images using lesion inpainting for morphometry or lesion mapping.” *Human Brain Mapping*, vol. 30, no. 4, pp. 1060–1067, 2009.
- [135] D. T. Chard, J. S. Jackson, D. H. Miller, and C. A. Wheeler-Kingshott, “Reducing the impact of white matter lesions on automated measures of brain grey and white matter volumes,” *Journal of Magnetic Resonance Imaging*, vol. 32, no. 1, pp. 223–228, 2010.
- [136] M. Battaglini, M. Jenkinson, and N. De Stefano, “Evaluating and reducing the impact of white matter lesions on brain volume measurements,” *Human Brain Mapping*, vol. 33, no. 9, pp. 2062–2071, 2012.